TAMPEREEN TEKNILLINEN YLIOPISTO
TAMPERE UNIVERSITY OF TECHNOLOGY

Ville-Markus Korpijärvi

High-Power Dilute Nitride Lasers Grown by Molecular Beam Epitaxy

Julkaisu 1346 • Publication 1346

Tampere 2015

Tampereen teknillinen yliopisto. Julkaisu 1346
Tampere University of Technology. Publication 1346

Ville-Markus Korpijärvi

High-Power Dilute Nitride Lasers Grown by Molecular Beam Epitaxy

Thesis for the degree of Doctor of Science in Technology to be presented with due permission for public examination and criticism in Tietotalo Building, Auditorium TB103, at Tampere University of Technology, on the 27th of November 2015, at 12 noon.

Tampereen teknillinen yliopisto - Tampere University of Technology
Tampere 2015

ISBN 978-952-15-3629-8 (printed)
ISBN 978-952-15-3706-6 (PDF)
ISSN 1459-2045

Abstract

Semiconductor lasers are the most widely used type of lasers. This is due to many beneficial properties including compact size, wavelength coverage, and high efficiency. Different semiconductor laser architectures and gain materials can be used to fulfill requirements of different applications. Semiconductor gain materials are easy to tune to emit at desired wavelengths by changing the composition of the material and they can cover a wide range of wavelengths from ultra-violet to mid-infrared. Still, there are some important gaps in the wavelength coverage. Two of these gaps are located at ~600 nm and ~1200 nm, i.e. just below and above the wavelength coverage of traditional GaAs-based semiconductors. Especially the yellow–red (580–620 nm) part of the visible spectrum is important for applications in the fields of medicine, spectroscopy, astronomy and laser projection.

This work targeted to cover both of the mentioned wavelength gaps by using dilute nitride GaInNAsSb/GaAs quantum well gain material in novel high-power lasers. This thesis discusses especially the fabrication of the dilute nitride gain materials using plasma-assisted molecular beam epitaxy. Incorporating few percent of nitrogen into InGaAs/GaAs QWs can increase the upper wavelength limit of GaAs-based semiconductors up to 1550 nm by reducing band gap and lattice strain. Using this dilute nitride material system, we fabricated the first multi-watt semiconductor disk lasers (SDLs) emitting at 1180 nm and 1230 nm. The output powers exceeded 10 W at both wavelengths. Although frequency doubling is out of the scope of this thesis, it should be mentioned that these lasers emitted multi-watt powers also at the corresponding frequency doubled wavelengths of 590 nm and 615 nm. In addition, this thesis

reports a GaInNAsSb/GaAs SDL emitting at 1550 nm, which is the longest wavelength demonstrated for a monolithic GaAs-based SDL.

SDLs, unlike other semiconductor lasers, can emit high-powers (up to 100 W) in nearly diffraction-limited beams and can be efficiently frequency doubled. However, not all applications require multi-watt output powers but would rather benefit from smaller size of the laser source. For this reason we studied also another laser architecture, namely edge-emitting laser diodes. A single-mode laser with record-high output power of 340 mW at 1180 nm, corresponding to yellow (590 nm) frequency-doubled wavelength, was demonstrated. The laser showed also excellent temperature stability, which is important for miniaturization of frequency-doubled lasers.

The laser demonstrations could not have been realized without good understanding of the basic properties of the GaInNAs(Sb) gain material and its fabrication. Studies related to these aspects and to calibration of PA-MBE reactors form an important part of this thesis. Especially, effects of growth temperature and As/III beam equivalent pressure ratio on the grown semiconductor structures were studied.

In summary, this work is concerned with plasma-assisted molecular beam epitaxy of GaInNAsSb/GaAs gain materials. The fabricated materials were used in novel lasers emitting at wide range of technologically important wavelengths that are difficult to reach otherwise.

Acknowledgments

The research described in this thesis was carried out at the Optoelectronics Research Centre (ORC), Tampere University of Technology, during 2008-2015. It was supported by Graduate School in Electronics, Telecommunications and Automation (GETA), the European Commission, the Finnish Funding Agency for Technology and Innovation (TEKES), Academy of Finland, Emil Aaltonen Foundation, The Industrial Research Fund of Tampere University of Technology, Walter Ahlström Foundation, HPY Research Foundation and Ulla Tuominen Foundation.

It has been a great pleasure to work at ORC. ORC is an inspiring research community with talented people and state-of-the-art equipment. I wish to thank the whole staff of ORC. In particular, I would like to thank my supervisor Prof. Mircea Guina. He is maybe the busiest man I know, but still always enthusiastic about new ideas and possibilities. I admire that. I thank Prof. Emeritus Markus Pessa, the founder of ORC, for giving me the opportunity to work at ORC in the first place. I acknowledge the work of Dr. Pekka Savolainen, Director of ORC, for keeping the department running and in good shape.

Dr. Tomi Leinonen knows not only how lasers work but also how to make them. Thank you for guiding and sharing your knowledge. Excellent researchers Emmi Kantola and Jussi-Pekka Penttinen made up the SDL team and had their contribution to this thesis as well. Not to mention the invaluable contributions of Dr. Antti Härkönen and Dr. Jussi Rautiainen. These people enabled the presented SDL research. Thank you.

I wish to thank the diode laser team as well. In particular, I want to express my gratitude to Dr. Jukka Viheriälä for developing the clean room and the diode laser technology. Thank you for sharing your expertise. Mervi Koskinen, Mariia Bister and others are gratefully acknowledged for processing the diode lasers. I wish to thank Dr. Antti Laakso for laser simulations and modelling.

CER measurements of Dr. Robert Kudrawiec from Wroclaw University of Technology are also gratefully acknowledged.

I spend most of my ORC time doing MBE. Fortunately, I could share this time with great fellow growers. Arto Aho, Dr. Antti Tukiainen, Riku Isoaho and Pekka Malinen shared with me the ups and downs of GEN20 reactor. Thank you for everything. Before that, I learned the basics of MBE with Janne Puustinen as taught by Pietari Tuomisto, Janne Konttinen and Dr. Pekka Laukkanen. Thank you AsN team. Dr. Tomi Leinonen (It is my pleasure to thank him twice), Dr. Mika Saarinen, Dr. Soile Suomalainen, Dr. Jari Lyytikäinen and other senior growers have always been available and willing to help. I appreciate that. Thank you, Ilkka Hirvonen, for keeping the facilities in operation.

I wish to thank the peer support group–J-P, Andreas, Ville P., Miki, Emmi, Jonna, Teemu, Antti R., Jari, Arto and others–for cultivated discussions in Semipub and Kultainen Apina as well as for the various sports activities.

Finally, my deepest gratitude goes to my family and friends for all their support.

Vantaa, October 2015
Ville-Markus Korpijärvi

Contents

List of Publications

The following publications are included in this thesis as appendices. In the text they are referred to as [P1]–[P6].

[P1] V.-M. Korpijärvi, M. Guina, J. Puustinen, P. Tuomisto, J. Rautiainen, A. Härkönen, A. Tukiainen, O. Okhotnikov and M. Pessa, "MBE grown GaInNAs-based multi-Watt disk lasers," *Journal of Crystal Growth,* vol. 311, pp. 1868-1871, 2009.

[P2] R. Kudrawiec, V.-M. Korpijärvi, P. Poloczek, J. Misiewicz, P. Laukkanen, J. Pakarinen, M. Dumitrescu, M. Guina and M. Pessa, "The influence of As/III pressure ratio on nitrogen nearest-neighbor environments in as-grown GaInNAs quantum wells," *Applied Physics Letters,* vol. 95, pp. 261909-3, 2009.

[P3] V. Korpijärvi, T. Leinonen, J. Puustinen, A. Härkönen and M. D. Guina, "11 W single gain-chip dilute nitride disk laser emitting around 1180 nm," *Optics Express,* vol. 18, pp. 25633-25641, 2010.

[P4] V.-M. Korpijärvi, A. Aho, P. Laukkanen, A. Tukiainen, A. Laakso, M. Tuominen and M. Guina, "Study of nitrogen incorporation into GaInNAs: The role of growth temperature in molecular beam epitaxy," *Journal of Applied Physics,* vol. 112, pp. 023504-5, 2012.

[P5] V.-M. Korpijarvi, E. L. Kantola, T. Leinonen, R. Isoaho and M. Guina, "Monolithic GaInNAsSb/GaAs VECSEL Operating at 1550 nm," *IEEE Journal of Selected Topics in Quantum Electronics*, vol. 21, pp. 1-5, 2015.

[P6] V.-M. Korpijärvi, J. Viheriälä, M. Koskinen, A.T. Aho, M. Guina, “High-power temperature-stable GaInNAs DBR laser emitting at 1180 nm,” Submitted to *Optics Letters.*

Author's Contribution

The results presented in this thesis have been obtained by teamwork. The author's role in these joint efforts is described below.

For papers [P1, P3, P5], which concern semiconductor disk lasers, I carried out the epitaxy of the semiconductor gain structures with the help of some of the coauthors. I also worked on the passive optical design of these structures and analysis of the results. Laser processing and characterization were done mostly by the coauthors. I am the main author of these publications, wrote the first manuscript versions and coordinated the writing and publication processes.

For papers [P2, P4], which are related to epitaxy and material properties, I carried out the epitaxy of most of the samples and did the majority of the measurements excluding contactless electroreflectance (CER) measurements presented in [P2]. In the study presented in [P2], I coordinated the research and writing at Tampere University of Technology while CER measurements were carried out by an external collaborator who also took the main responsibility of writing the manuscript. I am the main author of paper [P4], wrote the first manuscript version and coordinated the study and the publication process.

I carried out the epitaxy and most of the laser characterization presented in paper [P6]. I am the main author of the paper [P6], wrote the first manuscript version and coordinated the publication process. Device processing and design were done by coauthors.

List of Abbreviations and Symbols

Abbreviations

AR	Antireflective or anti-reflection
ASE	Amplified spontaneous emission
BAC	Band anticrossing
BEP	Beam equivalent pressure
CBM	Conduction band minimum
CER	Contactless electroreflectance
CW	Continuous wave
DBR	Distributed Bragg reflector
DFB	Distributed feedback
DPSSL	Diode pumped solid-state laser
EDS	Energy dispersive spectroscopy
EEL	Edge-emitting laser
FWHM	Full width at half maximum
GM	Gain mirror
HR	Highly reflective
LIDAR	Light detection and ranging
MBE	Molecular beam epitaxy
M1	Folding mirror in an SDL cavity
NN	Nearest neighbor
OC	Output coupler

OCT	Optical coherence tomography
OPSL	Optically pumped semiconductor laser
PA-MBE	Plasma-assisted molecular beam epitaxy
PL	Photoluminescence
QD	Quantum dot
QW	Quantum well
RF	Radio frequency
RPG	Resonant periodic gain
RWG	Ridge waveguide
SDL	Semiconductor disk laser
SEM	Scanning electron microscope
SESAM	Semiconductor saturable absorber mirror
SRO	Short-range ordering
STED	Stimulated emission depletion
TEC	Thermoelectric cooling
TEM_{00}	Fundamental, lowest-order transverse electromagnetic mode
VBM	Valence band maximum
VCSEL	Vertical-cavity surface-emitting laser
VCSOA	Vertical cavity semiconductor optical amplifier
VECSEL	Vertical-external-cavity surface-emitting laser
XRD(004)	X-ray diffraction scan of (004) planes

Symbols, Greek Alphabet

$\Delta\lambda$	Wavelength band
$\Delta\lambda_{99\%}$	Wavelength band with over 99 % DBR reflectivity
λ_{SDL}	Design wavelength of an SDL
Γ_{cav}	Enhancement of longitudinal confinement factor due to semiconductor microcavity
Γ_l	Longitudinal confinement factor
Γ_{RPG}	Gain enhancement due to RPG

Symbols, other

a_{EN}	BAC model fitting parameter
a_V	BAC model fitting parameter
B	Fitting parameter in plasma model
b_{EN}	BAC model fitting parameter
b_V	BAC model fitting parameter
$C(InGaAs)$	Bowing parameter for calculating band gap, for example, of InGaAs
c_{EN}	BAC model fitting parameter
c_V	BAC model fitting parameter
D	Desorption constant
d_{active}	Thickness of active material
D_{SPOT}	Diameter of the pump spot
E	Electric field amplitude of the laser mode
$E_{\pm}$	Conduction band subbands as described by BAC model
E_a	Activation energy for adsorption
$E_{ad}D$	Fitting parameter in plasma model
E_d	Activation energy for desorption
$E_g(GaInNAs)$	Band gap energy of GaInNAs
E_M	Band gap of the host material in BAC model
E_N	Energy level of nitrogen atoms used in BAC model
F	Nitrogen flow
G	Geometrical factor describing the reactor configuration
$Ga_{1-x}In_xN_yAs_{1-y}$	Compound semiconductor with compositions x and y
GR_{III}	Group-III growth rate
$ijH(L)$	Calculated energies for optical transitions between ith heavy(light) hole and jth conduction subband
k	Boltzmann constant
L_{cavity}	Thickness of semiconductor microcavity
M^2	Beam quality factor
$N\text{-}In_mGa_{4-m}$	Nearest neighborhood of N with m In atoms and 4-m Ga atoms
n_H	Refractive index higher than n_L
n_L	Refractive index lower than n_H

P_{RF}	Radio frequency power
R	Reflectivity
R_d	Dissociation rate of nitrogen
R_{SP}	Resistance of the RF system
S	Nitrogen sticking coefficient
S and M	Labels for two CER resonances close to QW transition from the first electron level to the first heavy-hole level
T_g	Growth temperature
T_{OC}	Transmission of an output coupler
V	Hybridization strength in BAC model

Chapter 1

Introduction

Semiconductor lasers have become the most widely used type of lasers due to their many favorable properties such as compact size, highly efficient (electrical) pumping, high modulation speed, and wavelength versatility offered by different gain material systems. Applications of these sources range from material processing and optical pumping of solid state lasers to data storage (CDs, DVDs, and Blue-ray disks) and optical fiber communication. Metrology, various medical treatments, and spectroscopy are also important applications.

The usability of lasers in different applications depends on the basic parameters of the laser source. These parameters include wavelength, output power, efficiency, and beam quality. Various types of semiconductor lasers have been developed to meet the requirements of different applications. While market for high-power laser diodes is expected to grow fastest, most of the semiconductor lasers sold today are still low-power diode lasers [1].

In terms of emission geometry, diode lasers can be divided into two main groups which are edge-emitting lasers (EELs, Figure 1.1(a)) and vertical-cavity surface-emitting lasers (VCSELs, Figure 1.1(b)). EELs emit in the direction parallel and VCSELs in the direction perpendicular to semiconductor junctions. In addition to laser diodes, optically pumped semiconductor disk lasers (SDLs, Figure 1.1(c)) have been developed and commercialized. They are also known as vertical-external-cavity surface-emitting lasers (VECSELs) or optically pumped semiconductor lasers (OPSLs). It depends on the requirements of the application which type of laser shows best performance. VCSELs are extremely compact, have good beam quality and operate in single longitudinal mode but their output power (as single emitters) is limited to mW range. Edge-emitting lasers can emit higher powers but their beam quality is worse than that of

VCSELs. EELs have also longer cavities and are, thus, longitudinally multimode if not forced to lase in single mode. SDLs were developed for emitting high powers in high-quality beams [2, 3]. On the downside, SDLs loose to laser diodes in compactness and efficiency. In fact they usually include an EEL for pumping. On the other hand, their external cavity allows the use of intra-cavity components, such as nonlinear crystals for efficient frequency doubling [4] or wavelength selective components for single mode operation [5]. SDLs should not only be compared to laser diodes, but also to optically pumped thin disk solid-state lasers [6]: SDLs combine the power scaling capability of the disk laser architecture with wavelength versatility of semiconductor gain materials.

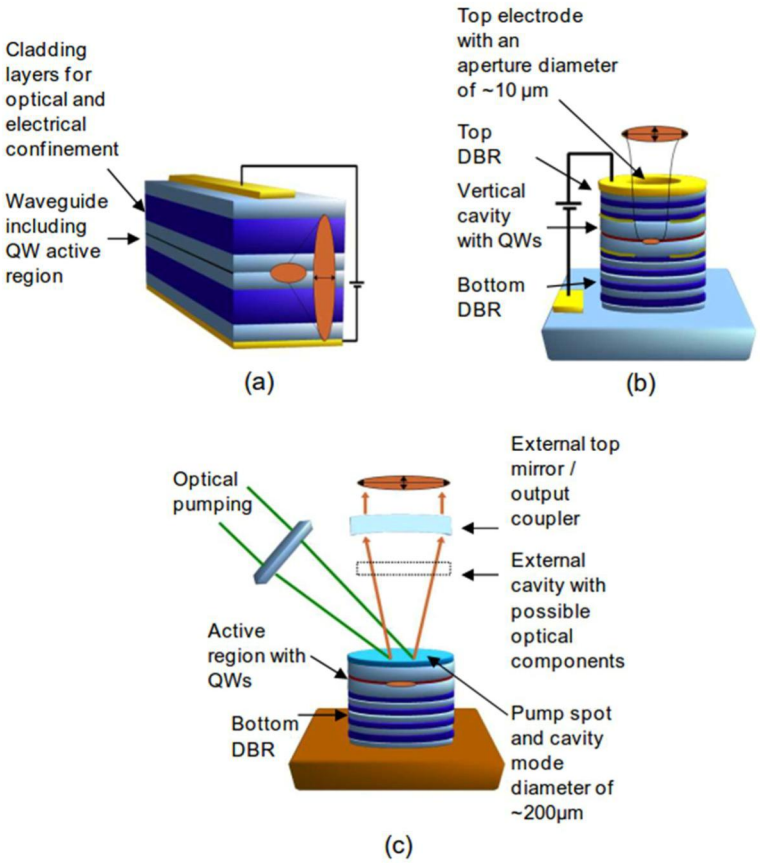

Figure 1.1. *Schematic representations of (a) an EEL, (b) a VCSEL, and (c) an SDL. In EELs the laser cavity is formed between cleaved facets and is parallel to semiconductor junctions whereas in VCSELs and SDLs the cavity is perpendicular to semiconductor layers. As compared to VCSELs, SDLs enable larger mode size with single transversal mode operation and introduction of nonlinear components into the external cavity.*

In addition to laser architecture, the most important design aspect of semiconductor lasers is the choice of gain material, which affects all the laser parameters and defines achievable wavelength range. In this thesis, EELs and SDLs were studied. We especially studied plasma-assisted molecular beam epitaxy of GaInNAs(Sb)/GaAs quantum well (QW) gain material and used this material in lasers for reaching new wavelength regions. This dilute nitride material shows great promise for frequency doubled lasers emitting at technologically important yellow–red wavelengths and complements InP technology at communication wavelength of 1.55 µm.

1.1 GaInNAsSb heterostructures

Nitrogen incorporated into GaInAs lattice reduces simultaneously both the band gap and lattice constant of the material. This unique effect reduces the compressive strain of GaInAs layers grown on GaAs and increases their emission wavelength [7, 8]. Without N, emission wavelength of GaInAs QWs is limited to below 1200 nm [9]. Thus, GaAs-based technology has a lack of long-wavelength lattice-matched gain materials. Longer wavelengths, especially fiber-optic communication wavelengths of 1.3 and 1.55 µm, have been traditionally covered by InP-based technology. Still, long-wavelength GaAs technology would have many benefits, including availability of AlAs/GaAs distributed Bragg reflector (DBR) mirrors that enable fabrication of monolithic vertical cavity lasers—a feature not available for InP technology. Large conduction band offset of GaInNAs/GaAs QWs is also expected to improve laser characteristics at high temperatures [7].

A major challenge in development of GaInNAs(Sb)/GaAs devices has been epitaxy of nitride layers with high enough quality. This can be understood by noting several differences between nitride epitaxy and standard GaAs epitaxy. First of all, GaInNAs is not thermodynamically stable material [10], and it has to be grown at low temperature in order to limit phase separation [11]. At low temperatures, relatively high nitrogen concentration at the growth front can be frozen in the bulk layers [11]. In addition to low growth temperature, phase separation can be limited by using Sb surfactant for limiting adatom diffusion length on the growth front [12, 13]. The longer is the emission wavelength, the higher are the required In and/or N compositions and the tendency for phase separation [14, 15]. Sb also incorporates to the crystal and decreases the band gap for longer emission wavelengths. In this dissertation Sb was used for fabrication of

longest wavelength SDL at 1.55 μm [P5]. Secondly, N_2 molecule is very stable and inert. For this reason, radio frequency plasma sources are used in epitaxy for nitrogen activation. These sources can damage growing crystals by generating flux of energetic ions, which should be removed by plasma source design and deflection plates [16, 17].

Low-temperature growth, nitrogen incorporation and use of plasma source create defects in the GaInNAs(Sb) lattice. N induces also short-range ordering (SRO) in the nearest neighborhood of nitrogen atoms. In order to remove the defects, post-growth annealing is routinely carried out for GaInNAs(Sb) device structures. Annealing treatment reduces the rate of nonradiative recombination and can improve photoluminescence intensity by orders of magnitude. Improvement is typically accompanied by a blueshift whose origin and amount depend on the growth and annealing conditions [18-20]. The importance of annealing for GaInNAs(Sb) devices is reflected in the large number of related research. Studies connecting growth and annealing conditions and SRO form part of this thesis as well [P2, P4].

1.2 Why dilute nitride lasers?

Combination of SDLs' high power, high beam quality and capability of highly efficient intra-cavity frequency doubling to visible wavelengths makes them very useful for many applications. Blue and green frequency doubled SDLs were developed first based on GaInAs/GaAs QWs [21, 22]. However, reaching yellow–red wavelengths using this gain material is increasingly difficult because of high lattice strain, and the longest wavelengths reached using this material system correspond to 1180 nm [23, 24]. Yellow-red spectral range is not difficult to reach only for frequency doubled SDLs, but also for lasers emitting directly at visible wavelengths. Only few demonstrations of direct lasers at these wavelengths have been published [25, 26]. In terms of performance, SDLs compete also with diode-pumped solid state lasers and fibre lasers which are both capable of reaching visible wavelengths by nonlinear frequency conversion [27, 28]. As compared to these types of lasers, semiconductor lasers benefit from simple architecture, relaxed requirements for pump lasers, high-efficiency and wavelength tunability. For these reasons, we developed GaInNAs/GaAs SDL gain structures emitting at 1.18 μm [P3] and 1.22–1.24 μm [P1] corresponding to frequency doubled visible wavelengths at ~590 nm [29] and ~615 nm [30-32]. Visible SDLs are attractive to many important applications. Yellow SDLs can

be used for creating laser guide stars for adaptive optics of earth-based telescopes [33, 34], stimulated emission depletion (STED) microscopy [35], eye surgery [36], flow cytometry [37] and treatment of vascular lesions (port wine stains) [38]. Red SDLs (at λ<630 nm, where direct emitting diode lasers do not work well) with high output power could be used in RGB laser projectors [39, 40] and photodynamic therapy [41, 42].

After demonstration of the visible frequency doubled SDLs, we pushed the limits of dilute nitride material system further to demonstrate the first monolithic GaAs-based SDL at 1.55 µm [P5]. This was achieved by using tensile strained GaNAs for compensating the compressive strain of the QWs and reactive Sb surfactant for improving material quality. 1.55 µm is an important fiber-optic communications wavelength but also an eye-safe wavelength with many applications outside the field of communications [43-46].

Not all applications require high output power in extremely high quality beams, but would rather benefit from smaller device size. Current GaAs-based laser diode technology is limited to wavelengths longer than 630 nm [47, 48] while GaN-based laser diode technology emitting at the yellow–red part of the spectrum is still relatively immature [25]. Thus, frequency doubling has to be used for yellow laser diodes. Although required 1180 nm EELs have been fabricated based on highly strained InGaAs/GaAs QWs [9, 49, 50], nitrogen incorporation improves electron confinement of the QWs and thus improves lasing characteristics at high temperatures. Improved temperature stability provided by GaInNAs/GaAs lasers would be important for miniaturization of frequency-doubled lasers, which is currently limited by thermal management [51]. If the frequency doubling crystal requires elevated temperatures for phase matching [51] or wavelength tuning [52], it would be beneficial to have laser diodes tolerating the elevated temperatures as well. Furthermore, lattice strain is reduced by nitrogen incorporation, which relaxes strain related design constraints. Because of lower lattice strain, increasing the number of QWs for further improvement of temperature characteristics [53] should be easier with GaInNAs QWs than it is with InGaAs QWs. This thesis includes a demonstration of a temperature-stable single-mode GaInNAs/GaAs distributed Bragg reflector (DBR) laser emitting at 1180 nm [P6].

1.3 Outline

This thesis is organized in five chapters. Chapter 2 introduces the basic properties and fabrication related aspects of GaInNAs. Especially it concerns plasma-assisted molecular beam epitaxy (PA-MBE) of GaInNAs(Sb). Band anticrossing (BAC) model for modelling GaInNAs band gap is described, and a new modified version is introduced for GaInNAsSb (Chapter 2.1) [54]. Effects of nitrogen on the material quality and related short-range ordering (SRO) are discussed in Chapter 2.2. Both the material quality and SRO can be modified after growth by annealing, which is then discussed in Chapter 2.3. Chapter 2.4 discusses three studies related directly to PA-MBE of GaInNAs: The studies concerned calibration of a radio frequency (RF) plasma source [55], influence of growth temperature on nitrogen incorporation [P4] and effect of As/III beam equivalent pressure ratio on short-range ordering of GaInNAs [P2].

Chapter 3 includes the studies concerning GaInNAs(Sb) SDLs. This chapter begins with a short description of motivation behind the work and also discusses pros and cons of alternative semiconductor gain material systems. Basic design aspects of semiconductor disk laser technology are discussed in Chapter 3.1. This is followed by a short description of fabrication and characterization of dilute nitride semiconductor disk lasers emitting at 1.18 µm (Chapter 3.2)[P3], 1.22–1.24 µm (Chapter 3.3)[P1] and 1.55 µm (Chapter 3.4)[P5].

Chapter 4 reports the fabrication and characterization of single-mode GaInNAs DBR-EEL emitting at 1.18 µm [P6]. In addition to the DBR laser, temperature characteristics of the gain material are discussed based on broad area edge-emitting laser characterization. Chapter 5 concludes this thesis with a short summary of results and gives an outlook for future research.

Chapter 2

Dilute Nitride Semiconductors

This Chapter reviews the basic properties of GaInNAs(Sb). In addition, some of the challenges related to this material are discussed. A simple band anticrossing model for band gap of GaInNAsSb is also described [54]. Emphasis is put on GaInNAs(Sb) growth by plasma-assisted molecular beam epitaxy (PA-MBE). Chapter 2.4 summarizes selected studies carried out in the framework of this dissertation and published in [P2, P4] and [55].

2.1 Effect of Nitrogen on the Band Structure

Rather than increasing towards GaN band gap value (E_g = 3.24 eV at a = 4.5 Å [56]), GaNAs band gap decreases strongly when small amount of N is added to GaAs. Thus it is possible to decrease both the band gap and the lattice constant by incorporating N into GaAs. This opens new opportunities for GaAs-based technology. For example, the compressive strain of GaInAs on GaAs can be compensated by N incorporation which simultaneously decreases the band gap and thus enables emission at wavelengths up to 1.55 µm. $Ga_{1-x}In_xN_yAs_{1-y}$ with $x \approx 2.8y$ is lattice matched to GaAs whereas compositions with $x > 2.8y$ and $x < 2.8y$ give compressive and tensile strained GaInNAs on GaAs, respectively. Room temperature (T = 300 K) band gap values and lattice constants are used throughout this chapter.

The band gap of GaNAs is poorly described by the normal quadratic approximation,

$$E_g(GaN(y)As(1-y)) = (1-y)E_g(GaAs)+yE_g(GaN)-y(1-y)C_{GaNAs}, \quad (2.1)$$

which includes a single composition-independent bowing parameter C_{GaNAs}. Instead, a so-called band anti-crossing (BAC) model can be used in describing the conduction band structure and

the related electron effective mass. The anomalous effect of N on the band gap is due to small size and large electronegativity of N atoms (radius ~ 0.068 Å, electronegativity ~ 3.04 in units of Pauling scale) as compared to As atoms (radius ~ 0.121 Å, electronegativity ~ 2.18). Such impurity atoms create localized energy levels close to the conduction band edge and, as a result, modify the conduction band structure of the alloy. BAC model describes this interaction. [56-59]

In GaAs, N atoms create a localized energy level, E_N, which lies about 0.25 eV above the conduction band edge. If N composition is increased to dilute regime i.e. to $y \approx 1\%$, the band structure is drastically modified. According to BAC model, the anti-crossing interaction between the band of localized N states and the conduction band of the host crystal leads to splitting of the conduction band into two sub-bands E_+ and E_-, which are located above and below, respectively, the band of N states and the conduction band edge of the host crystal. The band gap is now formed between the valence band maximum and the E_- band edge and is effectively decreased with increasing N concentration as the anti-crossing interaction pushes the E_- down in energy. According to BAC model, the dispersions of the two new sub-bands can be written as:

$$E_{\pm}(k) \quad \frac{1}{2}\left[\left(E_M(\mathbf{k})+E_N\right)\pm\sqrt{\left(E_M(\mathbf{k})-E_N\right)^2+4V^2y}\right] \tag{2.2}$$

where $E_M(k)$ is the conduction band dispersion of the host crystal (e.g. GaAs, GaInAs or GaInAsSb), E_N is the energy of the nitrogen band, V describes the hybridization strength, and y is the N composition for example in $Ga_{1-x}In_xN_yAs_{1-y}$. In addition to formation of the two new sub-bands and decrease of the fundamental band gap, Equation 2.2 describes reduction of the curvature of the E_- band, which corresponds to increase of effective electron mass. From the device engineer's point of view, BAC model can be thought of as a parameterization method whose two parameters, E_N and V, should be fitted with experimental data.

Figure 2.1 shows $Ga_{1-x}In_xN_yAs_{1-y}$ band gap for y = 1%, 2%, 3% and 4 % calculated with parameter values taken from references [56, 60]. It was assumed in the band gap calculation that only effect of N on the band gap value is by the changed conduction band structure [61, 62]. Lattice constants were calculated using linear interpolation between lattice constants of the binaries, also known as Vegard's law. It is also noted that care should be taken when BAC model is used for describing temperature or pressure (strain) dependent phenomena or when comparing materials with different growth and annealing conditions [61-63]. We have found

[64] that calculated values of Figure 2.1 are in good agreement with the ones measured for our annealed, nearly lattice-matched GaInNAs bulk samples. However, separate parameter values should be used for un-annealed samples.

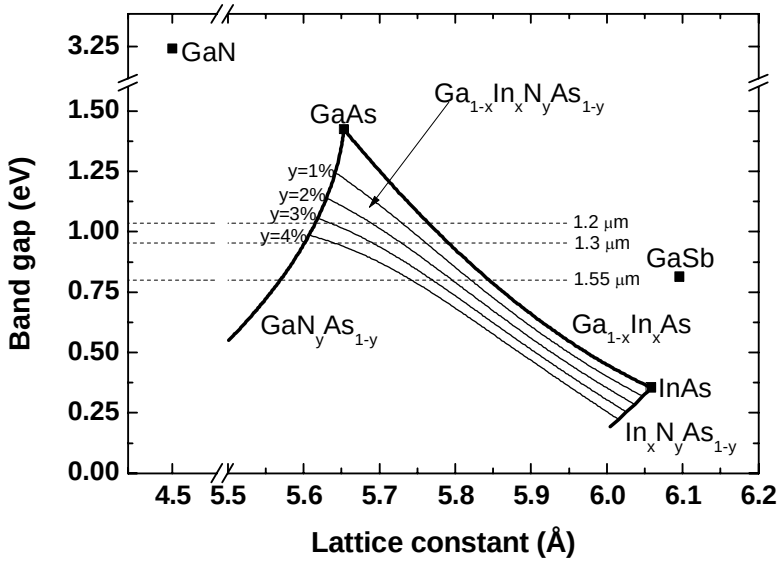

Figure 2.1. *Band gap and lattice constant of dilute nitride GaInNAs at room temperature. Important wavelengths are marked with dashed lines. Band gap and lattice constant values are calculated with parameters taken from references* [56, 60].

The use of antimony as an incorporating surfactant improves the optical quality of the QWs, widens the usable growth parameter window and also decreases the band gap for emission at longer wavelengths [13, 65]. Especially the growth temperature can be increased when Sb is used during growth, because addition of Sb allows avoiding phase separation. This is especially important for longer emission wavelengths where high In and N compositions are required. Many studies have been carried out and published on the epitaxy and incorporation dependencies of elements of GaInNAsSb [12, 66, 67] as well as on annealing and short-range ordering of GaInNAsSb [68]. However, a simple band gap model for GaInNAsSb has been lacking. For GaNAsSb, double-BAC model describing effect of N on the conduction band and antimony on the valence band has been previously reported [69].

Major obstacle for structuring the GaInNAsSb band gap model, has been the difficulty of measuring the composition of this five-element compound. Here, composition of the MBE-grown bulk GaInNAsSb crystals was determined by combining x-ray diffraction measurements with scanning electron microscope (SEM) measurements utilizing energy dispersive spectroscopy (EDS), as discussed in detail in reference [54]. All samples were annealed until their blueshift saturated in order to minimize the effect of short range ordering on the band gap value, which was measured by measuring the PL peak wavelength. With these composition and band gap measurements, we could show that standard band anti-crossing (BAC) model (Equation 2.2) can be utilized for GaInNAsSb if GaInAsSb is used in the model as a host material.

The band gaps of ternary GaInAs, GaInSb, GaAsSb and InAsSb were calculated by the second order polynomial (Equation 2.1) and using band gap values and bowing factors given in [60, 70]. Band gap of quaternary GaInAsSb was calculated by linear interpolation between ternary constituents [70] and was used as the host material value E_M for calculating $Ga_{1-x}In_xN_yAs_{1-y-z}Sb_z$ band gap using the BAC model (Equation 2.2). Energy of the N band, E_N, and hybridization strength V of BAC model were assumed to be independent of Sb composition. This is suggested also by the fact that Sb incorporation affects mainly the valence band while dilute nitride BAC model deals with changes of the conduction band structure [69, 71]. Thus, we treated these parameters as second order polynomial functions of In composition x,

$$E_N(x) \quad a_{En}(1-x) + b_{En}x - c_{En}x(1-x) \text{ and} \tag{2.3}$$

$$V(x) \quad a_V(1-x) + b_V x - c_V x(1-x), \tag{2.4}$$

and made only a slight change to a_V as compared to parameters suggested by Vurgaftman et al. [56] (Table 2.1). This change was made for improved fit with the measured band gap and composition values.

Table 2.1. *BAC model parameters used in this work for GaInNAsSb and the same parameters for GaInNAs from reference* [56].

BAC model parameters	a_{EN} (eV)	b_{EN} (eV)	c_{EN} (eV)	a_V (eV)	b_V (eV)	c_V (eV)
This work	1.65	1.44	0.38	2.55	2.00	3.50
Vurgaftman	1.65	1.44	0.38	2.70	2.00	3.50

With Equations 2.1–2.4 and parameters of Table 2.1, we could achieve good fit between calculated and measured band gap values as shown in Figure 2.2. Average deviation between measured and calculated values is only 20 meV. We note that for example short range ordering can cause 0–50 meV changes to band gap (although this effect was minimized in this work by annealing) and that band gap values measured by PL peak wavelength are systematically too large by 10–20 meV. There were no systematic errors with changing In, Sb or N compositions and all data points could be calculated with better than 95 % accuracy. In summary, we showed that only slightly modified BAC model can give accurate values for GaInNAsSb band gap.

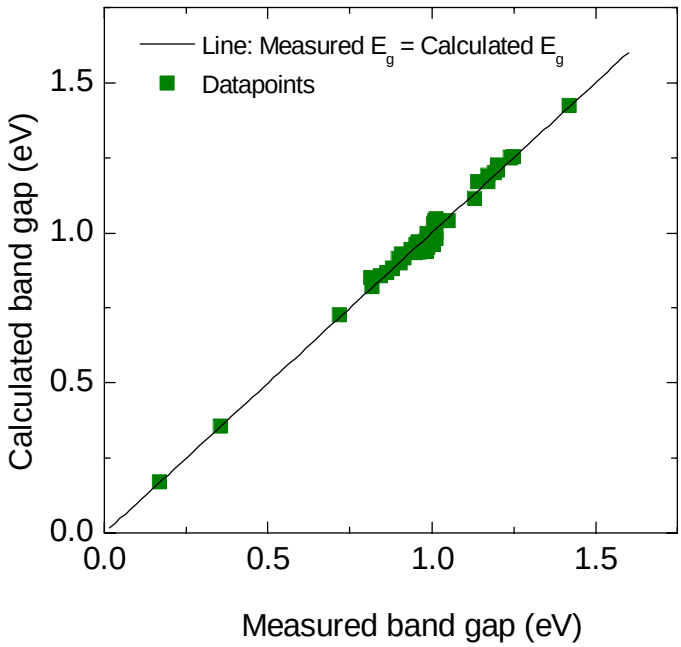

Figure 2.2. *Calculated band gap values plotted with those measured by PL (peak wavelength). Band gaps of end point binaries are also marked on the figure to show boundary conditions. Line indicates perfect match between calculated and measured values.* [54]

2.2 Effect of Nitrogen on Material Quality

Besides giving dilute nitride materials their interesting and beneficial properties, the large differences in the size and electronegativity of the N and As atoms as well as the different crystal structures of the endpoint ternaries (cubic fcc for GaInAs and hexagonal wurtzite for GaInN) complicate the fabrication of high quality GaInNAs. Particularly, they result in a large miscibility gap in the alloys. The solubility of N into Ga(In)As at thermal equilibrium is only a small fraction of a percent [10]. Incorporating higher amounts of N can cause clustering and phase separation [15], which have detrimental effect on the optical quality of the material. However, these problems can be avoided; single phase GaInNAs can be grown at kinetically limited conditions.

In the case of MBE, suitable growth conditions are created by using low growth temperature. The explanation for the high N compositions reported by many growers [72, 73] probably lies in the surface kinetics of the growing layer rather than in the bulk thermodynamics [11, 74-76]. Once the relatively high surface concentration of N is covered by the over grown layers, it will be frozen in due to the low diffusion of N atoms at low temperatures. This leads to far higher solubility than expected by bulk thermodynamic considerations. Thus, $GaInN_yAs_{1-y}$ layers with relatively high N content (y~10%) can be grown by MBE, but all layers that contain more than a negligible amount of N are metastable.

GaInNAs epitaxy is sensitive to growth conditions and surface reconstruction. Whereas the upper limit for the growth temperature of GaInNAs is set by the tendency towards phase separation, the lower limit is set by the formation of crystal point defects. These defects include As antisites, Ga vacancies, and As interstitials, which are observed also in GaAs grown at low temperature and under As-rich conditions [73], and a wide variety of N related defects [77]. Suitable growth temperature for GaInNAs is thus found as a compromise between phase separation at high temperatures and point defect formation at low temperatures [12]. Increasing either In or N content of the growing crystal increases the tendency of phase separation and 3-dimensional growth and, thus, decreases the optimum growth temperature [15].

In GaInNAs five different N-centered nearest neighbor (NN) environments can coexist. These can be labeled as $N\text{-}In_mGa_{4-m}$, where $0 \leq m \leq 4$ is the number of In atoms surrounding an N atom. This gives rise to short range ordering (SRO) or, in other words, nearest neighbor (NN)

effects. The question then is, what are the relative numbers of bonds between different kinds of atoms or, in other words, relative numbers of different NN environments and how the different configurations affect the optical properties of the crystal. [78] In GaInNAs the effect of SRO on the band gap is expected theoretically to be large due to the resonance between the states created by N atoms and the conduction band edge of the host crystal. Klar et al. were the first to show both theoretically and by photoreflectance measurements that five unequal band gap values corresponding to different NN environments can exist in a sample with a fixed composition (x,y) [79]. Also Kim et al. predicted this phenomenon theoretically [78]. Both these papers predict that energy of the N related E_N band and thus the band gap energy increases when the number of NN In atoms is increased from m = 0 to m = 4. In addition, the difference in the band gap values corresponding to different NN environments ($\triangle$=Eg(m=4)-Eg(m=0)) was calculated to increase with increasing amount of N or In in the crystal [79]. Klar et al. calculated that for $Ga_{0.67}In_{0.33}N_{0.01}As_{0.99}$ the difference in band gaps corresponding to m = 4 and m = 0 is about 50 meV and that the five band gap values corresponding to different NN configurations are evenly spread over this range [79]. Duboz et al. have suggested a simple correction to the BAC model for taking into account the effect of different NN configurations [80].

Lordi et al. showed that for a totally random $Ga_{0.7}In_{0.3}N_yAs_{1-y}$ alloy the most probable NN configuration corresponds to m = 1 [81] and found that their as-grown material was dominated by this configuration. Also Klar et al. reported that their as-grown material consisted mainly of m = 0 and m = 1 configurations [79]. This is, however, in contradiction with calculations showing that the crystal energy of a bulk material is minimized when m = 3 [78, 81]. This contradiction is generally thought to arise from an interplay between crystals elastic strain energy and chemical bonding energy [76, 79, 81]. The chemical bond energies are often estimated from the cohesive energies of the binaries which show the following trend: $E_{GaN}>E_{InN}>E_{GaAs}>E_{InAs}$. Similarly the elastic strain energy can be estimated from the lattice constants of the binaries which show the following trend: $a_{InAs}>a_{GaAs}>a_{InN}>a_{GaN}$. Thus, Ga-N (small atom – small atom) bonds are favored in terms of chemical bonding energy and In-N (large atom – small atom) bonds in terms of elastic strain energy. The increased number of Ga-N NN environments as compared to thermodynamically preferred m = 3 configuration is thought to arise from the domination of chemical bonding aspects over the elastic strain aspects at the growing surface where the elastic strain is relaxed more easily due to lower coordination

of the surface atoms [76, 79, 81]. Once the surface is grown over, the atomic configuration enriched with Ga-N bonds is kinetically frozen in due to low diffusivity of N atoms. In the bulk material, where atoms have higher coordination and the strain is not so easily relaxed, the elastic strain energy plays more important role in the total energy and a higher number of In-N bonds would be preferred. The number of In-N bonds can be increased towards m = 3 by providing sufficient amount of thermal energy for atomic diffusion that enables the reorganization of NN environments. The effect of thermal treatment, usually called annealing, on GaInNAs is discussed in the next Chapter 2.3.

Albrecht et al. also considered the effects of interplay between chemical bonding energy and elastic strain energy on the compositional dependence between In and N. Analogously to NN effects, they found that In-N interaction is repulsive at the surface and attractive in the bulk. Thus, increasing the In concentration can be expected to lower N solubility which is highly controlled by surface kinetics. Experimental support for this phenomenon has been reported by many groups [76, 82, 83], although contradictive reports can also be found [84]. It has been shown that the In segregation to the growth front is further increased with increasing N content [14, 82].

Interesting consequence from the above growth and surface considerations is that controlling surface conditions by changing growth parameters should enable control of NN configurations and N content [76]. Indeed, our results show that NN configuration can be controlled by As pressure during MBE growth (see Chapter 2.4.3) [P2] and N composition by growth temperature (see Chapter 2.4.2) [P4].

2.3 Effect of Annealing on Material Properties

Dilute nitride GaInNAs usually suffers from low luminescence efficiency due to non-radiative defects induced by low temperature growth, N incorporation, and ions from the plasma source. Additional reason for poor luminescence might lie behind the high number of Ga-N bonds in as-grown materials [68]. Thermal annealing has been shown to provide increase in the luminescence efficiency (photoluminescence intensity improvement by an order of magnitude is not uncommon) but is usually accompanied by large (several tens of nanometers) blueshift of the emission wavelength [18].

Mainly two methods are used for annealing the samples: so called in-situ annealing, which is performed in the same reactor as the growth itself, or post-growth rapid thermal annealing (RTA) performed in a separate furnace. In both cases, the surface has to be protected against As desorption and the related degradation of the surface quality. In the case of in-situ annealing this is done by applying an As overpressure on the surface [85, 86]. In the case of RTA the sample is covered with another GaAs wafer, enclosed in a box made of GaAs wafers [87] or capped with a dielectric film deposited on the surface [88, 89]. Typical annealing temperatures range from 580 °C (the growth temperature of GaAs) to 900 °C.

Whereas the increase in luminescence efficiency has been generally attributed to healing of non-radiative defects and improvement of interfacial quality of QWs, the blueshift behavior has been under keen investigation and several mechanisms have been suggested to cause it: change in nitrogen NN environment from gallium rich to indium rich [68, 79], N diffusion inside the QW, N-As interdiffusion across the QW boundaries, In diffusion inside the QWs, In-Ga interdiffusion across the QW boundaries, and healing of localized band gap variations due to point defects and N related clusters. For a review of different blueshift mechanisms, see references [18, 77] and references therein. Annealing behavior of GaInNAs varies considerably with changing growth and annealing conditions. Different growth conditions lead to materials with different defect population and SRO which affect annealing behavior of the material. Growth dependent SRO, especially, affects the blueshift of the material [P2, P4]. Materials used for surface protection during annealing have large effect on the results as well. For example, SiO2 capping of the sample surface has been shown to create Ga vacancy defects enhancing In-Ga interdiffusion [87].

Our practical knowledge is that when annealed at moderate temperatures around 700 °C for moderate times using GaAs box or the in-situ method, the blueshift is mostly explained by nitrogen NN reconfiguration from Ga-rich to In-rich [87]. At higher temperatures or when dielectric coatings are deposited at the surface, In-Ga interdiffusion becomes one of the main blueshift mechanisms. The surface damage and thermal etching of the sample surface are also more severe at elevated annealing temperatures. Still it should be noted that due to attractive interaction between N and In atoms in the bulk material [76], diffusion is suppressed in GaInNAs as compared to GaInAs [87]. GaNAs strain compensating and GaInNAs strain mediating layers around the QWs can be used to further suppress In or N outdiffusion [90-92].

One of the main advantages of performing annealing at relatively low temperatures around 700 °C is that the blueshift related to NN rearrangement (and potentially to defect annihilation) is saturable, whereas diffusion, which is mainly observed at higher temperatures, causes continuous blueshift. A well-defined saturable blueshift is highly desirable for device growths where the luminescence wavelength needs to be accurately controlled. In addition to intentional annealing, so called self-annealing, taking place during the growth of layers above the QWs, should be taken into account [19, 20].

2.4 Studies on Plasma-assisted Molecular Beam Epitaxy of GaInNAs

2.4.1 Radio Frequency Plasma Source Technology

N_2 molecules are extremely inert due to strong triple bond between their atoms. Thus, more reactive forms of N must be generated in order to incorporate N atoms into the crystal lattice. In this work a radio frequency (RF) plasma sources (Veeco UNI-BULB) were used for creating the active N. The sources consist of PBN crucible or a “bulb” which is surrounded by a hollow RF coil. Water was circulated inside the coil for cooling the cell. RF power at a frequency of 13.56 MHz and adjustable in the range of 0–500 W was supplied into the coil for generating the plasma inside the bulb. An automatic impedance matching network was used to ensure that all the fed RF power was converted into plasma power. Nitrogen (initially 99.9999% pure) was fed to the bulb through stainless steel tubing with filters for additional purification. A small window was attached to the feeding tube for visually monitoring the rear side of the plasma. Monitoring was however hindered because there was no unrestricted line of sight to the plasma itself. Instead, plasma was seen through the backside of the PBN bulb, which absorbed the UV wavelengths of the plasma emission. The N flow was controlled with a mass flow controller. Typically used flow values were in the range of 0.15–1.0 sccm. Nitrogen was extracted from the bulb through a PBN aperture plate with many small holes designed to direct the plasma uniformly on the sample and to increase pressure inside the bulb.

With the automated impedance matching, the two parameters controlling the plasma operation are RF power and N_2 flow. Not all possible flow-power combinations can produce stable

plasma. The pressure should be high enough to allow for sufficient collision rate between electrons and molecules. On the other hand, if pressure is too high particles cannot gain sufficient energy between successive collisions. The higher the pressure, the higher is the RF power required to provide this sufficient energy. The N plasma consists mainly of the following forms of N, with decreasing concentration [93, 94]: neutral molecules (N_2), excited molecular radicals (N_2*), neutral atoms (N), molecular ions (N_2+), and atomic ions (N+). The neutral atoms N and molecular radicals N_2* incorporate into the crystal lattice whereas the ions N_2^+ and N^+ damage the crystal [16, 77]. The ions can be deflected by generating an electric field between the deflector plates installed in front of the aperture plate. This possibility was available in Veeco GEN20 but not in VG V80H reactor. The standard operating conditions generally used and reported are those with relatively low power and high flow but so that plasma is stable against changes in vacuum environment and shutter movement. These parameters result in high pressure inside the bulb and relatively low particle energies, which translate into smaller ion concentration and energy, i.e. less damage on the crystal. The small aperture further increases the bulb pressure and decreases the ion concentration.

In both reactors used in this work, plasma source was enclosed into a vacuum chamber, which was separated from the growth chamber by a gate valve and pumped differentially by a turbomolecular pump. This allowed igniting and stabilizing the plasma without any effect on the growing crystal. Also the plasma source contamination with As and other species in the growth chamber was minimized. The gate valve was usually opened only a few seconds before the QW growth and closed immediately after so that unintentional N incorporation and damage was minimized.

Information about the plasma condition can be gained by monitoring its optical emission spectrum. Most importantly, this provides an insight into the relative concentrations of the active N species in the bulb and especially into the way these concentrations depend on the plasma source parameters [95-99]. The relative concentrations of N and N_2*, as determined from the intensities of the corresponding peaks in the plasma emission spectra, have been connected to N incorporation rate into both GaN [98, 99] and dilute nitride [95] crystals. Still, only relative and qualitative information about the amount of different particles in the plasma can be extracted from the emission spectra.

A typical optical emission spectrum of the GEN20 plasma source recorded through viewport is shown in Figure 2.3. This spectrum was measured for plasma operating with 250W RF power and 0.15 sccm N_2 flow. The spectrum consists of a number of broad bands (570–610 nm, 610–690 nm, 710–780 nm) originating from transitions between different vibrational states of excited molecular radicals N_2*. The molecular peaks are superimposed by atomic emission multiplets centered at about 745, 821, 866, and 942 nm. Absorption of ultra violet radiation by the PBN bulb hindered the possibility of observing the ion related emission peaks.[95, 96, 98]

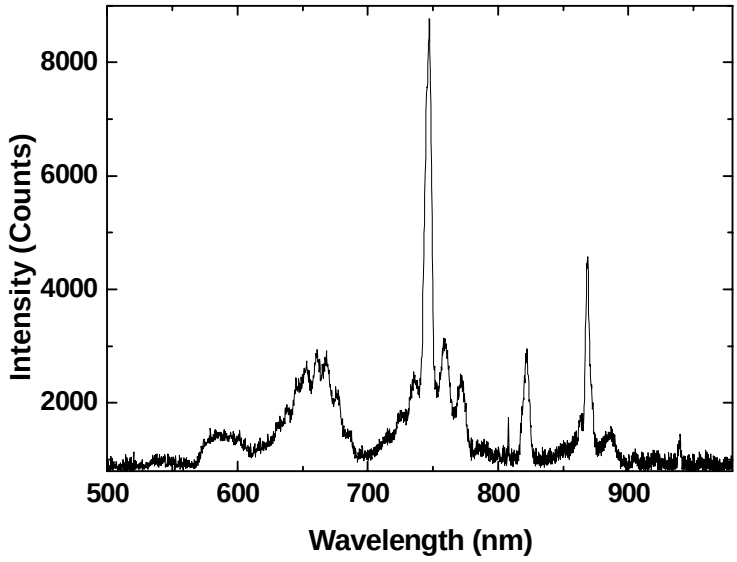

Figure 2.3. *A typical plasma emission spectrum recorded from plasma operating with 0.15 sccm N_2 flow and 250 W RF power.*

Here the intensities of atomic (N) and molecular radical (N_2*) peaks at 747 and 757 nm, respectively, were monitored as suggested in reference [95]. Figure 2.4 shows the peak intensities for different RF powers as a function of N_2 flow. It is seen that whereas the molecular peak intensity starts to saturate only at the highest measured flow values, the atomic peak intensities saturate and even decrease after 0.3 sccm. Qualitative explanation for the decrease in atomic peak intensity could be increased recombination of N atoms into molecules at higher pressures. Although not shown here, it should be mentioned that relative change in peak intensity is higher for atomic peak than for molecular peak with changing RF power.

Atomic peak intensity also shows less saturation with increasing RF power than does the molecular peak.

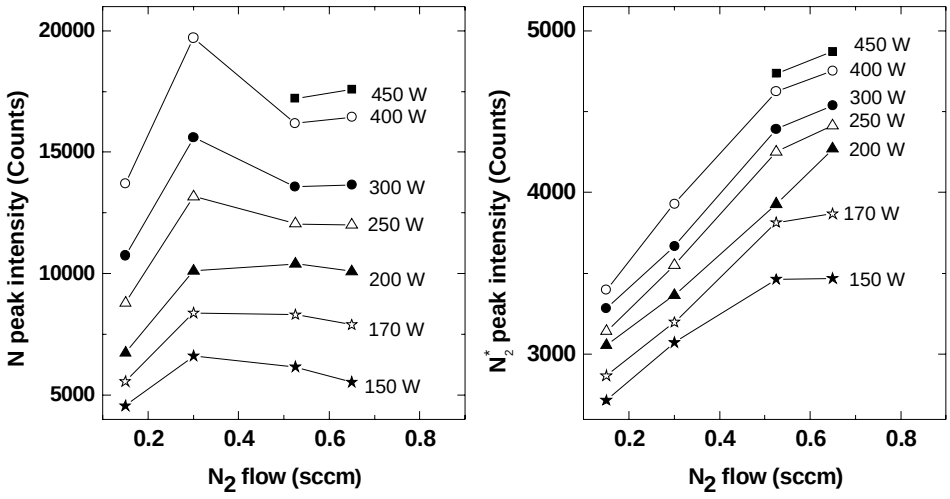

Figure 2.4. *Atomic peak intensity of the plasma emission for different RF powers as function of N_2 flow (on the left) and the corresponding molecular radical peak intensities (on the right).*

These observations can be linked to growth kinetics and N composition in GaInNAs by taking a look at a set of closely lattice matched $GaIn_{0.079}NAs$ samples with variable plasma parameters. Indium composition was determined by x-ray diffraction (XRD(004)) scan of a separate GaInAs calibration sample. Nitrogen concentration of GaInNAs samples was then determined also from XRD(004) rocking curves by assuming constant In content with changing plasma parameters. Nitrogen concentrations determined from these samples are shown in Figure 2.5 as a function of N_2 flow. Nitrogen content and thus its incorporation rate into the crystal are seen to saturate with increasing N_2 flow. Similar saturation was observed also for the molecular radical peak intensity. However, no decrease in incorporation is detected as it was detected for the atomic peak intensity. Because the peak intensities are thought to be directly proportional to the densities of active N particles in the plasma, it can be concluded that in addition to atomic N, there must be another form of N incorporating into the crystal, especially at high values of N_2 flow. Most likely this is the N_2^* radical [95, 97-99].

The same calibration sample set (Figure 2.5) was used for creating a model for incorporation of RF plasma activated N as described in reference [55]. The semi-empirical model predicts the N

composition as a function of the primary resistance of the radio frequency system, N_2 gas flow, RF power and group-III growth rate. The expression for N composition in the crystal is given according to the model by [55]:

$$N\ (\%) = \frac{SGR_d}{GR_{III}} = \frac{B}{GR_{III}} F(R_{sp}P_{RF})^{1/2} \exp\left(\frac{-E_{ad}D}{R_{sp}P_{RF}}\right) \quad (2.5)$$

Here G is geometrical factor describing the reactor and plasma source configuration, S is N sticking coefficient ($S \leq 1$ and depends on growth conditions), R_d is dissociation rate of N and GR_{III} is the group-III growth rate. P_{RF} and F denote radio frequency power and N_2 flow, respectively. R_{SP} is the resistance of the RF system, which can be determined from the RF power–voltage data and is nearly independent of the RF power but depends on the nitrogen flow. B and $E_{ad}D$ are fitting parameters. They are assumed to be independent of the nitrogen flow but were found to depend exponentially on the RF power. The model (Equation 2.5) could be used for Ga(In)NAs grown by two different MBE reactors with maximum deviation of less than 6 % from the experimental compositions [55].

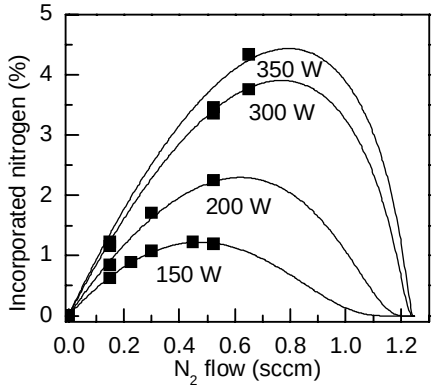

Figure 2.5. *Nitrogen content as determined by XRD measurements of GaInNAs bulk samples. For calibration purposes, N content is normalized to correspond to 1 μm/h growth rate by dividing it by the actual growth rate (0.75 μm/h). Figure shows also plots of Equation 2.5 fitted to the measured data points.* [55]

To test the above calibration with GaInNAs/GaAs QWs, three samples were grown with variable plasma settings so that the N content remained constant according to the calibration of Figure 2.5 and Equation 2.5. Each sample comprised two $GaIn_{0.25}N_{0.76}As$/GaAs QWs separated by 10 nm of GaAs. The PL spectra measured from these samples are shown in Figure 2.6. The

PL peak wavelength of all the samples is almost exactly the same indicating the accuracy of the calibration and model.

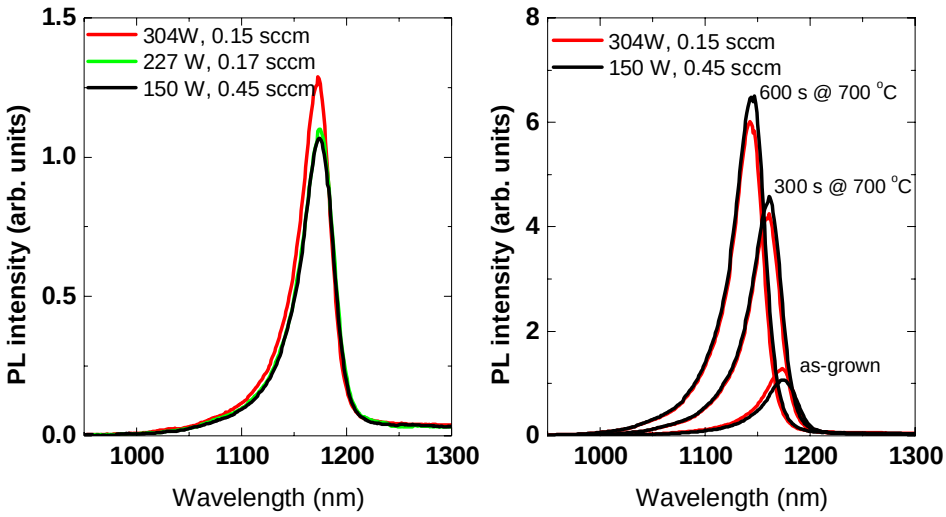

Figure 2.6. *PL spectra recorded from samples grown with different plasma settings. Left panel shows spectra for as-grown and right panel for annealed samples. For annealing, separate rapid thermal annealing chamber was used. GaAs proximity capping protected the samples.*

2.4.2 Influence of Growth Temperature on Nitrogen Composition: Thermally Activated Nitrogen Incorporation

Although the growth temperature (T_g) is one of the most important parameters affecting N solubility, the experimental findings on the effects of T_g have been controversial. [15, 20, 100-102] In particular, the redshift of emission wavelength with increasing T_g is not well understood. Previously, the annealing during the growth of other layers above GaInNAs has been found to induce this redshift. [20, 100-102] In fact, the annealing causes a blueshift through short range ordering within GaInNAs, which takes place more readily in the samples grown at lower T_g. [20, 100-102] Another explanation is phase separation of GaInNAs at elevated growth temperatures, which leads to formation of clusters or quantum dot like structures with redshifted emission. [15] Still another factor affecting the GaInNAs properties could be changes in defect concentration and type. [103, 104] Nevertheless, the previous reports have concluded that T_g of GaInNAs itself does not significantly affect the amount of N incorporated, except for the surface segregation and desorption, which lead to reduced N composition and emission

blueshift at elevated growth temperatures (Tg > 450 °C). [105, 106] However, we showed [P4] that N incorporation is enhanced with increasing growth temperature in the range of 300–450 °C. This observation was based on a combination of x-ray diffraction, photoluminescence, reflection high-energy electron diffraction, and photoelectron spectroscopy measurements and post-growth thermal annealing. Furthermore, this observation allowed us to treat N incorporation as a thermally activated process and to refine the kinetic N incorporation model by Pan et al. [105].

Two sample sets were used for this study. The first set comprised samples with two 7 nm $Ga_{0.75}In_{0.25}N_yAs_{1-y}$ QWs with nominal N composition of about y = 1%. The QW pair was embedded in GaAs and AlGaAs as described in reference [P4]. No annealing was performed in the MBE chamber except for the normal growth of upper layers at 580 °C. The photoluminescence wavelength of these samples showed unexpectedly strong increase with increasing growth temperature up to 430 °C as shown in Figure 2.7. Above 430 °C, blueshift of emission wavelength was observed which can be explained by desorption of N from the growth front leading to smaller N composition [105] or by phase separation of the crystal [15, 107, 108].

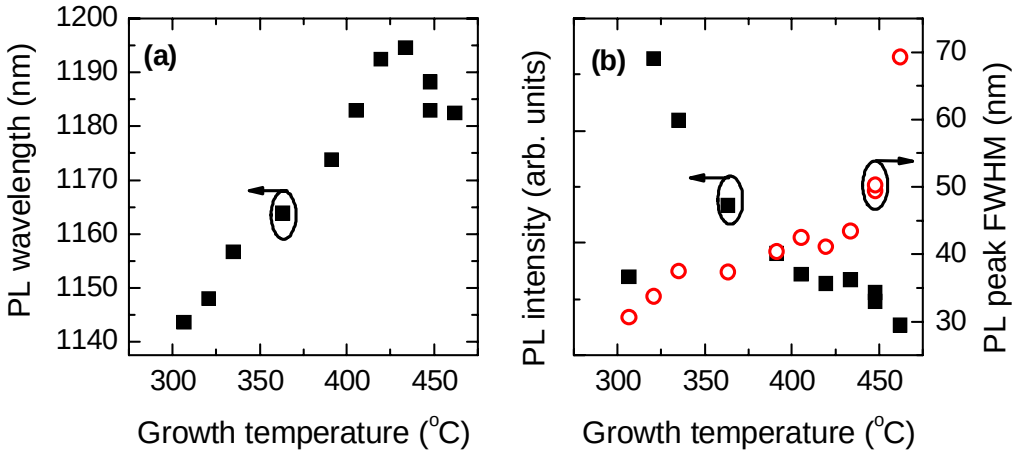

Figure 2.7. *(a) Photoluminescence peak wavelength, (b) peak intensity and peak width (full width at half maximum) as measured before annealing [P4].*

Because previous studies had suggested this redshift to be due to self-annealing [41-44], effect of annealing on these samples was studied. Post growth annealing was performed in a separate chamber at 700 °C, and sample surfaces were protected with GaAs proximity wafer. Photoluminescence (PL) peak wavelength blue shifted up to annealing time of 1200 s (Figure 2.8). The blueshift also increased with increasing temperature up to the second highest growth temperature. The decrease of the emission wavelength was accompanied by a large, from seven-fold up to 60-fold, increase of photoluminescence peak intensity, except for the lowest two growth temperatures (Figure 2.8). In addition, PL peak widths decreased indicating homogenization and improved quality of the material. Photoluminescence emission from the sample grown at the lowest temperature stopped after 600 s of annealing, while the one grown at the second lowest temperature showed only moderate, less than two-fold, intensity increase. The moderate annealing temperature of 700 °C and the use of GaAs proximity capping were chosen to limit diffusion of atoms across quantum well boundaries and thus the change of emission wavelength due to composition change. For these annealing conditions, the short range ordering of N nearest environments from Ga-rich to In-rich has been shown to be the main blueshift mechanism [18, 87].

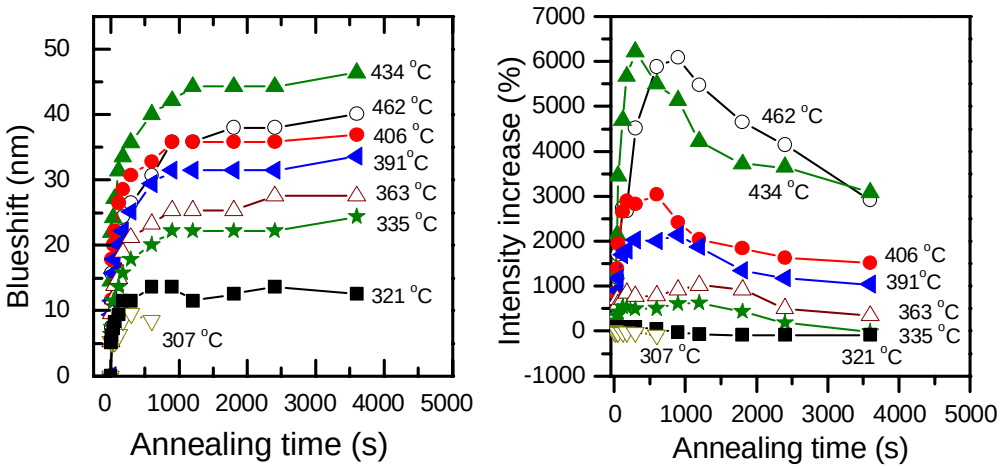

Figure 2.8. *Blueshift (left [P4]) and intensity increase (right) of QW samples grown at different temperatures and annealed at 700 °C using GaAs proximity capping.*

The emission wavelengths of the samples annealed for 2400 s are shown in the inset of Figure 2.9. The trend is similar as for the as-grown samples (Figure 2.7) except for the samples, which

were grown at the two lowest temperatures and showed also different annealing behavior. It is assumed that these samples, grown at the lowest temperatures, suffer from poor quality due to low growth temperatures. In order to have maintained good material quality at the lowest growth temperatures, As/III beam equivalent ratio should have been decreased when decreasing the growth temperature [73, 109]. Here As/III beam equivalent pressure ratio was kept constant at a value of about six. The low emission wavelength of the sample grown at the highest growth temperature of 462 °C is either due to lower N composition (N desorption from the growth front) [105] or due to phase separation which could not be recovered by annealing [15, 107, 108].

Figure 2.9 shows the normalized N compositions of the QW samples grown at temperature range from 335 °C to 462 °C and annealed for 2400 s. The two lowest growth temperatures are omitted here because of their annealing behavior, which deviates from other samples, assumedly due to decreased material quality. Figure 2.9 shows also two curves fitted to the measurement data. The black solid line is the incorporation model by Pan et al. [105] with constant incorporation rate and thermally activated desorption rate, which is described by Arrhenius exponential ($Dexp(-E_d/kT_g)$), where D is desorption constant, E_d is activation energy for desorption, k is Boltzmann constant and T_g is growth temperature. This model is not able to describe increase of N composition with increasing growth temperature. For this reason we modified the model to describe activated incorporation in addition to activated desorption. This gave the following expression for N composition [N] in the crystal:

$$[N] = \frac{Aexp(-E_a/kT_g)}{C+Dexp(-E_d/kT_g)}, \tag{2.6}$$

where E_a and E_d are activation energies for incorporation and desorption, respectively. A, C and D are temperature independent constants, which can be related to growth conditions. When Equation 2.6 is fitted to the N composition data of Figure 2.9 (green dashed line), activation energy for incorporation, $E_{a,}$ can be estimated to be 0.1 eV. Desorption activation energy of E_d = 2.1 eV, as reported in reference [105], was used for the fitting procedure.

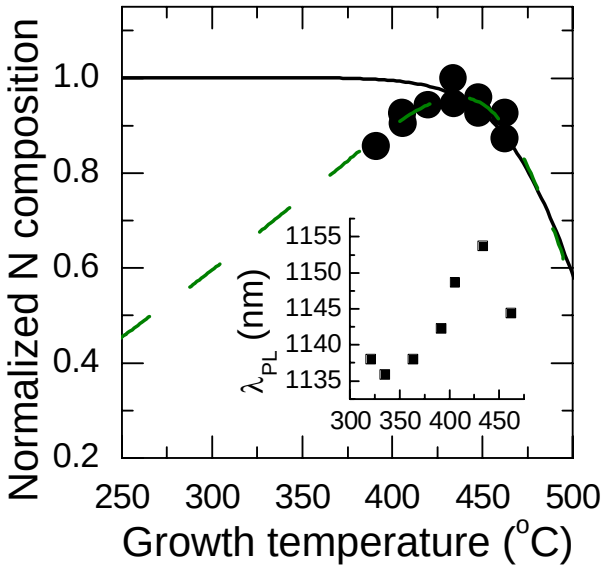

Figure 2.9. *Nitrogen composition of the QW samples deduced from simulation of QW PL peak wavelengths of samples annealed for 2400 s. Composition is normalized to 1%. Solid line shows fit of kinetic N incorporation model of Pan et al* [105] *and dashed green line shows the fit according to the kinetic model developed here (Equation 2.6). The inset shows the PL peak wavelengths of the samples annealed for 2400 s. [P4]*

According to simulations, PL wavelength increase with increasing growth temperature corresponds to N composition increase of 0.006%/°C for as-grown samples (Figure 2.7) and 0.002%/°C for annealed samples (Figure 2.9). Much larger value of as-grown samples can be explained by growth temperature dependent short range ordering. The smaller value of annealed samples is more related to actual change in composition. This was confirmed by comparing the slope of annealed QW samples with that measured by x-ray diffraction for bulk $Ga_{0.921}In_{0.79}N_{0.03}As_{0.97}$ samples. Compared to QW samples, x-ray diffraction characterization of these bulk samples is easier because they have higher N composition and each include only a single 500 nm GaInNAs layer. Dynamical XRD simulations were fitted to the measured XRD rocking curves. This allowed extracting N compositions assuming indium composition of 0.079 as calibrated with an InGaAs sample before the growth of these bulk samples. Inset of Figure 2.10 shows the N composition increase with increasing temperature. The linear fit has a slope of 0.006 %/°C which corresponds to 0.002 %/°C when normalized to N composition of 1 %. Thus, the increase of N incorporation rate in bulk samples corresponds to that of QW samples. The

increase of compressive strain in bulk samples (Figure 2.10) could, in principle, be due to increased indium composition, but this would however be in contradiction to observed redshift of photoluminescence wavelength. Thus, we concluded that N composition of MBE-grown dilute nitride GaInNAs increases with increasing growth temperature and that this increase can be modeled as a thermally activated incorporation process with an activation energy of about 0.1 eV.

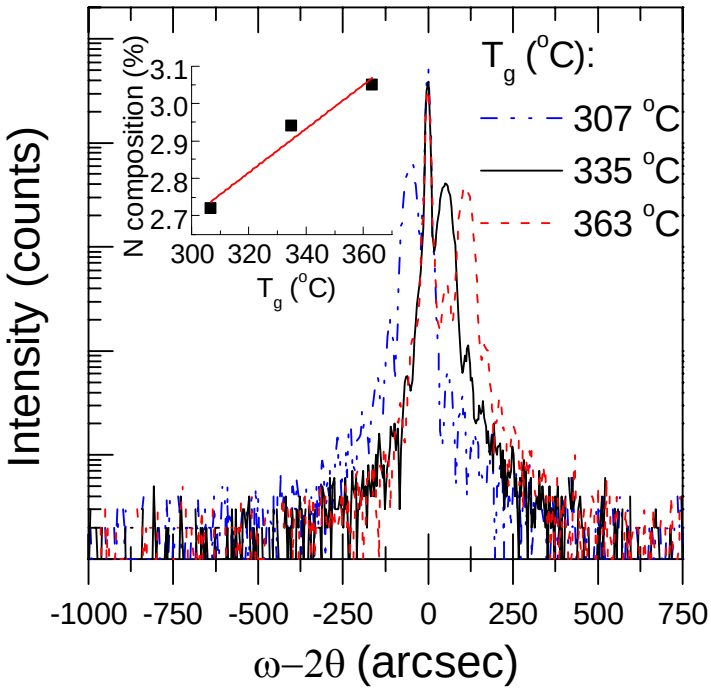

Figure 2.10. *XRD rocking curves for three 500nm $Ga_{0.921}In_{0.79}N_{0.03}As_{0.97}$ samples grown at different temperatures. Inset shows change of N composition with growth temperature and linear fit to the three data points. [P4]*

2.4.3 Influence of As/III Beam Pressure Ratio on Nitrogen Nearest Neighbor Environments

Similar to the growth temperature, which was discussed in the previous chapter, As/III beam equivalent pressure (BEP) ratio can be used to control N composition [73, 109] and annealing properties of GaInNAs [19]. Growth temperature and As/III BEP ratio are also very much dependent parameters. The lower the growth temperature, the higher the occupation probability

of surface sites by As atoms, because desorption rate decreases towards low temperatures. It is important to reduce As/III pressure ratio at low growth temperatures in order to maintain good material quality and to limit the formation of As-related defects [73]. Decreasing As/III pressure ratio also increases incorporation of N into GaInNAs [109]. Increased N incorporation at low As/III BEP ratios can be understood by competition between As and N atoms at the growth front; when As/III ratio is decreased there are more surface lattice sites available for N. Similarly, increased growth temperature decreases occupation of surface sites by As atoms due to desorption, thus leaving more sites available for N. This is one possible explanation for the increase of N incorporation rate with increasing growth temperature, which was discussed in the previous chapter and in publication [P4].

Similar to growth temperature, it is natural to study the effects of As/III pressure ratio on the short range ordering of GaInNAs. For this we used a set of four QW samples with QWs grown at different As/III BEP ratios of 3.8, 7.9, 10.0 and 12.1. Each sample contained three similar 6.5 nm $Ga_{0.62}In_{0.38}As_{0.0995}N_{0.005}$/GaAs QWs separated by 20 nm GaAs barriers. Quantum well growth parameters other than As/III BEP ratio were kept constant from sample to sample. QWs were grown at 455 °C (measured by thermocouple), and the nitrogen plasma source was operated at 205 W of forward RF power and 0.2 sccm nitrogen flow. MBE growth did not include separate annealing step, but GaAs on top of the QW group was grown at normal GaAs growth temperature of 580 °C, which might have caused some unintentional annealing. Only slight decrease in emission wavelength and slight increase in QW strain was detected by PL and XRD measurements, respectively, which indicated a minor decrease in N content with increasing As pressure.

The effect of As/III BEP ratio on the short range ordering was studied using contactless electroreflectance (CER) measurements. The basic idea of CER is to evaluate the derivative of the reflectivity spectrum with respect to modulating electric field. CER measurement involves placing the sample inside a capacitor like system. Sample is glued conductively to bottom electrode, whereas the upper electrode is separated from the sample surface by an air gap. Thus, no net current conduction takes place in the sample. The top electrode is semitransparent for measuring the reflectivity. The electric field inside the capacitor is then modulated and the fractional change in reflectivity is measured. The periodic modulation of the samples built-in electric field produces sharp spectral features at energies corresponding to interband transitions.

The derivative nature of this method makes it sensitive to transitions that are hardly if at all detectable by CW reflectivity or PL measurements.[110, 111]

CER spectra for the QW samples grown at different As pressures are shown in Figure 2.11. The spectrum of the sample grown at the lowest As/III BEP ratio of 3.8 shows clearly two resonances (labeled S and M) close to the QW transition from the first electron level to the first heavy-hole level (11H in the Figure 2.11). The resonances were separated by ~30 meV and could not be related to any other QW transition than to 11H. The broader resonance M is strong for samples grown with low As/III BEP ratio and can be attributed to different nitrogen NN environments none of which was clearly dominating [112].

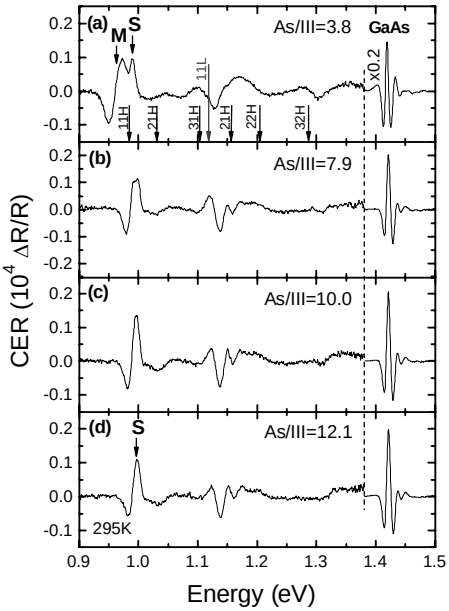

Figure 2.11. *CER spectra measured for the sample set with QWs grown at different As/III BEP ratios. Other growth conditions were kept constant and nitrogen source setting corresponded to 205 W forward RF power and 0.2 sccm nitrogen gas flow. Arrows and notation ijH(L) show calculated energies for optical transitions between ith heavy(light) hole and jth conduction subband. [P2]*

In the same measurement round we included also another sample set comprising 5 samples with the same structure as in the first series and QWs grown at As/III BEP ratio of 7.9. In this set nitrogen plasma settings were varied. All the samples of this series showed clear double

resonance in their CER spectra, similar to sample of the first set grown at As/III = 3.8. We quantified the degree of short-range ordering by measuring the relative intensities of resonances S and M and by plotting S / (M+S) intensity ratio of samples grown with different parameters (Figure 2.12). The intensities of the S and M peaks were determined from the fitted peaks as described in [P2]. This figure shows well how intensity related to M peak increases with decreasing As/III BEP ratio. Normal redshift of PL peak and CER resonances were observed (not shown) with increasing RF power and with the related increase of N composition in the crystal. Still the plasma parameters did not affect the S / (M+S) intensity ratio, i.e. the short range ordering, considerably in the studied parameter interval.

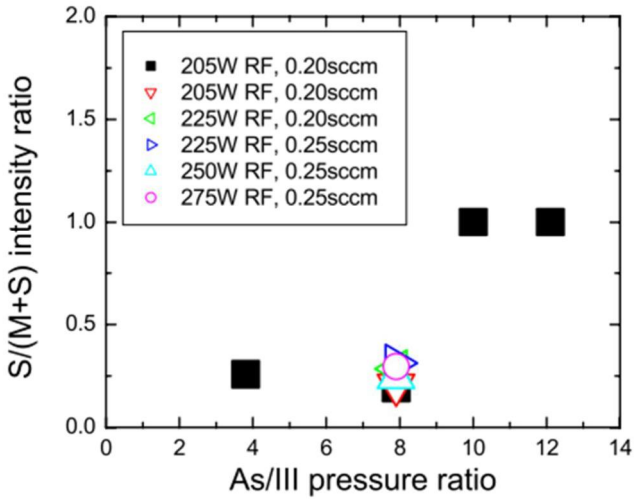

Figure 2.12. *Intensity ratio S/(M+S) of the narrow S and broad M resonances of the CER spectra measured for the samples grown at different As/III BEP ratios and nitrogen plasma settings. [P2]*

In order to study further the origin of the double resonance, we conducted separate annealing treatments on these samples, because annealing is a well-known method for changing the short range ordering in GaInNAs (Chapter 2.3). Annealing was carried out at three different temperatures (650, 750, and 850 °C) for 60 s and GaAs proximity capping was used to protect the samples. Figure 2.13 shows the CER spectra for four of the samples after different annealing treatments. In the QW samples grown at lower As/III BEP ratio, both M and S resonances are observed in as-grown samples, and the M resonance disappears with annealing.

This is in agreement with the hypothesis that the S resonance is due to the energetically most favorable N-In_3Ga_1 nitrogen nearest neighborhood [78, 81] and the broad resonance corresponds to nitrogen nearest neighborhoods with two or fewer surrounding In atoms. Annealing treatments are known [81] to drive short range ordering towards In-rich nitrogen nearest neighborhood configurations, which are energetically favorable in bulk crystal. Ga-rich configurations are favorable at the growth front and exist also in the bulk crystal because reconfiguration is kinetically limited. In addition to disappearance of the broad M resonance, annealing induced also blueshift of the S resonance and PL peak. This can be attributed to interdiffusion of atoms across the QW boundaries, which is stronger the higher the annealing temperature [18]. Homogenization of NN environments towards N-In_3Ga_1 configuration is a potential reason for narrowing of the CER resonance peaks with increasing annealing temperature, while reduced number of defects and improved interface quality are also expected to have an effect (Figure 2.13).

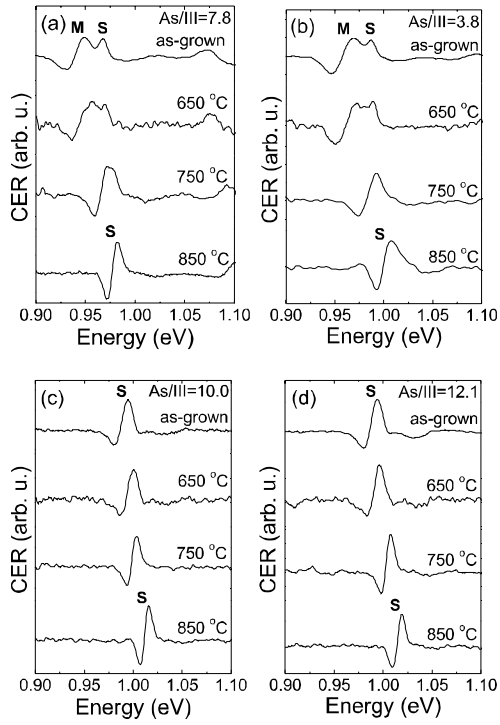

Figure 2.13. *CER spectra for GaInNAs/GaAs QWs grown at different As/III pressures and annealed. Spectrum (a) was measured for sample grown with nitrogen plasma source settings of 275 W and 0.25sccm and spectra (b), (c) and (d) for samples grown with 205W and 0.2 sccm flow. [P2]*

To conclude, also As/III BEP ratio clearly affects the short range ordering of nitrogen nearest neighborhoods. The M resonance of CER spectra, which corresponds to nitrogen nearest neighborhoods of N-In_mGa_{4-m} with $m \leq 2$, is clearly observed in the samples grown at lower As/III BEP ratios of 3.8 and 7.9. High As/III BEP ratio promoted formation of In-rich nitrogen nearest neighborhood, which is stable and energetically favorable form in the bulk crystal. These results suggest that effectiveness of formation of As-In and As-Ga bonds depends on the As/III BEP ratio or that high As/III BEP ratio enhances formation of As-related defects, which promote reorganization of the crystal towards favorable N-In_3Ga_1 configuration.

This finding as well as those related to growth temperature (chapter 2.4.2) and plasma source calibration (chapter 2.4.1) are important for the fundamental understanding of the mechanisms of PA-MBE growth of GaInNAs(Sb) and for the everyday work in the laboratory where the relation of growth parameters to crystal properties should be known for finding optimal growth conditions.

Chapter 3

Dilute Nitride Semiconductor Disk Lasers

It is difficult to achieve high output powers with symmetric and high quality beams by using traditional semiconductor lasers. Edge-emitting lasers (EELs) have limited performance in terms of beam profile and vertical-cavity surface-emitting lasers (VCSELs) in terms of output power. To overcome these limitations Kuznetsov et al. developed a new type of optically pumped semiconductor laser known as a vertical-external-cavity surface-emitting laser (VECSEL) [2, 3], which was later named a semiconductor disk laser (SDL) to emphasize its similarity to thin-disk solid-state lasers [6]. Groundwork for Kuznetsov was laid by several groups [113-118]. As compared with VCSELs, the most apparent difference is that in SDLs the top mirror is separated and located away from the so called gain mirror which consists of the gain region and integrated bottom mirror. This configuration allows scaling up the mode size on the gain mirror and, together with optical pumping, an increase in output power without sacrificing the high beam quality. Using this approach, Kuznetsov et al. could generate high output power in circular, high-quality output beam directly from a semiconductor laser.

Furthermore, the SDL geometry (Figure 1.1 (c)), enables introduction of optical elements into the free-space cavity where the optical intensity is the highest. The cavity may include, for example, nonlinear crystals for frequency conversion [119, 120], semiconductor saturable absorber mirrors (SESAMs) for ultra-short pulse generation [121], and filters for wavelength tuning [122] and single frequency operation [5]. In addition to optically pumped SDLs, electrically driven SDLs have been developed. Such a device has produced a relatively high power of 0.5 W with high beam quality [123]. Electrical pumping, however, gives rise to

problems related to doped DBR mirrors and current spreading, which makes uniform pumping of the gain material and, thus, increasing the output power difficult. On the other hand, electrically pumped SDLs are compact and can operate regardless of the availability of suitable pump lasers. In this thesis, only optically pumped SDLs were studied.

The increased interest in developing SDLs has been motivated partly by their ability to produce high-power, high beam quality visible laser radiation by efficient intra-cavity frequency doubling. Blue and green frequency doubled SDLs were demonstrated first [21, 22] as the fabrication of high quality GaAs-based AlAs/GaAs DBRs and GaInAs/GaAs QW gain materials for 940–1060 nm wavelengths is mature semiconductor technology. On the other hand, the development of yellow and red frequency doubled SDLs has been challenging due to lack of good semiconductor gain materials emitting at 1150–1240 nm spectral range and compatible with high quality GaAs-based DBRs. At best, SDLs based on GaInAs QWs have been able to reach 1180 nm fundamental wavelength [23, 24], which corresponds to yellow (590 nm) when frequency doubled [124, 125]. Further increase in emission wavelength using this material system is increasingly difficult due to large lattice mismatch between the QWs and the GaAs substrate. The high lattice strain may be detrimental to the lifetime of a device incorporating such QWs [126, 127].

As discussed in Chapter 2, the compressive strain of GaInAs on GaAs can be compensated by N incorporation which simultaneously decreases the band gap and thus enables emission at wavelengths up to 1.55 μm. Dilute nitride GaInNAs/GaAs QWs were initially developed due to their advantages over InP-based heterostructures used in laser diodes, which dominate the markets of 1.3 and 1.55 μm telecommunication lasers. Compared with InP-based lasers, GaInNAs lasers are expected to exhibit improved temperature stability due to better electron confinement, they use low-cost GaAs substrates, and they can utilize high-performance monolithic AlAs/GaAs DBR mirrors enabling vertical device geometry. [7, 8, 128] The possibility of growing long wavelength GaInNAs QWs monolithically on AlAs/GaAs DBRs has quickly led to demonstration and development of many vertical cavity devices such as VCSELs [129], vertical cavity semiconductor optical amplifiers (VCSOAs) [130], SESAMs [131] and also SDLs [132]. However, N incorporation can lead to deterioration in materials optical quality and device performance as discussed in chapter 2. Careful optimization of growth parameters, special growth techniques and post growth annealing are required to obtain device quality dilute nitrides, even more so at the longest wavelengths of 1.55 μm [12, 19, 73,

77]. At the 1.2 μm wavelength range both the N concentration and the lattice strain of the QWs can be kept at relatively low levels, and thus GaInNAs is a major candidate for a gain material of lasers at these wavelengths [133-136]. Together with frequency doubled SDL technology, this gain material system enables fabrication of high-power and high beam quality lasers emitting at yellow (fundamental wavelength of ~1180nm) [29] and red wavelengths (fundamental wavelength of ~1220 nm) [30]. This chapter covers fabrication and characterization of 1180 nm [P3], 1220nm [P1] and 1550 nm [P5] GaInNAs(Sb)/GaAs SDLs.

The main motivation for developing 1180 nm gain mirrors was to provide sources for creating laser guide stars for adaptive optics calibration in earth-based telescopes. In this application, the yellow SDL would be used to excite sodium (whose D_2 absorption line corresponds to a wavelength of 589.2 nm), which is naturally present in atmosphere at an altitude of 90 km. Re-emitted light from sodium atoms would then generate an artificial calibration star in the sky allowing adaptive optics system to compensate for atmospheric turbulence. [33, 34] Also LIDAR systems taking advantage of Na D_2 absorption have been developed [137]. Furthermore, yellow lasers can be used to benefit stimulated emission depletion (STED) microscopy [35]. Important applications of yellow SDLs are found also in eye surgery [36], flow cytometry [37] and treatment of vascular lesions (port wine stains) [38]. A yellow (578 nm) frequency-stable narrow-linewidth SDL could be an enabling technology for Yb-based optical lattice clocks, which are a candidate for future time standards [138].

Red SDL with high output power could be used in RGB laser projectors [39, 40]. Watt level red lasers are needed also in photodynamic therapy [41, 42]. Both the yellow and red SDLs would also find a wide variety of applications in the field of spectroscopy. 1.2 μm SDLs find potential applications for example in optical coherence tomography (OCT) [139] and as pump sources for Raman amplifiers [136] and thulium doped tellurite glass lasers [140].

While the telecom band around 1550 nm is covered also by Er-doped fibre lasers [141, 142], SDLs could still bring certain advantages to this wavelength band. For example, SDLs can be readily mode locked to give high repetition rates [121, 143, 144], which is important for communication applications. Longitudinally single-mode 1550 nm SDLs could be used in laser communications, light detection and ranging (LIDAR), spectroscopy, sensing, and as seed lasers for high power amplified systems [43]. A potential application for 1550 nm SDLs with low noise can be found in microwave radio antenna systems [44]. When frequency doubled to

700 – 800 nm, these lasers could provide an alternative to bulky Ti:sapphire lasers, or to GaAs-based diode lasers in applications where high beam quality is required [45]. SDLs at slightly shorter wavelengths around 1480 nm could find application as pump sources of Raman amplifiers [46].

In addition to dilute nitride GaInNAs(Sb) QWs, there are other SDL gain material systems capable of producing 1.18–1.23 μm or 1.55 μm laser radiation. Also SDLs emitting directly at red wavelengths have been demonstrated. As mentioned in the beginning of this chapter, highly strained GaInAs/GaAs QWs have been used to demonstrate SDLs with wavelengths up to 1180 nm corresponding to yellow frequency doubled light [24, 124], but further increase in wavelength using these QWs is increasingly difficult. SDLs based on GaAsSb/GaAs QWs have been demonstrated at 1.18–1.22 μm and frequency doubled to yellow and red. GaAsSb QWs, however, suffer from low electron confinement, which makes them temperature sensitive and less promising for high power applications. [145, 146] SDLs based on GaInAs/GaAs quantum dots (QDs) are interesting because they show low lasing threshold, good temperature stability and large tuning range. The small gain of QD layers has been somewhat an obstacle to producing watt-level powers by QD SDLs [147], but recently multi-watt output powers have been measured from 1.18 μm SDLs based on 39 layers of GaInAs QDs [148-150]. The upper wavelength limit of quantum dot SDLs is around 1.3 μm based on the current reports [151]. As discussed above, one of the main drawbacks of InP-based gain materials is the lack of good lattice-matched DBR materials. InP-based DBRs do not provide sufficient heat removal for high power flip-chip SDLs and are difficult to fabricate because of high number of layer pairs required due to low refractive index contrast. However, a few reports on 1.55 μm InP-based SDLs can be found in the literature [5, 152]. In addition, different ways to circumvent the DBR problem of InP-based SDLs have been developed. Maybe the most promising approach is wafer fusion technology. It has led to the demonstration of SDLs at 1.55, 1.3, and 1.2 μm with AlAs/GaAs DBRs and InP-based gain regions [153-155]. Still, the complex fabrication process including two epitaxial growth runs and the wafer fusion makes this technique less favorable. SDLs based on a GaInP/AlGaInP/GaAs material system are capable of producing direct red emission [26]. This material system is limited to wavelengths longer than 630 nm by the lack of good QW barrier materials and, thus complements frequency doubled GaInNAs technology on the long wavelength side. The advantages and disadvantages of SDL gain materials having

potential for operation at yellow–red wavelengths, 1.18–1.24 μm or 1.55 μm are summarized in Table 3.1.

Table 3.1. *Potential gain material systems for SDLs operating at yellow–red wavelengths, 1.18–1.24 μm or 1.55 μm.*

Material system	Advantages	Disadvantages
Material systems for direct yellow–red SDLs		
GaInP/GaAs [26]	• Red wavelengths at λ_{SDL} > 630 nm feasible • AlAs/GaAs DBRs	• Slightly too long wavelength for many applications • Lack of pump laser diodes
Material systems for 1.18 μm and 1.22 μm SDLs		
GaInAs/GaAs [24, 124]	• Mature growth technology • High gain • Good power scalability • Low threshold • AlAs/GaAs DBRs	• λ_{SDL} < 1.2 μm • Quality of highly strained QWs degrades at long wavelengths
GaAsSb/GaAs [145, 146]	• λ_{SDL}=1.18–1.22 μm feasible • AlAs/GaAs DBRs	• Poor electron confinement • Poor output power • Poor high temperature operation • Highly strained QWs
(Ga)InAs QDs/GaAs [148-151]	• λ_{SDL}=1.18–1.22 μm feasible • Broad QD gain spectrum • High temperature stability of laser characteristics • AlAs/GaAs DBRs	• High number of QD layers required due to small gain of a single layer
Material systems for 1.3–1.55 μm SDLs		
AlGaInAs/InP or GaInAsP/InP [5, 152]	• Mature growth technology • Mature telecom laser technology • λ_{SDL} = 1.3–1.55 μm feasible	• Poor characteristics of InP-based DBRs • Potentially poor operation at shorter, ~1.2 μm wavelengths
InP-based gain region + hybrid metal–metamorphic AlAs/GaAs mirror [156]	• Single round of epitaxy	• Metamorphic • Only low power demonstrated
AlGaInAs/InP wafer fused with AlAs/GaAs DBR [153-155]	• Mature growth technology of both the InP-based active region and GaAs-based DBR • λ_{SDL} = 1.2–1.55 μm feasible	• Complicated gain mirror fabrication • Potentially poor operation at shorter, ~1.2 μm wavelengths

3.1 Basics of Semiconductor Disk Lasers

3.1.1 Optical Pumping and External Cavity

Semiconductor disk lasers combine the advantages of diode-pumped solid-state lasers and semiconductor gain medium. As such, SDLs are an extension of the thin-disk diode pumped solid-state laser (DPSSL) technology [6]. Together with external cavity, optical pumping allows scaling up the pumped mode size in the active region and thus efficient power scaling. The external cavity with high intra-cavity circulating power makes SDLs also very suitable for intra-cavity frequency doubling. [3]

In a simple form, an SDL consists of a gain mirror, one or more external mirrors and a pump laser. The gain mirror comprises a QW or QD gain section for providing the gain and a DBR mirror acting as one of the cavity end mirrors. External mirrors are used to define the optical cavity. At least one of these mirrors is used as an output coupler and is only partially reflective. The main function of the external cavity in SDLs is to define the TEM_{00} that has an optimum spatial overlap with the pumped volume of the gain medium [3, 157]. The pumped area on the gain mirror acts as a gain aperture decreasing the gain of higher order cavity modes, which in optimized case lie largely outside the pumped region. Too large pump spot as compared to cavity mode size leads to amplification of higher order cavity modes, and too small pump spot size reduces the laser efficiency due to losses in the unpumped regions [158]. This transverse overlap is described by transverse confinement factor Γ_t. Excellent beam quality (beam quality factor M^2 close to 1) with only few percent penalty in output power could be achieved [158] by setting mode diameter ~10 % larger than pump spot diameter.

The gain mirror is usually pumped with a diode laser. The pump laser beam is typically incident on the gain mirror at a convenient angle and focused into a spot having a diameter in the range of 50–900 μm. The pump light is absorbed in the semiconductor providing the excited carriers required for population inversion. The choice of pump wavelength depends on the semiconductor design as wells as on the availability of suitable pump lasers. Naturally, pump lasers whose wavelength is short enough to stimulate interband absorption should be used. Suitable cost-effective pump laser diodes with high-power and sufficient beam quality are most

readily available at the wavelengths of 808 nm (corresponding to AlGaAs/GaAs material system) and 980 nm (InGaAs/GaAs).

The most common SDL semiconductor design is such that the whole active region, including the QWs and the barrier layers between them, absorbs the pump light (for a schematic layer structure, see Figure 3.1). Because the thickness of barrier layers and thus the net absorption in them is an order of magnitude higher as compared to the QWs, this pumping scheme is often called barrier pumping. The high absorption coefficient of GaAs-based semiconductors allows efficient use of the pump energy. For example taking the GaAs absorption coefficient to be 13900 cm^{-1} [159] it can be calculated that about 89 % of pump power is absorbed into 1.45 µm thick semiconductor (the active region thickness of the 1.18 µm SDL introduced later in the thesis) in a single pass. This simplistic calculation demonstrates clear advantages of using semiconductor gain materials. In contrast to thin-disk DPSSLs, no pump light circulation optics is required to compensate for the low single pass absorption. In addition, the small thickness of the active region requires matching of the cavity mode and pumped volume effectively only at a single plane because divergence in the thin active region is negligible. This alleviates the requirements on the focus depth and beam quality of the pump sources. In addition, the wide interband absorption bandwidth of semiconductors alleviates the spectral linewidth requirements for the pump sources.

The main problem of barrier pumping is that the laser emission wavelength is much longer than the pump wavelength. This is described by a quantity known as quantum defect and defined as the difference in pump photon and emitted photon energies. Each electron excited by a pump photon gives up an energy corresponding to the quantum defect as phonons, i.e. as heat, when it decays to occupy the QW ground state. The higher the quantum defect, the more energy is lost as waste heat in the semiconductor. A high quantum defect decreases the laser efficiency and requires efficient cooling mechanisms. Device heating is still a main obstacle to power scaling SDLs. This issue can sometimes be alleviated by using so-called in-well pumping scheme in which the barrier layer band gap is higher than the pump photon energy and the pump light is absorbed only in the QWs [6, 160-163]. However, the small thickness of the QWs gives a relatively low absorption of the pump light in a single pass.

In both the barrier and in-well pumping schemes, the amount of pump light reflected from the gain mirror surface, and thus wasted, is usually reduced by depositing an anti-reflection (AR)

coating on the gain mirror surface. This can affect also reflectivity at the signal wavelength and resonance properties of the semiconductor gain mirror. [164]

SDLs are low gain devices due to the small total thickness of the QWs. This introduces stringent requirements for the cavity; the parasitic cavity losses should be minimized, and the total cavity losses should be dominated by the output extraction [157]. Increasing the transmission of the coupler, however, has two competing effects on the output: The output power tends to increase due to higher extraction of photons from the cavity, and simultaneously to decrease due to increased cavity losses or, in other words, decreased number of cavity photons. For SDLs, a low output coupler transmission of T_{OC} = 1–10 % is usually found to give the optimum efficiency. The higher the T_{OC}, the smaller is the effect of parasitic losses. However, a high T_{OC} also results in high threshold pump power and carrier density, and thus in higher rate of nonradiative recombination rate [158].

3.1.2 Structure of Semiconductor Gain Mirror

The active component in SDLs is a semiconductor chip that both provides the gain and acts as a cavity end mirror. Hence it is often called a gain or an active mirror. Figure 3.1 shows a schematic band gap profile of a typical semiconductor gain mirror.

The distributed Bragg reflector (DBR) at the bottom of the gain mirror acts as one of the mirrors defining the laser cavity. A few layer pairs of the DBR are shown schematically in Figure 3.1. Most often it consists of layers with an optical thickness corresponding to a quarter of the signal wavelength ($\lambda_{SDL}/4$) and with adjacent layers having alternating high and low refractive indices (n_H and n_L, respectively).

In SDLs, a very low-loss cavity is required due to low single pass gain. For this reason, DBR should have a reflectivity above 99 %. This requires both high index contrast between n_H and n_L and high number of layers. A 29.5-pair AlAs/GaAs DBR gives a reflectivity of 99.97 % and a stop-band width of $\Delta\lambda_{99\%}$ = 102 nm at λ_{SDL} = 1.22 µm. In addition to decreased reflectivity, deviation from the design wavelength, λ_{SDL}, introduces a phase shift in the light reflected from the DBR. In order to maximize the reflectivity and the tolerance for growth errors, devices are usually designed to operate at the wavelength corresponding to stop band center [165].

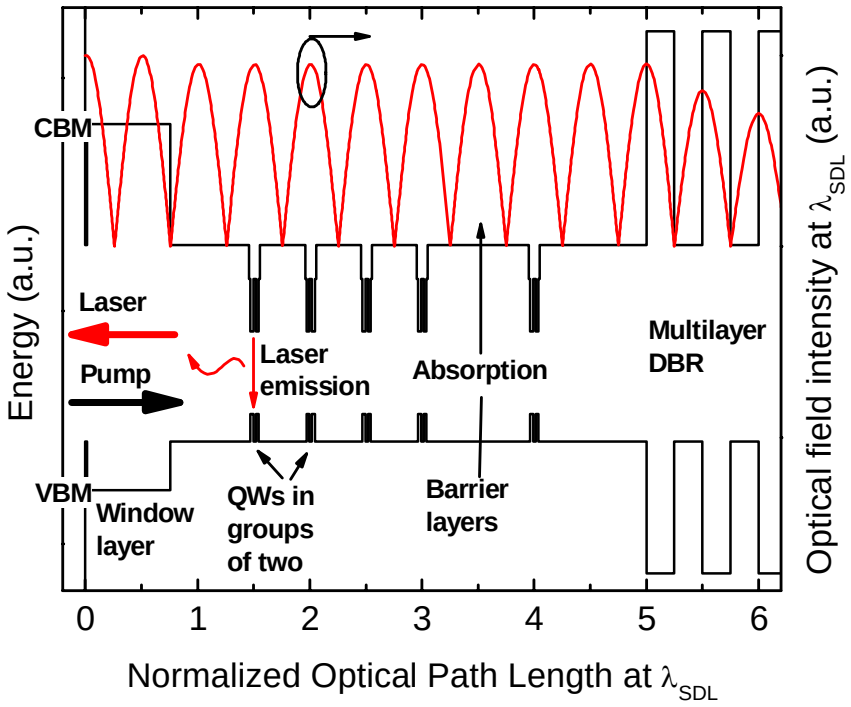

Figure 3.1. *A schematic band gap diagram of an SDL gain mirror (left axis) and optical field intensity in it (right axis). This layer design was used for 1.18 µm gain mirror (wafer ID AsN2897) and 1.22 µm gain mirror A (AsN2527) reported later in this thesis. Semiconductor–air interface is located at zero on the horizontal axis. Semiconductor band gap is formed between conduction band minimum (CBM) and valence band maximum (VBM). Absorption takes place in the barriers and QWs (barrier pumping) and emission in the QWs. Below the gain region, a DBR acts as a cavity end mirror.*

Above the DBR lies an active region for providing the gain. The single-pass gain of a vertical cavity QW device is very small because the interaction of laser mode and gain is limited to the thin QW planes. The small gain is usually compensated by using a high number of QWs and by maximizing their coupling with the laser mode. The latter is achieved by placing the QWs periodically at the antinodes of the optical standing wave formed in the semiconductor microcavity. The microcavity is defined by the DBR and the semiconductor top surface. This periodic gain scheme is called resonant periodic gain (RPG) [166, 167]. To place the QWs at the field anti-nodes, they should be separated by layers whose optical thickness corresponds to a

multiple of $\lambda_{SDL}/2$. The longitudinal confinement factor, which describes spatial overlap between the QWs and the laser mode, is defined as

$$\Gamma_l \quad \frac{\int_{QWs} E^2 dz}{\int_{cavity} E^2 dz} \tag{3.1}$$

where E is the electric field amplitude of the laser mode. The integral in the numerator is taken over QWs, and the one in denominator over the semiconductor microcavity. If the maxima of the E^2 overlap spatially with the QWs, Γ_l is increased. For a homogenous gain material Γ_l equals a so called fill factor which is defined as a ratio of active material thickness to the total thickness of microcavity, d_{active} / L_{cavity}. In other words, enhancement due to RPG as compared to homogenous gain material is given as $\Gamma_{RPG} = \Gamma_l/(d_{active}/L_{cavity})$ which approaches a value of 2 as the fill factor approaches zero. [163, 166, 167] The Γ_l and modal gain can be enhanced also by grouping several QWs at each anti-node.

In addition to RPG gain, Γ_l is also affected by the total thickness of the cavity. This is described by a quantity Γ_{cav}, with the longitudinal confinement factor then given as a product of confinement factors due to RPG and semiconductor cavity, i.e. $\Gamma_l = \Gamma_{cav}\Gamma_{RPG}(d_{active}/L_{cavity})$. Microcavity can be either resonant or antiresonant with the signal radiation. These extreme cases correspond to optical microcavity thickness of even and odd multiples of $\lambda_{SDL}/4$, respectively. In a resonant structure optical field intensity inside the microcavity is enhanced. Typically, intrinsic material gain can be enhanced by a factor of $\Gamma_l = 7$ by using a resonant microcavity together with RPG. [163] In Figure 3.1, resonant microcavity with RPG is formed between the DBR and semiconductor-air interface. In an anti-resonant case, the optical field intensity inside the semiconductor is reduced thus reducing Γ_{cav} and the modal gain [157].

Both the resonant and antiresonant SDLs have their own advantages and disadvantages. The resonant cavity with RPG gives a narrow gain spectrum with higher sensitivity to variations in either wavelength or semiconductor thickness. For maximum gain, both the spatial separation of QWs and microcavity thickness should equal a multiple of half a wavelength. Deviation from this match decreases Γ_{RPG}, Γ_{cav}, or both at the design wavelength. Moreover, it should be noted that for maximum modal gain, the intrinsic QW gain spectrum maximum should match the

narrow spectrum of Γ_1. This can be somewhat a problem in high-power SDLs because the two spectra redshift at different rates with increasing temperature. In general, the narrow Γ_1 spectrum has the disadvantages of increasing the temperature sensitivity of the device and decreasing the gain bandwidth for wavelength tuning and mode locking. In resonant structures an antinode of the optical field is always positioned at the semiconductor surface, which might enhance optical losses. On the other hand, the high peak gain of resonant structures is more tolerant of losses, for example those introduced by intra-cavity elements such as frequency doubling crystals. Despite the lower peak gain, antiresonant structures have wide bandwidth of Γ_1, which results in wide gain spectrum useful for mode-locked or tunable lasers. Also the match between intrinsic QW gain and Γ_1 spectra is more readily achieved in this case, which results in increased temperature stability. [157]

The topmost layer of the gain mirror is usually a so-called window or cladding layer. This layer creates an energy barrier for the excited carriers in the active region and prevents them from diffusing to the semiconductor surface where they could recombine nonradiatively. The window layer band gap is chosen large enough to be transparent for both the signal and pump radiation.

One of the main problems in reaching new wavelength regions with the SDL technology is the lack of suitable gain materials compatible with high quality DBRs and substrates. Often this combination is prevented by the lattice mismatch between the otherwise preferable materials. As discussed, the lattice mismatch of GaInAs/GaAs can be alleviated by incorporating N into the QWs for reaching wavelengths above 1100 nm. Still a substantial net strain can accumulate in MQW structures, as a low N concentration is usually preferred to ensure high emission efficiency. In order to keep the MQW active regions structurally stable, strain compensation is often used. This means incorporating layers with an opposite sign of mismatch, as compared to QWs, into the structure. In the GaInAs/GaAs system tensile GaAsP strain compensation layers are widely used [168]. In the GaInNAs/GaAs system tensile GaNAs has been a natural choice and is used also in this thesis. In addition to strain compensation, GaNAs layers provide an additional redshift of the emission wavelength as they are usually placed next to QWs where they decrease energy barrier of the QWs [90-92]. On the downside GaNAs layers are thought to increase the temperature sensitivity and non-radiative recombination of the device [65, 169]. The structural stability of MQW structures can be studied theoretically [170] and by experimental methods such as x-ray diffraction [77, 168]. In a fully strain compensated gain region, where the barrier strain exactly balances the QW strain, virtually infinite number of

layers can be grown pseudomorphically as long as no single layer exceeds its critical thickness. However in most cases partial strain compensation is sufficient for ensuring structural stability [168, 170]. Whereas strain compensating layers reduce the net strain of the structure, they do the opposite at the layer interfaces where two layers with opposite strains are in contact. In order to avoid high interfacial strain and the related deterioration of optical properties, so called strain mediating layers with intermediate value of strain can be used between the QW and the oppositely strained barrier. A thin GaInNAs layer with moderate compressive strain and placed between GaInNAs QW and GaNAs strain compensating layer has been found to improve both the structural and optical properties of the QW system [92].

3.1.3 Thermal Management and Power Scaling

Power scaling [171] is one of the main advantages of SDL technology as compared to laser diodes. Assuming efficient one-dimensional heat extraction from the gain mirror surface or bottom, power scaling of SDLs can be achieved by increasing the pump and laser mode area on the gain mirror in proportion to pump and output power. Thus, the intensities of pump and signal light as well as the gain mirror temperature can be kept virtually constant with increasing power.

Mainly two device configurations are used to ensure efficient heat extraction from the gain mirror. These are intra-cavity heat spreader and thin-device, also known as flip-chip, configurations (Figure 3.2). Both target in minimizing the heat conduction through the relatively thick substrate by either forming an alternative heat conduction path (intra-cavity heat spreader) or by removing the substrate (thin-device).

A gain mirror for intra-cavity heat spreader SDL is typically grown starting from the DBR on the substrate and followed by the active region and the window layer. A heat spreader transparent for both the pump and signal radiation is then attached to a gain mirror chip by capillary bonding. Typically for SDLs emitting around 1 μm as well as in this thesis, diamond is chosen as the heat spreader material [172]. It shows both excellent thermal conductivity and transmittance of pump and signal radiation. The heat spreader-gain mirror combination is attached to a copper mount using indium foil to ensure good thermal contact. The copper mount can be cooled either thermoelectrically (TEC) or by circulating water. Heat spreader approach

can be refined into microchip SDL by depositing a mirror coating on the heat spreader, which then forms the external cavity [173, 174].

A gain mirror for a thin-device SDL is grown in reverse order. Growth is started with an etch-stop layer which often acts also as a window layer. The growth of etch-stop layer is followed by the growth of active region and DBR. The as-grown wafer surface, i.e. the DBR side, is then metallized and most of the substrate on the other side is removed. Then the thinned wafer is cut into chips whose metallized DBR side is soldered onto heat sinks or heat spreaders. The rest of the substrate is removed by etching which reveals the etch-stop layer, i.e. the gain mirror surface. [3]

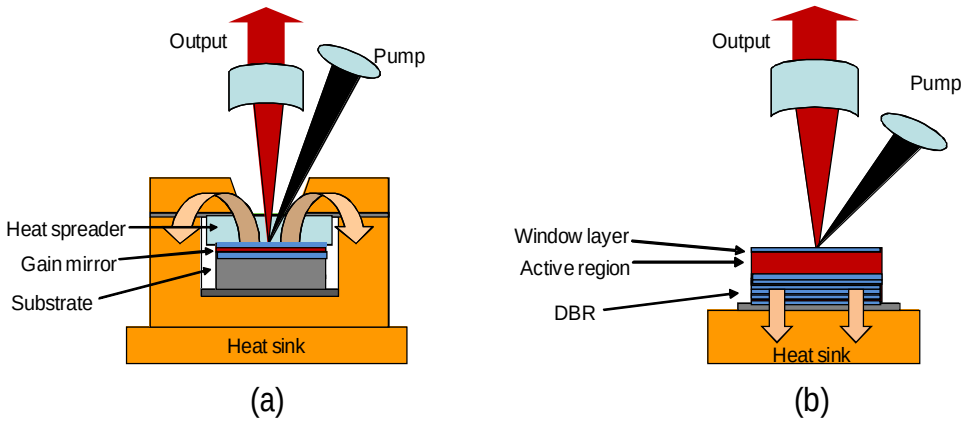

Figure 3.2. *Schematic representations of (a) an intra-cavity heat spreader SDL and (b) a thin-device, also known as flip-chip, SDL. In the former heat is extracted from semiconductor surface through a heat spreader located inside the laser cavity. In the latter substrate is removed and heat is extracted through the DBR.*

Neither of the thermal management concepts are fully capable of keeping the gain mirror temperature constant with increasing pump power, even though pump intensity would be kept constant. Thus the heat extraction limits the power scaling of SDLs. Whereas the thermal resistance for heat extraction should present $1/(pump\,spot\,area)^2$ dependency for true power scaling, real devices show dependency in the range of $1/(pump\,spot\,area)^1$ – $1/(pump\,spot\,area)^{1.7}$. [4, 172] The thin device approach is best suited for SDLs emitting around 1 µm which can use binary AlAs/GaAs DBRs with relatively high thermal conductivity. The limits of this approach are met with other material systems or at longer wavelengths where

DBR conductivities are lower and thicker layers are required, especially so with long-wavelength InP- and GaSb-based devices [5, 175-177]. The heat spreader does not require heat flow through the DBR and is thus more generic with respect to wavelength range and material system used [177]. Intra-cavity heat spreader approach has been utilized for demonstrating an 1180 nm SDL with an output power of 50 W [24], while the thin-device approach was used for a 1028 nm SDL achieving so far the highest SDL output power of 106 W [178]. Both of these SDLs were based on InGaAs/GaAs gain mirrors. In order to overcome limitations regarding the inadequate heat extraction with increasing spot size, SDLs with multiple gain mirrors have been manufactured [179-181]. Output powers of these devices were reported to scale linearly with increasing number of gain elements. A three gain mirror device described in reference [181] could produce over 50 W of output power both at infrared and at frequency doubled green wavelength of 532 nm.

Maybe the most noticeable difference between the two types of SDLs is found in spectral characteristics. Whereas thin-device SDL in its simplest form is free from intra-cavity components, the intra-cavity heat spreader forms an etalon inside the cavity and modifies modal gain and output spectra of the device. The spectra are modulated with a period given by the free spectral range of the Fabry-Pérot etalon. This kind of feature in the output spectrum is undesired if for example modelocked or continuously tunable laser is targeted. Heat spreader introduces also refractive index adaptation between semiconductor and air $\left(n_{air} < n_{heatspreader} < n_{gainmirror}\right)$ thus broadening the spectrum [172]. Advantage can also be taken from the etalon effect if the free spectral range of the etalon is increased above the natural linewidth of the laser emission by decreasing the heat spreader thickness. In this way the laser can be forced to operate with narrow linewidth [5] but at the expense of lower thermal conductivity. Wedged and AR coated heat spreaders are often used to recover continuous gain and emission spectra. The possible birefringence of the intra-cavity heat spreaders should be taken into account when polarization sensitive elements, such as frequency doubling crystals, are used with this type of SDLs [182].

Temperature increase should be accounted for already in the design phase of the gain mirror. Otherwise the temperature induced wavelength offset between the QW gain spectrum and the spectrum of gain enhancing Γ_1 becomes a main limiting factor for maximum output power and efficiency at elevated temperatures. Other limiting factors are increased rate of nonradiative

recombination, spontaneous emission, and carrier leakage out from the QWs. The offset between peak wavelengths of QW gain and Γ_1 at increased temperatures is inevitable because, although they both redshift with increasing temperature, the shift rate is much higher for the QW gain than for Γ_1. Typical redshift rate is about 0.4 nm/K for the QW gain and 0.1 nm/K for the Γ_1 [135, 175, 183, 184] [P3]. The different shift rates are usually taken into account in the gain mirror design by detuning the room-temperature QW photoluminescence peak about 30-40 nm and the resonance wavelength of the microcavity about 5 nm shorter than the designed operation wavelength. This detuning has the advantage of postponing thermal roll-over by increasing the modal gain at high-power operation where the gain mirror temperature is high. On the downside, the threshold pump power is increased due to lower gain at low pumping levels and temperature, which results in increased carrier density and losses. Thus the detuning is a matter of optimization.

3.2 1.18 µm Semiconductor Disk Lasers

This 1.18 µm semiconductor disk laser [P3] was developed for frequency doubling to yellow spectral region around 590 nm. As discussed in the beginning of Chapter 3, this spectral region is relevant for laser guide star applications (Na D2 line is at 589 nm) and various applications in medicine and life sciences.

3.2.1 Gain Mirror Design and Fabrication

The gain mirror (wafer ID AsN2897) for 1180 nm SDL comprised five pairs of 7 nm GaInNAs QWs and a 25.5-pair AlAs/GaAs DBR, as shown in Figure 3.1. Strain-compensating GaNAs layers surrounded and separated the QWs in the QW pairs. The GaInNAs and GaNAs layers were grown at low growth temperature of 460 °C as measured by thermocouple located between the substrate and the heater element behind the substrate. Low growth temperature is important for kinetically limiting phase separation as well as the strain relaxation of the highly compressive QWs [15, 23, 185, 186]. After the growth, the wafer was in-situ annealed in the manipulator at 680 °C (as measured by a pyrometer) and under As pressure for 7 min. Annealing (see Chapter 2.3) is important for improving the material quality of GaInNAs and was carried out for all laser structures reported in this thesis.

Figure 3.3 shows room temperature reflectivity and photoluminescence spectra of the as-grown gain mirror and their evolution with increasing temperature. The detuning between intrinsic QW PL peak wavelength (1146 nm as measured from a separate calibration sample) and the designed operation wavelength was 34 nm at room temperature. The gain mirror PL was affected by the resonant semiconductor structure, as revealed by the narrower linewidth and increased wavelength (1170 nm) as compared with the calibration sample. It shifted with temperature at a rate of 0.3 nm/K while the reflectivity stop-band redshifted at a rate of 0.06 nm/K. Thus, the detuning between QW absorption edge and the resonance wavelength was decreased with increasing temperature as shown by the increased resonance enhanced absorption dip in the stop-band. The gain mirror PL intensity, however, decreased with increasing temperature regardless of the improving resonance, probably due to increased rate of nonradiative recombination. The PL peak and absorption dip wavelengths reached 1182 nm at 85 °C, which corresponds to lasing wavelength with 5 W output power (Figure 3.4).

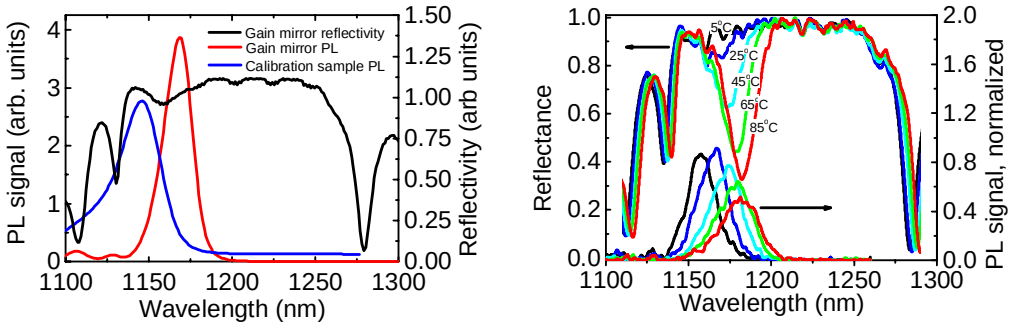

Figure 3.3. *Left: PL and reflectance spectrum measured from as-grown gain mirror surface. PL measured from a separate QW calibration sample shows the QW emission without the effect of gain mirror microcavity. Right: Change of reflectance and PL spectra with increasing temperature. Setup did not allow temperatures above 85 °C.*

3.2.2 Laser Characterization

The output power characteristics for a V-cavity SDL with wedged AR coated diamond heat spreader are shown in Figure 3.4. [187] Laser showed a high output power of about 7 W at the mount temperature of 15 °C. The slope efficiency was 28 % as determined between the threshold pump power of 5 W and a pump power of 20 W. When the mount temperature was decreased to 5 °C, the threshold decreased to 4.4 W and the slope efficiency increased to 30 %. Pump and output powers were limited by the cooling capacity of TEC heat sink. The spectrum

was quite well centered at the target wavelength at high power operation (Figure 3.4). Redshift with increasing temperature took place at a rate of approximately 0.3 nm/K similar to PL measurements.

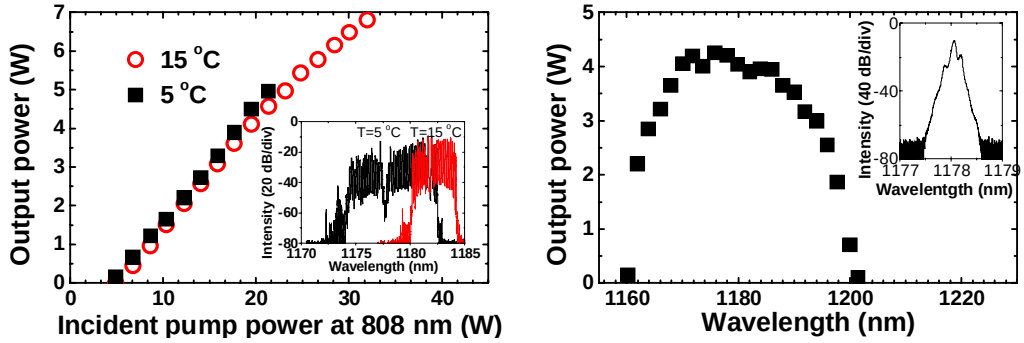

Figure 3.4. *Left: Power conversion characteristics of the 1.18 μm SDL with mount temperatures set to 5 and 15 °C. Output power was limited by the cooling capacity of the TEC heat sink. Inset: Output spectra measured at the two temperatures and at output power of 5.0 W. Right: Tuning characteristics of the 1.18 μm SDL at pump power of 21 W and mount temperature of 5 °C. Output power at different wavelengths as controlled by the intra-cavity birefringent filter. Inset shows the output spectrum tuned to 1178 nm.*

The tuning range of this laser was studied by placing a 3 mm quartz birefringent filter between the folding mirror and the output coupler. The tuning range, with over 2 W of output power, was 34 nm centered at 1180 nm. Figure 3.4 shows the output powers with respect to wavelengths selected by the filter. The Figure inset shows a spectrum tuned to 1178 nm. The spectrum still consisted of multiple Fabry-Pérot modes of the output coupler. Beam quality factors M^2 = 1.58 and 1.12 (in the horizontal and vertical directions, respectively) were measured for this laser with 5 W output power and emission tuned to 1178 nm.

Because the TEC cooling limited the output power in the first laser, the power scaling with the 1.18 μm gain mirror was characterized more thoroughly in a slightly different V-cavity, and with a water-cooled microchannel mount. [P3]

The first factor investigated was the output coupler transmission. The power conversion characteristics corresponding to different output couplers are shown in Figure 3.5. For these measurements, a pump spot with a diameter of D_{SPOT} = 320 μm and cooling water temperature of 16 °C were used. No lasing was achieved with the output coupler having the highest transmission of T_{OC} = 8%. As expected, the slope efficiency increased with increasing output

coupling as the parasitic cavity losses played less pronounced role in the total cavity losses [158]. However, roll-over was reached at smaller pump powers for the highest output coupling ratios. Possible explanation for this is the higher gain required to match the increased output coupling ratio, which means higher carrier concentration and, thus, higher rate of non-radiative recombination. Ultimately, the 1.5% output coupler resulted in the highest output power of 7.5 W at a pump power of 41.1 W. The maximum slope efficiency with 3.0% output coupling ratio was about 27%.

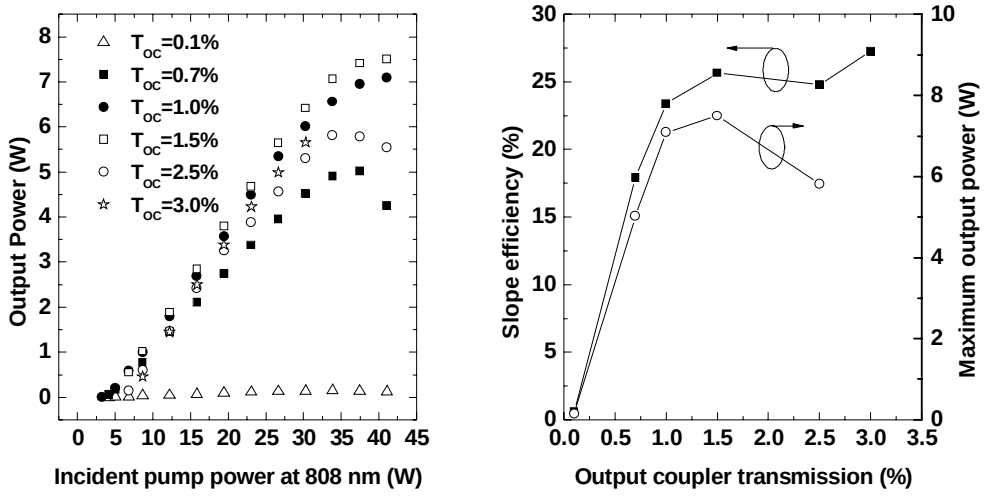

Figure 3.5. *Output characteristics of the 1.18 µm SDL with cooling water temperature set to 16 °C and pump spot diameter of D_{SPOT} = 320 µm. Slope efficiency was determined from linear fits in the range between threshold and a pump power of 20 W.*

In order to further increase the output power, cooling water temperature was set to 1 °C. This was expected to alleviate deterioration of slope efficiency at high pump powers due to non-radiative recombination. Accordingly, the slope efficiency increased, especially with higher output coupling, and roll-over was shifted to higher pump powers. Maximum output power of over 9 W was achieved with 1.5 % output coupler as shown in Figure 3.6.

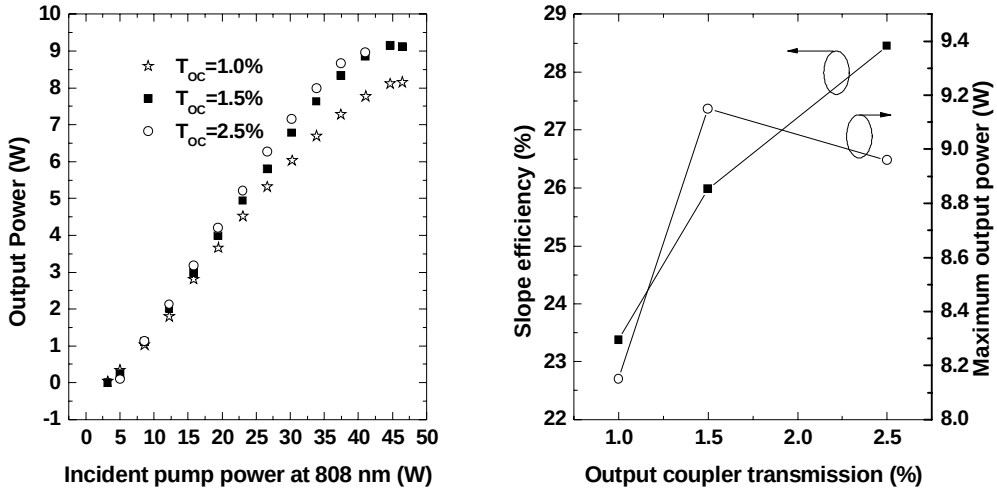

Figure 3.6. *Output characteristics of the 1.18 μm SDL with cooling water temperature set to 1 °C. Pump spot diameter was D_{SPOT} = 320 μm. Slope efficiency was determined from linear fits in the range between threshold and a pump power of 20 W.*

Next, different pump spot sizes were tested with cooling water temperature kept at 1 °C. Different output couplers were tested with each tested spot size, but the 1.5 % output coupler was found to be optimum, with respect to maximum achievable output power, in all cases. The pump spot size was changed by changing the focusing lens of the pump laser. Figure 3.7 shows that over 11 W of output power was generated by the SDL with the largest pump spot diameter of D_{SPOT} = 460 μm. As the figure suggests, this result was achieved due to a shift in the thermal roll-over point because the pump intensity for a given pump power decreased with increased pump spot size.

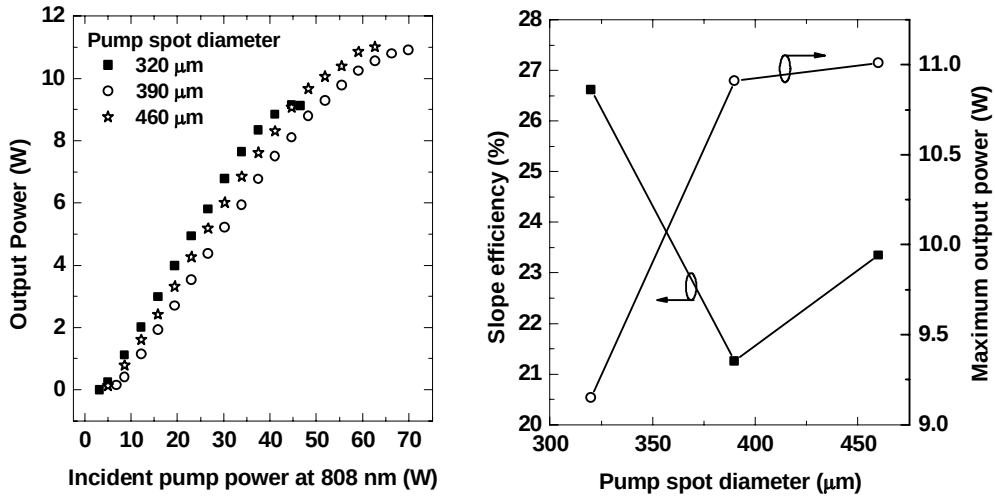

Figure 3.7. *Power conversion characteristics of the 1.18 µm gain mirror with different pump spot sizes. Cooling water temperature was set to 1 °C. Output coupler had a transmission of* T_{OC} *= 1.5 %.*

3.3 1.23 µm Semiconductor Disk Lasers

The 1.22–1.24 µm gain mirrors were developed for frequency doubled SDLs emitting at 610–620 nm. The advantages of frequency doubled red SDLs as compared to directly emitting red SDLs are the ability to reach shorter wavelengths (<630 nm) and readily available, efficient and affordable 808 nm pump diode lasers. As compared to direct red laser diodes, frequency doubled SDLs benefit from high-quality circular beam, higher power per emitter and freedom to choose emission wavelength. Here two gain mirror structures are reported. Gain mirror A (wafer ID AsN2527) was grown using VG Semicon V80H reactor, whereas VEECO GEN20 MBE reactor was used for fabricating gain mirror B (G1190).

3.3.1 Gain Mirror Design and Fabrication

The first 1.22 µm gain mirror (gain mirror A) had the same design as the 1.18 µm gain mirror described above (Figure 3.1), but with the optical thicknesses of GaAs and Al(Ga)As layers scaled to match the longer operation wavelength. In addition, window layer had slightly higher Al composition ($Al_{0.37}GaAs$) and higher number (29.5) of AlAs/GaAs DBR pairs was used. [P1]

The growth temperature, as measured by a thermocouple between the heater and the back surface of the substrate, was decreased to 470 °C for the QW growth. After the growth, the gain mirror was in-situ annealed in the manipulator at 680 °C and under As pressure for 5 min.

The PL and reflectance spectra measured for the as-grown gain mirror wafer are shown in Figure 3.8. For comparison, QW PL emission without semiconductor microcavity is plotted as measured from a gain mirror chip without DBR. The QW emission at room temperature and under low-intensity pumping was detuned by 26 nm from the design wavelength of 1220 nm and by 36 nm from 1230 nm, where the laser operated at higher powers.

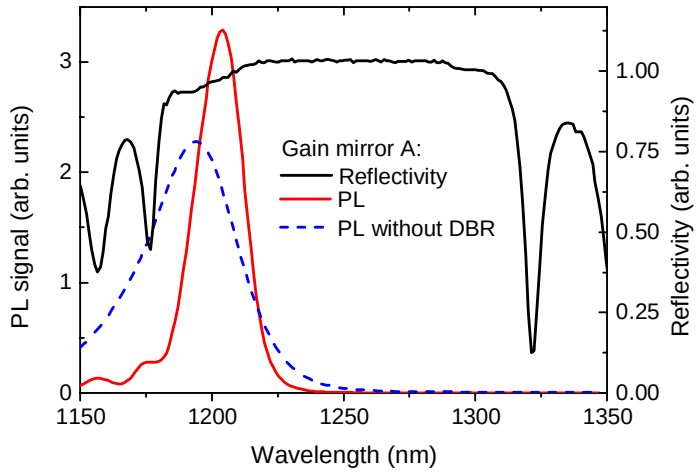

Figure 3.8. Room-temperature *PL and reflectance spectra measured from as-grown gain mirror A surface. PL spectrum measured from a chip without DBR reveals QW emission without microcavity enhancement.*

In addition to the gain mirror A described above and in [P1], another GaInNAs/GaAs gain mirror (gain mirror B) was fabricated more recently. The gain region design was updated and the structure (wafer ID G1190) was grown with a different MBE reactor. Similarly to the first gain mirror, this gain mirror comprised ten QWs. However, only one QW was positioned per optical standing wave antinode and no strain compensating GaNAs barrier layers were used (Figure 3.9). Because the GaAs barriers were higher in energy, band gap of the QWs had to be made smaller. On the other hand, nonradiative recombination in the GaNAs barriers, which has been suggested to be a major problem and cause of temperature sensitive operation [169] is

expected to be hindered. Total accumulated strain of the new gain region is expected to be higher than for the early gain mirror with strain compensation. On the other hand, the QWs were surrounded by relatively thick GaAs barriers, which stabilize the structure [170]. Still another change in the designs was the use of thin lattice matched InGaP window layer instead of $0.75x\lambda_{SDL}$ $Al_{0.37}GaAs$. The change was made, because thinner layers have smaller thermal resistance and the reduced window layer thickness of 50 nm is enough to confine the carriers to the active region. InGaP window layers are also used as etch-stop layers in flip-chips SDLs, which will be the next development stage.

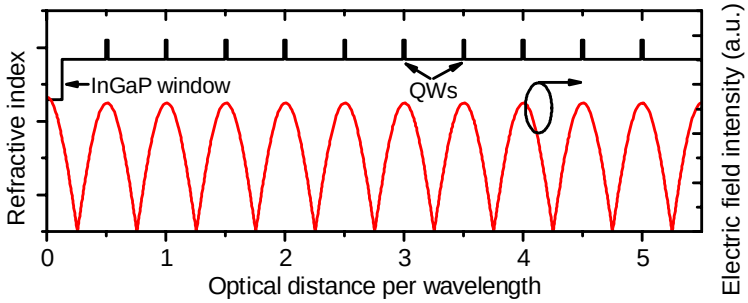

Figure 3.9. *Active region design for the gain mirror B operating at 1230 nm.*

One effect of changing the QW distribution from two QWs to one QW per antinode was the increase of active region thickness. This increased the pump absorption efficiency due to longer pump absorption length. The pump absorption efficiency can be estimated using GaAs absorption coefficient of 13900 cm^{-1} [159] and simplistic exponential decay of pump intensity due to pump absorption. For the gain mirror A, the active region thickness was 1510 nm, which corresponds to pump absorption efficiency of 88 % per single pass. The high absorption efficiency could be achieved due to thicker barriers around the bottommost QW pair which increased the absorption length (Figure 3.1). The active region thickness was 1930 nm for the gain mirror B with one QW per antinode, which corresponds roughly to 93 % pump absorption efficiency. With increasing cavity thickness, an issue with uneven carrier distribution could arise because pump intensity decreases exponentially away from the sample surface and excitation rate is thus smaller deeper in the structure. There is certain evidence [188], however, that carrier diffusion can even out the carriers across the active region, at least in samples with active region thicknesses around 1.5 µm. More experiments and modelling would be required to study the carrier distribution in the case of the lasers reported here.

The QWs of the gain mirror B were grown at low growth temperature of 375 °C (thermocouple set point 476 °C) in order to limit N related phase separation. As/III BEP ratio during the QW growth was 14, and growth rate was high for (1.383 µm/h) for keeping N composition low (Equation 2.5). The nominal QW composition was $GaIn_{0.31}N_{0.05}As$. The gain structure was annealed after growth in the MBE reactor for 4 minutes at 720 °C. The PL peak wavelength of an active region sample without DBR was 1189 nm. With respect to lasing wavelength at high output powers (Figure 3.12), the active region PL spectra was detuned by 41 nm.

3.3.2 Laser Characterization

The laser characterization of the 1.22 µm gain mirror A was started in a linear cavity and with a diamond heat spreader that had no AR coatings [P1]. With this setup the power conversion characteristics were measured at several cooling water temperatures ranging from 8 to 35 °C (Figure 3.10). Output coupling ratio was 1 %. Pump spot size on the gain mirror had a diameter of 180 µm. The maximum output power, limited by the available pump power, was 3.14 W at the minimum cooling water temperature of 8 °C. Slope efficiency, as determined between threshold pump power and a pump power of 10 W, was about 20 % at 8 °C and 16 % at 35 °C. Output spectra of this SDL at the maximum pump power are shown in Figure 3.10 for mount temperatures of 8 and 35 °C. The spectrum redshifted at a rate of 0.3 nm/°C.

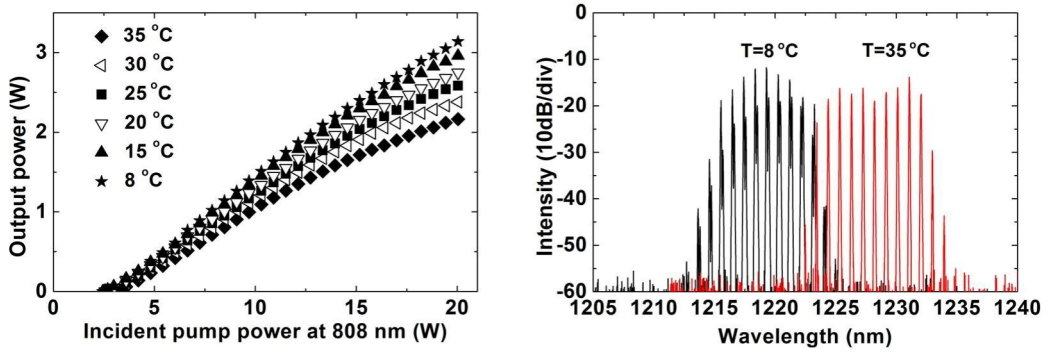

Figure 3.10. *Left: Power conversion characteristics of the 1.22 µm linear cavity SDL using gain mirror A and measured at different cooling water temperatures. Right: Output spectra of the SDL at two cooling water temperatures. Incident pump power was 20 W. [P1]*

After the successful initial characterization of the gain mirror A, the laser was arranged in a V-cavity set up. This SDL used the same gain mirror material but now the diamond was AR coated in order to reduce its etalon effect and to minimize the reflected and wasted pump power.

With this setup we were able to increase the pump spot diameter to 290 µm and to compare two different planar output couplers with transmissions of 1% and 2.5%. Because the output power of the linear cavity SDL was pump power limited, a more powerful 788 nm pump was used for this SDL. With the 2.5% output coupler, slope efficiency was higher (23 %) and this SDL reached an output power of over 5 W with 38 W of pump power corresponding to optical-to-optical conversion efficiency of 14 % (Figure 3.11).

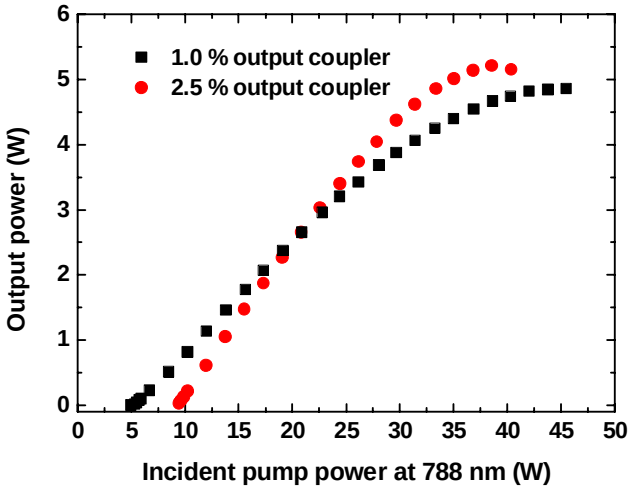

Figure 3.11. *Power conversion characteristics of the V-shaped 1.22 µm SDL using gain mirror A and characterized with two different output couplers. The cooling water temperature was set to 15 °C. [P1]*

The new gain mirror B was characterized in slightly different V-shaped cavity. The highly reflective folding mirror M1 had radius of curvature of 75 mm. The flat output coupler (OC) had a transmittance of 1 or 2.5 %. The cavity dimensions were D_{GM-M1} = 72 mm and D_{M1-OC} = 48 mm. Flat 300 µm AR-coated intra-cavity diamond was used for heat extraction from the gain mirror to a water cooled copper mount. The cooling water temperature was set to 16 °C. The gain mirror was pumped by an 808 nm laser. The pump spot diameter on the gain mirror was about 440 µm, whereas the simulated fundamental mode size on the gain mirror was 260 µm (tangential) and 300 µm (sagittal).

The SDL lased above threshold pump power of 5.8 W or 10.4 W corresponding to 1 or 2.5 % output couplers, respectively. The maximum output powers were almost the same for the two

output couplers (10.45 W–10.65 W). However, the 2.5 % output coupler gave better slope efficiency of 26 %, and thus the maximum output power of 10.45 W was reached at lower pump power of 57 W. This corresponds to optical- to-optical conversion efficiency of 18 %. This is a two-fold increase in the output power of 1.22–1.24 µm SDLs as compared with the first gain mirror and publication [P1]. Optical-to-optical conversion efficiency at maximum output power was increased by 5 % points.

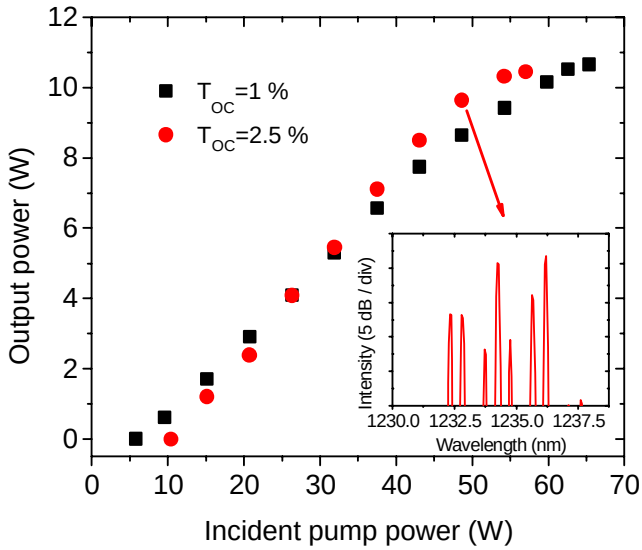

Figure 3.12. *Power conversion characteristics of the 1.23 µm SDL with the new gain mirror B and two different output couplers. The cooling water temperature was set to 16 °C and pumping wavelength was 808 nm.*

3.4 1.55 µm Semiconductor Disk Laser

The main driving force for developing 1.55 µm GaInNAsSb QWs on GaAs has been the need of a material system that enables monolithic fabrication of vertical cavity devices such as SDLs at this important wavelength. As compared with InP-based SDLs, GaAs-based devices benefit from superior refractive index contrast and high thermal conductivity of AlAs/GaAs DBRs. Here we demonstrate the first monolithic GaAs-based SDL operating at 1.55 µm using GaInNAsSb QWs [P5].

3.4.1 Gain Mirror Design and Fabrication

The 1.55 µm gain mirror comprised 4 pairs of GaInNAsSb quantum wells located at the antinodes of the optical standing wave formed in the resonant semiconductor microcavity [P5]. The lower number of QWs was chosen because this was the first time that we grew several QW pairs stacked at this wavelength, and we were not sure how we could maintain the material quality. The quantum wells within each pair were separated by 21 nm GaNAs layers, which also surrounded the QW pairs on the outer edges of the QW pairs. Pump absorbing GaAs barriers were used between the QW pairs. Below the active region, a monolithic 29.5-pair AlAs/GaAs DBR was acting as an end mirror of the laser cavity. Above the active region a 50 nm AlGaAs window layer confined the carriers to the active region. The QWs were grown at low temperature of 350 °C and the whole structure was annealed after growth at 730 °C for 30 minutes. The required annealing time was longer than that optimized and used for the GaInNAs gain mirros emitting around 1.2 µm. A possible explanation for this is that regardless of the use of Sb surfactant and low growth temperature, phase separation had taken place in the QWs during growth. Such QWs might require longer annealing time or higher annealing temperature to homogenize [15].

Reflectance and PL spectra measured from the as-grown gain mirror are shown in Figure 3.13. The high-reflectivity band was centered at 1530 nm. The target resonance wavelength for the semiconductor microcavity was 1545 nm and enhancement of gain mirror PL is seen at this wavelength. Figure 3.13 shows also a PL spectrum measured from a separate QW calibration sample grown before the gain mirror. This PL spectrum peaks at 1504 nm, which is very close to the PL peak wavelength of 1508 nm measured from the gain mirror. Detuning between the QW PL and lasing wavelengths was thus about 40 nm allowing redshift due to pump-induced heating of the gain mirror.

X-ray diffraction (XRD) rocking curve showed sharp and clear features (Figure 3.13) corresponding to simulated rocking curve (not shown). Dynamic fitting of a simulated rocking curve with a curve measured for the QW calibration sample indicated that the compressive QWs had a lattice misfit of -1.7 % while tensile GaNAs strain compensation layers had misfit of 0.45 % with respect to GaAs substrate. Thus the *thickness x misfit* product is similar but of opposite sign for QW pair (-24 nm%) and for the three GaNAs layers related to each QW pair (28 nm%). This means that the compressive strain of the QWs is roughly compensated by the

tensile strain of GaNAs barriers. Still, the compressive strain of the relatively thick DBR mirror was not compensated.

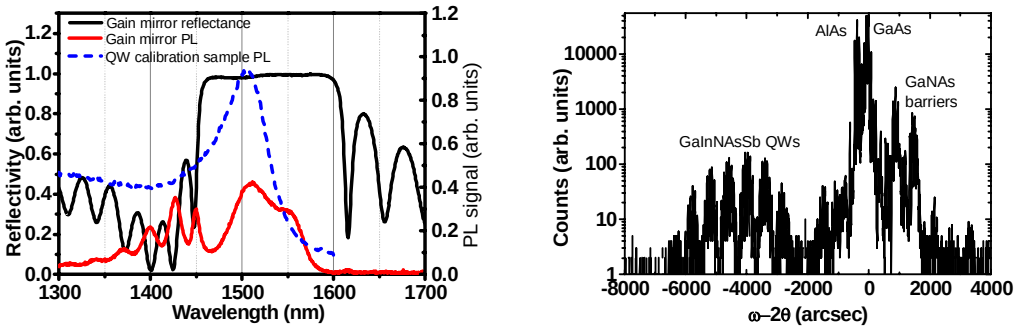

Figure 3.13. *Left: PL and reflectance spectra measured from the gain mirror wafer and PL spectrum measured from a separate QW sample grown using the same growth parameters. Right: X-ray diffraction rocking curve measured from the gain mirror wafer.*

3.4.2 Laser Characterization

Heat was conducted from the gain mirror to a water-cooled copper mount by a flat 300 µm capillary-bonded diamond heat spreader without coatings. The gain mirror was characterized in a straight cavity and with output coupler transmittance of less than 0.2 %. The gain mirror was pumped using an 808 nm diode laser.

1.55 µm SDL lased above threshold pump power of 10.3 W as shown in Figure 3.14. The maximum output power was 78 mW, which was achieved at a pump power of 30.2 W. The laser spectra, which consisted of several peaks due to intra-cavity etalon introduced by the uncoated diamond heat spreader, was centered at 1550 nm at an output power of 42 mW. During the characterization cooling water temperature was set to 1 °C, but the mount temperature increased to 16 °C at the highest pump powers.

Because of the limited output power in continuous wave (CW) mode, the SDL was characterized also in pulsed pump mode. The pump laser was pulsed by its current driver producing 1.5 µs pulses at a repetition rate of 10 kHz. In pulsed pump mode, average pump power is lower which alleviated problems related to gain mirror heating. In accordance, mount temperature corresponded closely to cooling water temperature. Here cooling water temperature was set to 16 °C. Thus mount temperatures were similar in pulsed mode and at the highest powers during CW operation. A maximum peak output power of 210 mW was achieved in

pulsed pump mode. The full width at half maximum (FWHM) duration of the output pulse at the maximum power was 0.94 µs and decreased with decreasing power as marked in Figure 3.14 for each measurement point.

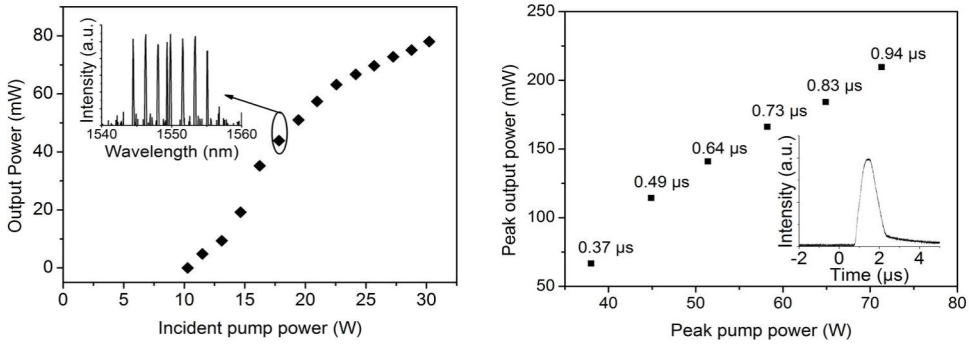

Figure 3.14. *Left: Output characteristics of the 1.55 µm SDL in CW mode. Right: Output characteristics in pulsed pump mode. The inset shows the output pulse shape at the maximum output power. [P5]*

There are many possible reasons for the low output power and efficiency of the 1.55 µm SDL. It is possible that the high N content used for the QWs has led to material quality problems and lower emission efficiency. On the other hand, it is also known that 1.55 µm GaInNAsSb QWs are more sensitive to temperature increase than GaInNAs at shorter wavelengths [169, 189]. This problem might be strengthened here by the heat load related to the large quantum defect between the pump and operation wavelengths. Comparing with the 1.23 µm gain mirrors, efficiency related to quantum defect $\eta_{quant} = \lambda_{pump}/\lambda_{SDL}$ was decreased from 66% to 52% due to longer emission wavelength. Moreover, it can be calculated using exponential pump intensity decay [159] that in the current design with 0.9 µm thick active region only 71 % of the pump power is absorbed in the active region and as much as 29 % is transmitted to the DBR. This pump absorption efficiency η_{abs} can be compared to 93 % calculated for 1.23 µm gain mirror B. By noting that the slope efficiency $\eta_{diff} = \eta_{out}\eta_{quant}\eta_{abs}$ is very much determined by absorption and quantum defect efficiencies, low output power and efficiency can be at least partly explained. Thus, it is expected that increasing active region thickness would improve the pump absorption efficiency and, as a result, also the overall efficiency of the laser. At the same time, the number of quantum wells could be increased. This should reduce the gain per QW required to reach the threshold, and thus, reduce the carrier density in each QW during lasing. The reduced carrier density should reduce the Auger recombination rate leading to higher

efficiency of the laser. On the other hand, the gain should be increased to allow operation at higher output coupling ratio. This would increase output efficiency η_{out}. High intracavity losses are another possible explanation for small differential efficiency and high threshold even at small output coupling ratio. With higher output coupling ratio, also the effect of intracavity loss would be hindered.. Still, further improvement of the pumping efficiency could be achieved by the use of antireflection coating to minimize the pump power that is reflected from the diamond surface. Roughly 15 % of the pump power was reflected from the first air-diamond interface, while the power reflected from an AR coated SDL gain mirror can be reduced to below 1 % by careful design. Longer pump wavelengths and alternative designs can also be considered for reducing the quantum defect. Also QW and barrier composition and material quality optimization should be continued for reducing threshold power and carrier density.

Chapter 4

1.18 µm DBR Laser Diode

Many applications would benefit from small visible lasers with high electro-optical conversion efficiency. For this reason, we have studied also 1.18 µm EELs. Similar to 1.18–1.24 µm SDLs, the work on EELs was motivated by frequency doubling to visible wavelengths.

Efficient frequency doubling requires typically high intensity, narrow spectrum and good beam quality. In SDLs these can be achieved inside the cavity, which is designed transversally single mode and includes components for spectral narrowing. Also external cavity EELs can be fabricated, but the most compact architecture is to form the laser cavity within the semiconductor chip and mount the nonlinear crystal in close proximity of the semiconductor chip [51]. In this case, wavelength control and operation in single longitudinal mode can be achieved monolithically by processing distributed feedback (DFB) or distributed Bragg reflector (DBR) gratings into the semiconductor cavity. Transversally single mode operation can be ensured by narrow ridge waveguide (RWG) structure with optimized etch depth. Single-mode operation is important in both directions because spectral bandwidth of the fundamental lasers should be in the range of 100 pm, and good beam quality is important for coupling into waveguide frequency doubling crystals or for frequency doubling efficiency when bulk crystals are used [51]. Miniaturization of frequency doubled EELs using bulk crystals can benefit from enhanced temperature stability of the fundamental laser. Miniaturization requires positioning the laser chip, which typically requires cooling, and nonlinear crystal, which are often designed to operate at elevated temperatures, close to each other. For most compact devices these components should be placed on the same heat sink. [51]

Single-mode DBR lasers at ~1060 nm and based on InGaAs QWs on GaAs can emit over 700 mW [190] and show high reliability [191]. By using tapered configuration, output powers up to 12 W at 979 nm have been demonstrated in single longitudinal mode and with good beam quality [192]. There are fewer reports on 1180 nm single mode lasers because of the high strain of InGaAs QWs at this wavelength. Still, 200 mW DBR laser emitting at 1180 nm and based on these QWs have been recently reported [9, 50]. By tapering, the output power at 1180 nm could be increased to 2 W [49].

As compared with InGaAs QWs, GaInNAs QWs offer lower lattice strain and better temperature stability due to higher conduction band offset. The temperature stability can be increased further by increasing number of QWs. This will be more straightforward using GaInNAs QWs with lower strain. Good operation of laser diodes at elevated temperatures could allow mounting of heated nonlinear crystals closer to laser chip and on the same mount. This would allow further miniaturization of frequency doubled laser diodes [51] or tuning by changing the temperature of the nonlinear crystal [52]. This chapter and publication [P6] describe the fabrication and characterization of a temperature-stable, high-power and single-mode GaInNAs/GaAs DBR laser diode emitting at 1180 nm.

4.1 Design and Fabrication

The semiconductor structure for the 1180 nm DBR laser (Figure 4.1) was grown on n-GaAs(100). A 7-nm $GaIn_{0.31}N_{0.005}As$ QW and 10 nm GaAs layers around it were grown at low temperature of 380 °C. Other layers were grown at normal growth conditions around 600 °C. The QW was embedded in the middle of 1 µm GaAs waveguide, which was clad by $Al_{0.25}GaAs$ claddings. Upper cladding was grown thinner for ease of DBR etching and for increasing heat conductivity through it to heat sink. Annealing treatment of 4 min at 719 °C was chosen based on test lasers annealed at different temperatures, as described in [P6].

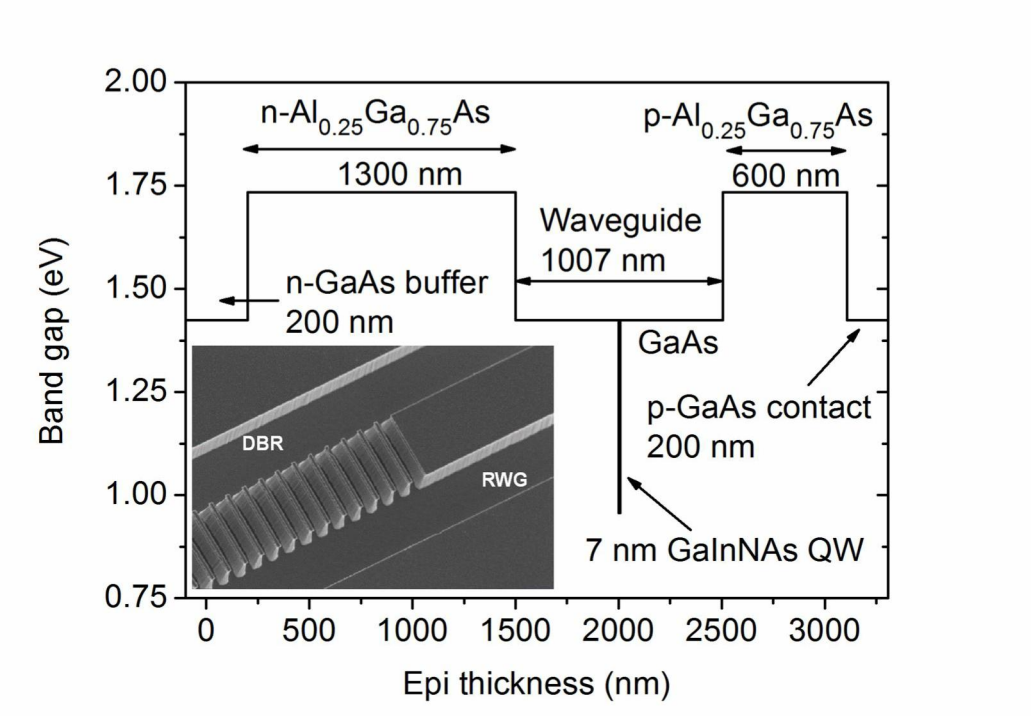

Figure 4.1. *Semiconductor heterostructure used for 1180 nm DBR laser. Inset shows a scanning electron microscope image taken from a DBR laser. RWG = Ridge wave guide.*

For studying gain material characteristics, part of the wafer was first processed into broad area oxide stripe lasers with stripe width of 83 µm and length of 1600 µm. Broad are lasers were mounted p-side upwards and were thus not optimized for high power CW operation. The actual DBR laser comprised a 2-mm long passive 3rd order DBR section whose reflectivity was estimated to be about 15 %. The passive DBR selected single longitudinal lasing mode and stabilized the wavelength. A 3-mm long ridge wave guide section with a ridge width of 3.2 µm provided gain for lasing in a single transversal mode (see inset of Figure 4.1). Heat extraction of the DBR lasers was improved by mounting them p-side down. Chips were first soldered with AuSn to AlN submount with thermal conductivity of 170 W/mK. The submount was then bonded on conductively cooled copper mount with indium solder. Both cleaved facets were AR coated.

4.2 Characterization

Broad area oxide stripe lasers showed good characteristics at elevated temperatures as described by high values of T_0 = 110 K and T_1 = 160 K, which describe stability of threshold current and slope efficiency, respectively, with increasing temperature [P6]. These parameters were measured in pulsed mode. Oxide stripe lasers showed good characteristics also in CW mode regardless of the p-side up mounting leading to poor cooling of active semiconductor junction: Oxide stripe laser reached an output power of 1.2 W (0.6 W per as-cleaved facet) with 31 % electro-optical conversion efficiency at mount temperature of 25 °C (Figure 4.2).

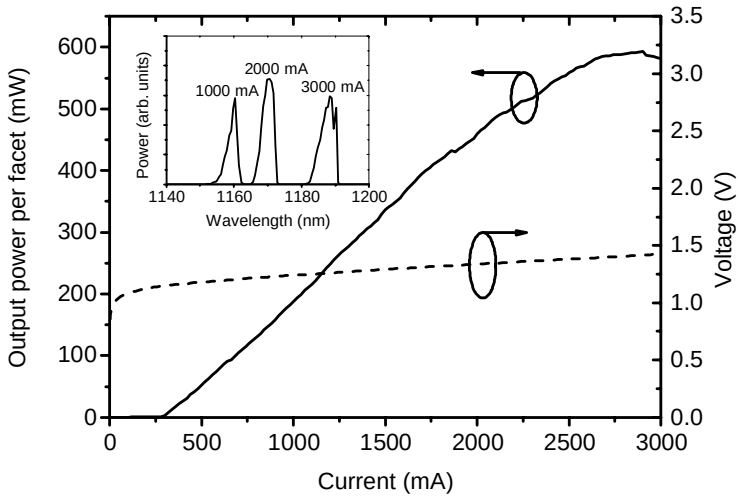

Figure 4.2. *CW characteristics for a p-up mounted broad area 83 µm x 1600 µm oxide stripe laser with mount temperature set to 25 °C.*

Output characteristics of the DBR laser are shown in Figure 4.3. The laser had a threshold current of 300 mA and emitted maximum power of 340 mW at a driving current of 1170 mA and forward voltage of 1.67 V. This corresponds to electro-optical conversion efficiency of 17 %. Maximum conversion efficiency of 20 % was reached at slightly lower power levels (driving current of 876 mA and output power of 269 mW).

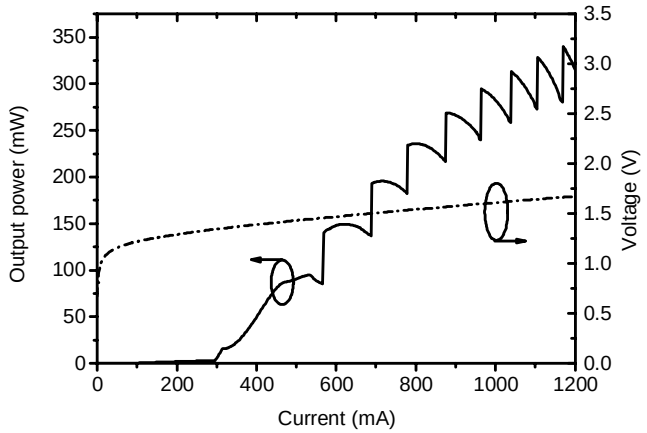

Figure 4.3. *Light-current-voltage characteristics of the 1180 nm DBR laser in CW mode and mount temperature set to 20 °C.*

High detuning between the peak wavelengths of the DBR reflectivity and semiconductor gain maximum was used for the DBR laser. Whereas the laser operated at 1180 nm, the amplified spontaneous emission (ASE) spectrum was centered at 1142 nm at room temperature and 500 mA driving current. Temperature-stable GaInNAs gain material combined with the high detuning allowed high-power operation at elevated temperatures; output powers measured at 1000 mA decreased only 30 % with temperature increase from 20 °C to 80 °C. Because of the high detuning threshold current decreased considerably when temperature was increased. Change of these laser characteristics with temperature is plotted in Figure 4.4.

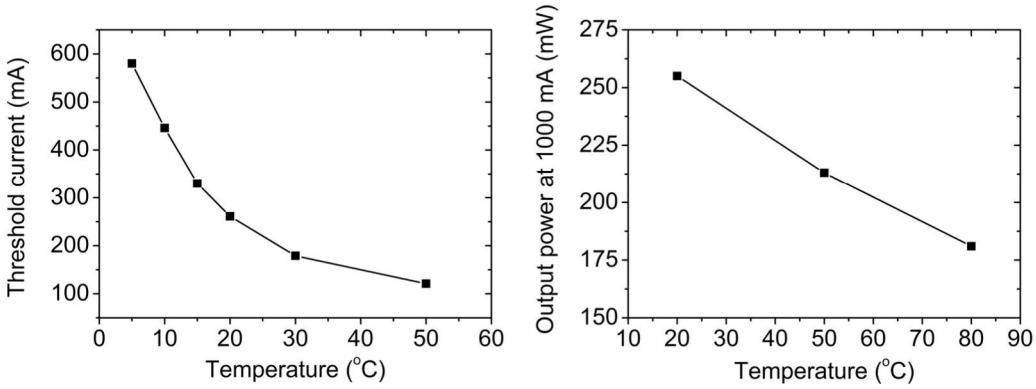

Figure 4.4. *Effect of mount temperature on threshold current (left) and output power measured at 1000 mA (right).*

The kinks observed in the output power (Figure 4.3) are related to change between consecutive longitudinal cavity modes, which redshift due to increasing active region temperature, matching the maximum DBR reflectivity [190]. Mode hops were observed also as abrupt changes of wavelength at the corresponding currents as shown in Figure 4.5. The output spectrum was centered at 1180 nm and was measured to have FWHM of 0.05 nm corresponding to resolution of the used optical spectrum analyzer. In reality spectrum might be even narrower but this is to be confirmed by dedicated linewidth measurements. Between the mode hops, lasing wavelength was tunable at a rate of 1.1 pm/mA while the average tuning rate was 0.5 pm/mA. The wavelength tuning rate with temperature was 0.1 nm/°C. Laser showed no degradation due to preliminary lifetime test where it was operated for 125 hours at drive current of 900 mA at mount temperature of 20 °C.

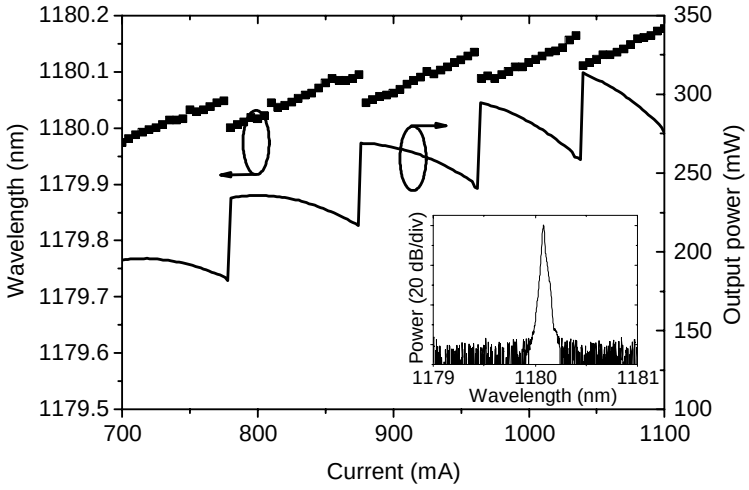

Figure 4.5. *Wavelength tuning with driving current. Change between consecutive lasing modes is seen as abrupt changes in wavelength and output power. Inset shows the output spectrum measured at 800 mA. [P6]*

These results show considerable improvement in terms of output power and temperature stability as compared with previous reports on 1180 nm laser diodes [9, 50]. Using tapered configuration, output power exceeding 2 W is expected [49]. Improved temperature stability provided by GaInNAs/GaAs lasers is expected to allow further miniaturization of frequency-doubled lasers, which is currently limited by thermal management issues.

Chapter 5

Conclusions

The topic of this thesis was the development of dilute nitride GaInNAs(Sb)/GaAs quantum well gain materials and their use in novel lasers emitting at new wavelengths important for applications. In particular, plasma-assisted MBE growth was studied and utilized for the fabrication of these structures. Special emphasis was put on the fabrication of lasers that can be frequency doubled to emit at the visible yellow-red part of the spectrum. This was realized by fabricating a single-mode DBR laser diode emitting at 1180 nm corresponding to yellow frequency doubled wavelength and semiconductor disk lasers emitting at 1180–1240 nm corresponding to yellow–red wavelengths. In addition, we expanded the wavelength coverage of GaAs-based disk laser technology to 1550 nm.

The basis for the laser demonstrations was laid by good understanding of the basic properties and growth of GaInNAs(Sb). We studied the calibration of RF plasma sources [55], effect of Sb on the GaInNAsSb band gap [54] and effects of growth parameters, namely As/III BEP ratio [P2] and growth temperature [P4], on the N composition and short range ordering. In publication [P2], we showed that varying the As/III BEP ratio controls the short range ordering in GaInNAs. Short range ordering is a major factor affecting emission wavelength of GaInNAs. We could also show that growth temperature affects not only the short range ordering but also the N composition of GaInNAs [P4]. In order to model this effect, we treated N incorporation as a thermally activated process and refined a previously published [105] N incorporation model accordingly [P4].

The fabricated semiconductor disk lasers, whose development and characterization was reported in [P1], [P3] and in this thesis, were the first multi-watt SDLs emitting at 1180 nm and 1230 nm. Output powers at both wavelengths exceeded 10 W. These SDLs were also efficiently frequency doubled to produce multi-watt emission at the targeted yellow [P3] [29] and red [30-32] wavelengths. In addition to the visible wavelengths, we extended the wavelength coverage to other direction as well, namely to 1550 nm which is an important eye-safe optical communications wavelength. The demonstrated 1550 nm GaInNAsSb/GaAs SDL emits at the longest wavelength reported for GaAs-based SDLs although its efficiency and output power should still be increased [P5].

SDLs are suitable for achieving high power, beam quality and frequency doubling efficiency. Still some applications would benefit from smaller visible-emitting laser sources at the cost of reduced output power. For this reason we studied also fabrication of edge-emitting laser diodes. Again the work was motivated by applications at the visible wavelengths. In order to achieve high brilliance required by the frequency doubling crystals and some applications, we fabricated a single-mode DBR laser diode. This laser emitted record high output power of 340 mW at the target wavelength of 1180 nm [P6], which corresponds to frequency doubled yellow wavelength of 590 nm. This laser showed both higher power and enhanced temperature stability as compared with similar InGaAs/GaAs lasers without N [50].

Besides the demonstrated wavelength versatility, temperature-stability of laser characteristics and design flexibility are thought to be the main assets of the GaInNAsSb materials as compared with other gain material systems. Temperature stability is important especially in applications where miniaturization or high integration densities are required. These applications include frequency-doubled edge emitting lasers [51] and hybrid integration of GaInNAsSb/GaAs devices on silicon for photonic integrated circuits [193, 194]. Outside the scope of this thesis, multijunction solar cells are maybe the fastest growing application area where GaInNAsSb and the results of this work can be used. The design flexibility of GaInNAsSb/GaAs is well realized using plasma assisted molecular beam epitaxy, which allows relatively independent control of different growth parameters and elemental compositions.

Bibliography

[1] "Semiconductor laser market growing at 7.1% CAGR," *Semiconductor Today*, vol. 10, pp. 8, 2015.

[2] M. Kuznetsov, F. Hakimi, R. Sprague and A. Mooradian, "High-power (> 0.5-W CW) diode-pumped vertical-external-cavity surface-emitting semiconductor lasers with circular TEM00 beams," *Photonics Technology Letters, IEEE*, vol. 9, pp. 1063-1065, 1997.

[3] M. Kuznetsov, F. Hakimi, R. Sprague and A. Mooradian, "Design and characteristics of high-power (> 0.5-W CW) diode-pumped vertical-external-cavity surface-emitting semiconductor lasers with circular TEM 00 beams," *Selected Topics in Quantum Electronics, IEEE Journal Of*, vol. 5, pp. 561-573, 1999.

[4] S. Calvez, J. E. Hastie, M. Guina, O. G. Okhotnikov and M. D. Dawson, "Semiconductor disk lasers for the generation of visible and ultraviolet radiation," *Laser & Photonics Reviews*, vol. 3, pp. 407-434, 2009.

[5] H. Lindberg, A. Larsson and M. Strassner, "Single-frequency operation of a high-power, long-wavelength semiconductor disk laser," *Opt. Lett.*, vol. 30, pp. 2260-2262, Sep, 2005.

[6] A. Giesen and J. Speiser, "Fifteen years of work on thin-disk lasers: results and scaling laws," *Selected Topics in Quantum Electronics, IEEE Journal Of*, vol. 13, pp. 598-609, 2007.

[7] M. Kondow, K. Uomi, A. Niwa, T. Kitatani, S. Watahiki and Y. Yazawa, "GaInNAs: a novel material for long-wavelength-range laser diodes with excellent high-temperature performance," *Japanese Journal of Applied Physics*, vol. 35, pp. 1273, 1996.

[8] M. Kondow, T. Kitatani, S. Nakatsuka, M. C. Larson, K. Nakahara, Y. Yazawa, M. Okai and K. Uomi, "GaInNAs: a novel material for long-wavelength semiconductor lasers," *Selected Topics in Quantum Electronics, IEEE Journal Of*, vol. 3, pp. 719-730, 1997.

[9] F. Bugge, K. Paschke, G. Blume, D. Feise, U. Zeimer and M. Weyers, "Growth of laser diode structures with emission wavelength beyond 1100nm for yellow–green emission by frequency conversion," *J. Cryst. Growth*, vol. 414, pp. 205-209, 2015.

[10] I. Ho and G. Stringfellow, "Solubility of nitrogen in binary III–V systems," *J. Cryst. Growth*, vol. 178, pp. 1-7, 1997.

[11] H. Abu-Farsakh and J. Neugebauer, "Enhancing nitrogen solubility in GaAs and InAs by surface kinetics: An ab initio study," *Physical Review B*, vol. 79, pp. 155311, 2009.

[12] J. S. Harris, R. Kudrawiec, H. Yuen, S. Bank, H. Bae, M. Wistey, D. Jackrel, E. Pickett, T. Sarmiento and L. Goddard, "Development of GaInNAsSb alloys: growth, band structure, optical properties and applications," *Physica Status Solidi (B)*, vol. 244, pp. 2707-2729, 2007.

[13] H. B. Yuen, S. R. Bank, H. Bae, M. A. Wistey and J. S. Harris, "The role of antimony on properties of widely varying GaInNAsSb compositions," *J. Appl. Phys.*, vol. 99, 2006.

[14] E. Luna, A. Trampert, E. Pavelescu and M. Pessa, "Nitrogen-enhanced indium segregation in (Ga, In)(N, As)/GaAs multiple quantum wells grown by molecular-beam epitaxy," *New Journal of Physics*, vol. 9, pp. 405, 2007.

[15] W. McGee, R. Williams, M. Ashwin, T. Jones, E. Clarke, J. Zhang and S. Tomić, "Structure, morphology, and optical properties of Ga x In 1− x N 0.05 As 0.95 quantum wells: Influence of the growth mechanism," *Physical Review B*, vol. 76, pp. 085309, 2007.

[16] J. Miguel-Sánchez, Á Guzmán, A. Hierro, E. Muñoz, U. Jahn and A. Trampert, "Impact of nitrogen ion density on the optical and structural properties of MBE grown GaInNAs/GaAs (100) and (111)B quantum wells," in *Dilute III-V Nitride Semiconductors and Material Systems*, A. Erol, Ed. Springer Berlin Heidelberg, 2008, pp. 35-63.

[17] M. A. Wistey, S. R. Bank, H. B. Yuen, H. Bae and J. S. Harris Jr., "Nitrogen plasma optimization for high-quality dilute nitrides," *J. Cryst. Growth*, vol. 278, pp. 229-233, 5/1, 2005.

[18] M. Hugues, B. Damilano, J. Chauveau, J. Duboz and J. Massies, "Blue-shift mechanisms in annealed (Ga, In)(N, As)⁄ Ga As quantum wells," *Physical Review B,* vol. 75, pp. 045313, 2007.

[19] D. Bisping, D. Pucicki, M. Fischer, S. Höfling and A. Forchel, "Influence of arsenic flux on the annealing properties of GaInNAs quantum wells for long wavelength laser applications around 1.6 μm," *J. Cryst. Growth,* vol. 311, pp. 1715-1718, 2009.

[20] E. -. Pavelescu, T. Jouhti, M. Dumitrescu, P. J. Klar, S. Karirinne, Y. Fedorenko and M. Pessa. Growth-temperature-dependent (self-)annealing-induced blueshift of photoluminescence from 1.3 μm GaInNAs/GaAs quantum wells. *Appl. Phys. Lett. 83(8),* pp. 1497-1499. 2003.

[21] L. Fan, T. Hsu, M. Fallahi, J. T. Murray, R. Bedford, Y. Kaneda, J. Hader, A. R. Zakharian, J. V. Moloney and S. W. Koch, "Tunable watt-level blue-green vertical-external-cavity surface-emitting lasers by intracavity frequency doubling," *Appl. Phys. Lett.,* vol. 88, pp. 1117, 2006.

[22] J. Lee, S. Lee, T. Kim and Y. Park, "7 W high-efficiency continuous-wave green light generation by intracavity frequency doubling of an end-pumped vertical external-cavity surface emitting semiconductor laser," *Appl. Phys. Lett.,* vol. 89, pp. 241107-241107-3, 2006.

[23] L. Fan, C. Hessenius, M. Fallahi, J. Hader, H. Li, J. V. Moloney, W. Stolz, S. W. Koch, J. T. Murray and R. Bedford, "Highly strained InGaAs/GaAs multiwatt vertical-external-cavity surface-emitting laser emitting around 1170 nm," *Appl. Phys. Lett.,* vol. 91, 2007.

[24] E. Kantola, T. Leinonen, S. Ranta, M. Tavast, J. Penttinen and M. Guina, "1180nm VECSEL with 50 W output power," *Proc.SPIE,* vol. 9349, pp. 93490U-93490U-6, 2015.

[25] T. Frost, A. Banerjee, Kai Sun, Shun Lien Chuang and P. Bhattacharya, "InGaN/GaN Quantum Dot Red (lambda =630 nm) Laser," *Quantum Electronics, IEEE Journal Of,* vol. 49, pp. 923-931, Nov, 2013.

[26] J. Hastie, S. Calvez, M. Dawson, T. Leinonen, A. Laakso, J. Lyytikäinen and M. Pessa, "High power CW red VECSEL with linearly polarized TEM00 output beam," *Opt.Express,* vol. 13, pp. 77-81, 01, 2005.

[27] Y. Wang, Q. Zheng, Y. Yao and X. Chen, "Intracavity sum-frequency diode side-pumped all-solid-state generation yellow laser at 589 nm with an output power of 20.5 W," *Appl. Opt.,* vol. 52, pp. 1876-1880, Mar, 2013.

[28] Y. Feng, L. R. Taylor and D. B. Calia, "25 W Raman-fiber-amplifier-based 589 nm laser for laser guide star," *Opt.Express,* vol. 17, pp. 19021-19026, Oct, 2009.

[29] T. Leinonen, V. Korpijärvi, A. Härkönen and M. Guina, "7.4 W yellow GaInNAs-based semiconductor disk laser," *Electron. Lett.,* vol. 47, pp. 1139-1440, 2011.

[30] J. Rautiainen, A. Härkönen, V. -. Korpijärvi, P. Tuomisto, M. Guina and O. G. Okhotnikov, "2.7 W tunable orange-red GaInNAs semiconductor disk laser," *Optics Express,* vol. 15, pp. 18345-18350, 12/24, 2007.

[31] E. Kantola, T. Leinonen, J. Penttinen, V. Korpijärvi and M. Guina, "615 nm GaInNAs VECSEL with output power above 10 W," *Opt.Express,* vol. 23, pp. 20280-20287, Aug, 2015.

[32] J. Rautiainen, A. Harkonen, V. -. Korpijarvi, J. Puustinen, L. Orsila, M. Guina and O. G. Okhotnikov, "Red and UV generation using frequency-converted GaInNAs-based semiconductor disk laser," in *Conference on Lasers and Electro-Optics, 2009 and 2009 Conference on Quantum Electronics and Laser Science Conference.CLEO/QELS 2009.* 2009, pp. 1-2.

[33] C. E. Max, S. S. Olivier, H. W. Friedman, J. An, K. Avicola, B. V. Beeman, H. D. Bissinger, J. M. Brase, G. V. Erbert and D. T. Gavel, "Image improvement from a sodium-layer laser guide star adaptive optics system," *Science,* vol. 277, pp. 1649-1652, 1997.

[34] P. L. Wizinowich, D. Le Mignant, A. H. Bouchez, R. D. Campbell, J. C. Chin, A. R. Contos, M. A. van Dam, S. K. Hartman, E. M. Johansson and R. E. Lafon, "The WM Keck Observatory laser guide star adaptive optics system: overview," *Publications of the Astronomical Society of the Pacific,* vol. 118, pp. 297-309, 2006.

[35] J. N. Farahani, M. J. Schibler and L. A. Bentolila, "Stimulated emission depletion (STED) microscopy: from theory to practice," *Microscopy: Science, Technology, Applications and Education,* vol. 2, pp. 1539, 2010.

[36] C. F. Blodi, S. R. Russell, J. S. Pulido and J. C. Folk, "Direct and feeder vessel photocoagulation of retinal angiomas with dye yellow laser," *Ophthalmology,* vol. 97, pp. 791-797, 1990.

[37] W. G. Telford, E. Illy, H. Karlsson and P. Prabhat, "Orange laser sources for life sciences research," *Biophotonics*, vol. 17, pp. 2628, 2010.

[38] O. T. Tan, J. M. Carney, R. Margolis, Y. Seki, J. Boll, R. R. Anderson and J. A. Parrish, "Histologic responses of port-wine stains treated by argon, carbon dioxide, and tunable dye lasers: a preliminary report," *Arch. Dermatol.*, vol. 122, pp. 1016-1022, 1986.

[39] U. Steegmüller, M. Kühnelt, H. Unold, T. Schwarz, R. Schulz, S. Illek, I. Pietzonka, H. Lindberg, M. Schmitt and U. Strauss, "Green laser modules to fit laser projection out of your pocket," in *Lasers and Applications in Science and Engineering*, 2008, pp. 687117-687117-8.

[40] N. Madamopoulos and F. Papageorgiou, "Laser Based Projection System for Displays, Signageand Illumination," *J.Display Technol.*, vol. 10, pp. 804-811, Oct, 2014.

[41] T. J. Dougherty, C. J. Gomer, B. W. Henderson, G. Jori, D. Kessel, M. Korbelik, J. Moan and Q. Peng, "Photodynamic therapy," *J. Natl. Cancer Inst.*, vol. 90, pp. 889-905, Jun 17, 1998.

[42] L. Brancaleon and H. Moseley, "Laser and non-laser light sources for photodynamic therapy," *Lasers in Medical Science*, vol. 17, pp. 173-186, 2002.

[43] A. Rantamäki, J. Rautiainen, A. Sirbu, A. Mereuta, E. Kapon and O. G. Okhotnikov, "1.56 µm 1 watt single frequency semiconductor disk laser," *Opt.Express*, vol. 21, pp. 2355-2360, Jan, 2013.

[44] G. Baili, L. Morvan, G. Pillet, S. Bouchoule, Z. Zhao, J. Oudar, L. Ménager, S. Formont, F. V. Dijk, M. Faugeron, M. Alouini, F. Bretenaker and D. Dolfi, "Ultralow Noise and High-Power VECSEL for High Dynamic Range and Broadband RF/Optical Links," *J. Lightwave Technol.*, vol. 32, pp. 3489-3494, Oct, 2014.

[45] A. Rantamäki, J. Rautiainen, J. Lyytik\ainen, A. Sirbu, A. Mereuta, E. Kapon and O. G. Okhotnikov, "1 W at 785 nm from a frequency-doubled wafer-fused semiconductor disk laser," *Opt.Express*, vol. 20, pp. 9046-9051, Apr, 2012.

[46] J. Lyytikainen, J. Rautiainen, A. Sirbu, V. Iakovlev, A. Laakso, S. Ranta, M. Tavast, E. Kapon and O. G. Okhotnikov, "High-Power 1.48-µm Wafer-Fused Optically Pumped Semiconductor Disk Laser," *Photonics Technology Letters, IEEE*, vol. 23, pp. 917-919, July, 2011.

[47] B. Qiu, S. McDougall, D. Yanson and J. H. Marsh, "Analysis of thermal performance of InGaP/InGaAlP quantum wells for high-power red laser diodes," *Opt. Quant. Electron.*, vol. 40, pp. 1149-1154, 2008.

[48] T. Onishi, K. Inoue, K. Onozawa, T. Takayama and M. Yuri, "High-power and high-temperature operation of Mg-doped AlGaInP-based red laser diodes," *Quantum Electronics, IEEE Journal Of*, vol. 40, pp. 1634-1638, 2004.

[49] K. Paschke, F. Bugge, G. Blume, D. Feise and G. Erbert, "High-power diode lasers at 1178 nm with high beam quality and narrow spectra," *Opt. Lett.*, vol. 40, pp. 100-102, 2015.

[50] K. Paschke, F. Bugge, G. Blume, D. Feise, W. John, S. Knigge, M. Matalla, H. Wenzel and G. Erbert, "Watt-level continuous-wave diode lasers at 1180 nm with InGaAs quantum wells," *Proc.SPIE*, vol. 8965, pp. 896509-896509-7, 2014.

[51] A. Jechow, R. Menzel, K. Paschke and G. Erbert, "Blue-green light generation using high brilliance edge emitting diode lasers," *Laser & Photonics Reviews*, vol. 4, pp. 633-655, 2010.

[52] K. A. Fedorova, G. S. Sokolovskii, P. R. Battle, D. A. Livshits and E. U. Rafailov, "574-647 nm wavelength tuning by second-harmonic generation from diode-pumped PPKTP waveguides," *Opt. Lett.*, vol. 40, pp. 835-838, Mar, 2015.

[53] N. Tansu and L. J. Mawst, "Current injection efficiency of InGaAsN quantum-well lasers," *J. Appl. Phys.*, vol. 97, pp. -, 2005.

[54] A. Aho, V. -. Korpijärvi, R. Isoaho, P. Malinen, A. Tukiainen, M. Honkanen and M. Guina, "Band gap and composition determination of GaInNAsSb compounds grown on GaAs by molecular beam epitaxy," *Journal of Crystal Growth*, Submitted.

[55] A. Aho, V. -. Korpijärvi, A. Tukiainen, J. Puustinen and M. Guina. Incorporation model of N into GaInNAs alloys grown by radio-frequency plasma-assisted molecular beam epitaxy. *J. Appl. Phys. 116(21)*, 2014.

[56] I. Vurgaftman and J. Meyer, "Band parameters for nitrogen-containing semiconductors," *J. Appl. Phys.*, vol. 94, pp. 3675-3696, 2003.

[57] W. Walukiewicz, W. Shan, J. Wu, K. M. Yu and J. W. Ager III, "Chapter 10 - band anticrossing and related electronic structure in III-N-V alloys," in *Dilute Nitride Semiconductors*, M. Henini, Ed. Amsterdam: Elsevier, 2005, pp. 325-359.

[58] E. P. O'Reilly, A. Lindsay, S. Fahy, S. Tomić and P. J. Klar, "Chapter 11 - A tight-binding based analysis of the band anti-crossing model and its application in ga(in)NAs alloys," in *Dilute Nitride Semiconductors*, M. Henini, Ed. Amsterdam: Elsevier, 2005, pp. 361-391.

[59] W. Walukiewicz, K. Alberi, J. Wu, W. Shan, K. M. Yu and Ager,J.W.,,III, "Electronic band structure of highly mismatched semiconductor alloys," in , A. Erol, Ed. Springer Berlin Heidelberg, 2008, pp. 65-89.

[60] I. Vurgaftman, J. Meyer and L. Ram-Mohan, "Band parameters for III–V compound semiconductors and their alloys," *J. Appl. Phys.*, vol. 89, pp. 5815-5875, 2001.

[61] W. Shan, W. Walukiewicz, J. W. Ager, E. E. Haller, J. F. Geisz, D. J. Friedman, J. M. Olson and S. R. Kurtz, "Band Anticrossing in GaInNAs Alloys," *Phys. Rev. Lett.*, vol. 82, pp. 1221-1224, Feb, 1999.

[62] V. Lordi, "Band-Edge Optical Properties of GaInNAs(Sb) and the Relation to Atomic Structure," pp. 215, 2004.

[63] I. Suemune, K. Uesugi and W. Walukiewicz, "Role of nitrogen in the reduced temperature dependence of band-gap energy in GaNAs," *Appl. Phys. Lett.*, vol. 77, pp. 3021-3023, 2000.

[64] P. Malinen, "GaInNAs-puolijohteen energia-aukon mallintaminen," pp. 30, 2013.

[65] S. R. Bank, H. Bae, L. L. Goddard, H. B. Yuen, M. A. Wistey, R. Kudrawiec and J. S. Harris, "Recent Progress on 1.55- μm Dilute-Nitride Lasers," *Quantum Electronics, IEEE Journal Of*, vol. 43, pp. 773-785, 2007.

[66] J. Harmand, G. Ungaro, L. Largeau and G. Le Roux, "Comparison of nitrogen incorporation in molecular-beam epitaxy of GaAsN, GaInAsN, and GaAsSbN," *Appl. Phys. Lett.*, vol. 77, pp. 2482-2484, 2000.

[67] T. Ma, Y. Lin and H. Lin, "Incorporation behaviors of group V elements in GaAsSbN grown by gas-source molecular-beam epitaxy," *J. Cryst. Growth*, vol. 310, pp. 2854-2858, 2008.

[68] V. Lordi, H. B. Yuen, S. R. Bank, M. A. Wistey, J. S. Harris and S. Friedrich, "Nearest-neighbor distributions in Ga 1− x In x N y As 1− y and Ga 1− x In x N y As 1− y− z Sb z thin films upon annealing," *Physical Review B*, vol. 71, pp. 125309, 2005.

[69] Y. Lin, T. Ma, T. Chen and H. Lin, "Energy gap reduction in dilute nitride GaAsSbN," *Appl. Phys. Lett.,* vol. 93, pp. -, 2008.

[70] S. Adachi, "Band gaps and refractive indices of AlGaAsSb, GaInAsSb, and InPAsSb: Key properties for a variety of the 2–4-μm optoelectronic device applications," *J. Appl. Phys.,* vol. 61, pp. 4869-4876, 1987.

[71] J. Wu, W. Shan and W. Walukiewicz, "Band anticrossing in highly mismatched III–V semiconductor alloys," *Semiconductor Science and Technology,* vol. 17, pp. 860, 2002.

[72] K. M. Yu, S. V. Novikov, R. Broesler, I. N. Demchenko, J. D. Denlinger, Z. Liliental-Weber, F. Luckert, R. W. Martin, W. Walukiewicz and C. T. Foxon, "Highly mismatched crystalline and amorphous GaN1−xAsx alloys in the whole composition range," *J. Appl. Phys.,* vol. 106, pp. -, 2009.

[73] G. Jaschke, R. Averbeck, L. Geelhaar and H. Riechert, "Low threshold InGaAsN/GaAs lasers beyond 1500 nm," *J. Cryst. Growth,* vol. 278, pp. 224-228, 5/1, 2005.

[74] S. B. Zhang and S. Wei, "Nitrogen solubility and N-induced defect complexes in epitaxial GaAs : N," *Physica B: Condensed Matter,* vol. 308–310, pp. 839-842, 12, 2001.

[75] S. Zhang and A. Zunger, "Surface-reconstruction-enhanced solubility of N, P, As, and Sb in III-V semiconductors," *Appl. Phys. Lett.,* vol. 71, pp. 677-679, 1997.

[76] M. Albrecht, H. Abu-Farsakh, T. Remmele, L. Geelhaar, H. Riechert and J. Neugebauer, "Compositional correlation and anticorrelation in quaternary alloys: Competition between bulk thermodynamics and surface kinetics," *Phys. Rev. Lett.,* vol. 99, pp. 206103, 2007.

[77] J. S. Harris Jr., H. Yuen, S. Bank, M. Wistey, V. Lordi, T. Gugov, H. Bae and L. Goddard, "Chapter 1 - MBE growth and characterization of long wavelength dilute nitride III–V alloys," in *Dilute Nitride Semiconductors*, M. Henini, Ed. Amsterdam: Elsevier, 2005, pp. 1-92.

[78] K. Kim and A. Zunger, "Spatial correlations in GaInAsN alloys and their effects on band-gap enhancement and electron localization," *Phys. Rev. Lett.,* vol. 86, pp. 2609, 2001.

[79] P. J. Klar, H. Grüning, J. Koch, S. Schäfer, K. Volz, W. Stolz, W. Heimbrodt, A. M. K. Saadi, A. Lindsay and E. P. O'Reilly, "(Ga, In)(N, As)-fine structure of the band gap due to nearest-neighbor configurations of the isovalent nitrogen," *Phys.Rev.B*, vol. 64, 09, 2001.

[80] J. Duboz, J. Gupta, Z. Wasilewski, J. Ramsey, R. Williams, G. Aers, B. Riel and G. Sproule, "Band-gap energy of In x Ga 1-x N y As 1-y as a function of N content," *Physical Review B*, vol. 66, pp. 085313, 2002.

[81] V. Lordi, V. Gambin, S. Friedrich, T. Funk, T. Takizawa, K. Uno and J. S. Harris, "Nearest-neighbor configuration in (GaIn)(NAs) probed by X-ray absorption spectroscopy," *Phys. Rev. Lett.*, vol. 90, pp. 145505, 2003.

[82] H. Liu, N. Xiang and S. Chua, "Influence of N incorporation on In content in GaInNAs⁄ GaNAs quantum wells grown by plasma-assisted molecular beam epitaxy," *Appl. Phys. Lett.*, vol. 89, pp. 071905, 2006.

[83] S. Rubini, G. Bais, A. Cristofoli, M. Piccin, R. Duca, C. Nacci, S. Modesti, E. Carlino, F. Martelli and A. Franciosi, "Nitrogen-induced hindering of In incorporation in InGaAsN," *Appl. Phys. Lett.*, vol. 88, pp. 141923-141923-3, 2006.

[84] E. Tournie, M. Pinault, S. Vezian, J. Massies and O. Tottereau, "Long wavelength GaInNAs/GaAs quantum-well heterostructures grown by solid-source molecular-beam epitaxy," *Appl. Phys. Lett.*, vol. 77, pp. 2189-2191, 2000.

[85] H. F. Liu, S. Karirinne, C. S. Peng, T. Jouhti, J. Konttinen and M. Pessa, "In situ annealing effect on the structural properties of near-surface GaInNAs/GaAs quantum wells," *J. Cryst. Growth*, vol. 263, pp. 171-175, 3/1, 2004.

[86] B. Damilano, J. Barjon, J. -. Duboz, J. Massies, A. Hierro, J. -. Ulloa and E. Calleja, "Growth and in situ annealing conditions for long-wavelength (Ga, In)(N, As)/GaAs lasers," *Appl. Phys. Lett.*, vol. 86, pp. -, 2005.

[87] J. Pakarinen, C. S. Peng, J. Puustinen, P. Laukkanen, V. -. Korpijarvi, A. Tukiainen and M. Pessa, "Postgrowth annealing of GaInAs/GaAs and GaInAsN/GaAs quantum well samples placed in a proximity GaAs box: A simple method to improve the crystalline quality," *Appl. Phys. Lett.*, vol. 92, pp. 232105, 2008.

[88] H. Liu, C. Peng, E. Pavelescu, T. Jouhti, S. Karirinne, J. Konttinen and M. Pessa, "Annealing effects on optical and structural properties of 1.3-μm GaInNAs/GaAs quantum-well samples capped with dielectric layers," *Appl. Phys. Lett.*, vol. 84, pp. 478-480, 2004.

[89] H. Liu, C. Peng, J. Likonen, T. Jouhti, S. Karirinne, J. Konttinen and M. Pessa, "Influence of nitride and oxide cap layers upon the annealing of 1.3 μm GaInNAs/GaAs quantum wells," *J. Appl. Phys.*, vol. 95, pp. 4102-4104, 2004.

[90] H. Liu, N. Xiang, S. Chua and M. Pessa, "Structural and optical properties of GaInAs/GaAs and GaInNAs/GaNAs multiple quantum wells upon postgrowth annealing," *Appl. Phys. Lett.*, vol. 88, pp. 181912-181912-3, 2006.

[91] C. Peng, E. Pavelescu, T. Jouhti, J. Konttinen, I. Fodchuk, Y. Kyslovsky and M. Pessa, "Suppression of interfacial atomic diffusion in InGaNAs/GaAs heterostructures grown by molecular-beam epitaxy," *Appl. Phys. Lett.*, vol. 80, pp. 4720-4722, 2002.

[92] E. Pavelescu, C. Peng, T. Jouhti, J. Konttinen, W. Li, M. Pessa, M. Dumitrescu and S. Spanulescu, "Effects of insertion of strain-mediating layers on luminescence properties of 1.3-μm GaInNAs/GaNAs/GaAs quantum-well structures," *Appl. Phys. Lett.*, vol. 80, pp. 3054-3056, 2002.

[93] M. A. Wistey, "Growth of 1.5 μm GaInNAsSb Vertical cavity surface emitting lasers by molecular beam epitaxy," pp. 1-219, 2005.

[94] N. Newman, "The energetics of the GaN MBE reaction: a case study of meta-stable growth," *J. Cryst. Growth*, vol. 178, pp. 102-112, 6/2, 1997.

[95] H. Carrere, A. Arnoult, A. Ricard, X. Marie, T. Amand and E. Bedel-Pereira, "Nitrogen-plasma study for plasma-assisted MBE growth of 1.3 μm laser diodes," *Solid-State Electronics*, vol. 47, pp. 419-423, 2003.

[96] J. M. Reifsnider, S. Govindaraju and A. L. Holmes Jr, "Use of optical emission intensity to characterize an RF plasma source for MBE growth of GaAsN," *J. Cryst. Growth*, vol. 243, pp. 396-403, 2002.

[97] M. M. Oye, T. J. Mattord, G. A. Hallock, S. R. Bank, M. A. Wistey, J. M. Reifsnider, A. J. Ptak, H. B. Yuen, J. S. Harris and A. L. Holmes, "Effects of different plasma species (atomic N, metastable N 2*, and ions) on the optical properties of dilute nitride materials grown by plasma-assisted molecular-beam epitaxy," *Appl. Phys. Lett.*, vol. 91, pp. 191903-191903-3, 2007.

[98] E. Iliopoulos, A. Adikimenakis, E. Dimakis, K. Tsagaraki, G. Konstantinidis and A. Georgakilas, "Active nitrogen species dependence on radiofrequency plasma source operating parameters and their role in GaN growth," *J. Cryst. Growth*, vol. 278, pp. 426-430, 2005.

[99] T. Kikuchi, A. Somintac, O. Ariyada, M. Wada and T. Ohachi, "Role of excited nitrogen species in the growth of GaN by RF–MBE," *J. Cryst. Growth*, vol. 292, pp. 221-226, 2006.

[100] E. -. Pavelescu, J. Wagner, H. -. Komsa, T. T. Rantala, M. Dumitrescu and M. Pessa. Nitrogen incorporation into GaInNAs lattice-matched to GaAs: The effects of growth temperature and thermal annealing. *J. Appl. Phys. 98(8)*, 2005.

[101] R. Kudrawiec, E. -. Pavelescu, J. Andrzejewski, J. Misiewicz, A. Gheorghiu, T. Jouhti and M. Pessa. The energy-fine structure of GaInNAs⁄GaAs multiple quantum wells grown at different temperatures and postgrown annealed. *J. Appl. Phys. 96(5)*, pp. 2909-2913. 2004.

[102] S. Karirinne, E. Pavelescu, J. Konttinen, T. Jouhti and M. Pessa, "The behaviour of optical and structural properties of GaInNAs/GaAs quantum wells upon annealing," *New Journal of Physics*, vol. 6, 2004.

[103] Q. D. Zhuang, A. Krier and C. R. Stanley, "Strain enhancement during annealing of GaAsN alloys," vol. 101, pp. 103536, 2007.

[104] G. Stenuit and S. Fahy, "First-principles calculations of the mechanical and structural properties of GaNxAs1-x: Lattice and elastic constants," *Phys.Rev.B*, vol. 76, pp. 035201, jul, 2007.

[105] Z. Pan, L. H. Li, W. Zhang, Y. W. Lin and R. H. Wu, "Kinetic modeling of N incorporation in GaInNAs growth by plasma-assisted molecular-beam epitaxy," *Appl. Phys. Lett.*, vol. 77, pp. 214-216, 2000.

[106] V. Odnoblyudov, A. Kovsh, A. Zhukov, N. Maleev, E. Semenova and V. Ustinov, "Thermodynamic analysis of the growth of GaAsN ternary compounds by molecular beam epitaxy," *Semiconductor Science and Technology*, vol. 35, pp. 533-538, 2001.

[107] X. Kong, A. Trampert, E. Tournié and K. H. Ploog, "Decomposition in as-grown (Ga,In)(N,As) quantum wells," vol. 87, 2005.

[108] A. Hierro, J. -. Ulloa, J. -. Chauveau, A. Trampert, M. -. Pinault, E. Tournié, A. Guzmán, J. L. Sánchez-Rojas and E. Calleja, "Annealing effects on the crystal structure of GaInNAs quantum wells with large In and N content grown by molecular beam epitaxy," vol. 94, pp. 2319-2324, 2003.

[109] F. Ishikawa, A. Trampert and K. H. Ploog, "Low substrate temperature and low As-pressure growth concept for the molecular beam epitaxial growth of (Ga,In)(N,As) multiple quantum wells," *J. Cryst. Growth,* vol. 301–302, pp. 529-533, 4, 2007.

[110] J. Misiewicz, R. Kudrawiec and G. Sek, "Chapter 9 - photo- and electro-reflectance of III–V-N compounds and low dimensional structures," in *Dilute Nitride Semiconductors*, M. Henini, Ed. Amsterdam: Elsevier, 2005, pp. 279-324.

[111] M. Motyka, R. Kudrawiec and J. Misiewicz, "On the deepness of contactless electroreflectance probing in semiconductor structures," *Physica Status Solidi (a)*, vol. 204, pp. 354-363, 2007.

[112] R. Kudrawiec, G. Seęk, J. Misiewicz, D. Gollub and A. Forchel. Explanation of annealing-induced blueshift of the optical transitions in GaInAsN/GaAs quantum wells. *Appl. Phys. Lett. 83(14)*, pp. 2772-2774. 2003.

[113] J. Sandusky and S. Brueck, "A CW external-cavity surface-emitting laser," *Photonics Technology Letters, IEEE,* vol. 8, pp. 313-315, 1996.

[114] N. G. Basov, O. Bogdankevich and A. Grasyuk, "9B4 - Semiconductor lasers with radiating mirrors," *Quantum Electronics, IEEE Journal Of*, vol. 2, pp. 594-597, 1966.

[115] G. Stillman, M. Sirkis, J. Rossi, M. Johnson and N. Holonyak Jr, "VOLUME EXCITATION OF AN ULTRATHIN SINGLE-MODE CdSe LASER," *Appl. Phys. Lett.*, vol. 9, pp. 268-269, 1966.

[116] H. Le, S. Di Cecca and A. Mooradian, "Scalable high-power optically pumped GaAs laser," *Appl. Phys. Lett.*, vol. 58, pp. 1967-1969, 1991.

[117] W. Jiang, S. Friberg, H. Iwamura and Y. Yamamoto, "High powers and subpicosecond pulses from an external-cavity surface-emitting InGaAs/InP multiple quantum well laser," *Appl. Phys. Lett.*, vol. 58, pp. 807-809, 1991.

[118] W. Xiang, S. Friberg, K. Watanabe, S. Machida, Y. Sakai, H. Iwamura and Y. Yamamoto, "Sub-100 femtosecond pulses from an external-cavity surface-emitting InGaAs/InP multiple quantum well laser with soliton-effect compression," *Appl. Phys. Lett.*, vol. 59, pp. 2076-2078, 1991.

[119] R. Smith, "Theory of intracavity optical second-harmonic generation," *Quantum Electronics, IEEE Journal Of*, vol. 6, pp. 215-223, 1970.

[120] T. Raymond, W. Alford, M. Crawford and A. Allerman, "Intracavity frequency doubling of a diode-pumped external-cavity surface-emitting semiconductor laser," *Opt. Lett.*, vol. 24, pp. 1127-1129, 1999.

[121] U. Keller and A. C. Tropper, "Passively modelocked surface-emitting semiconductor lasers," *Physics Reports*, vol. 429, pp. 67-120, 2006.

[122] L. Fan, M. Fallahi, J. T. Murray, R. Bedford, Y. Kaneda, A. R. Zakharian, J. Hader, J. V. Moloney, W. Stolz and S. W. Koch, "Tunable high-power high-brightness linearly polarized vertical-external-cavity surface-emitting lasers," *Appl. Phys. Lett.*, vol. 88, pp. 021105, 2006.

[123] J. McInerney, A. Mooradian, A. Lewis, A. Shchegrov, E. Strzelecka, D. Lee, J. Watson, M. Liebman, G. Carey and B. Cantos, "High-power surface emitting semiconductor laser with extended vertical compound cavity," *Electron. Lett.*, vol. 39, pp. 523-525, 2003.

[124] M. Fallahi, L. Fan, Y. Kaneda, C. Hessenius, J. Hader, H. Li, J. V. Moloney, B. Kunert, W. Stolz, S. W. Koch, J. Murray and R. Bedford, "5-W Yellow Laser by Intracavity Frequency Doubling of High-Power Vertical-External-Cavity Surface-Emitting Laser," *Photonics Technology Letters, IEEE*, vol. 20, pp. 1700-1702, 10, 2008.

[125] E. Kantola, T. Leinonen, S. Ranta, M. Tavast and M. Guina, "High-efficiency 20 W yellow VECSEL," *Opt.Express*, vol. 22, pp. 6372-6380, Mar, 2014.

[126] K. Beernink, P. K. York, J. Coleman, R. Waters, J. Kim and C. Wayman, "Characterization of InGaAs-GaAs strained-layer lasers with quantum wells near the critical thickness," *Appl. Phys. Lett.*, vol. 55, pp. 2167-2169, 1989.

[127] J. Jiménez, "Laser diode reliability: crystal defects and degradation modes," *Comptes Rendus Physique*, vol. 4, pp. 663-673, 2003.

[128] J. Yong, J. M. Rorison and I. H. White, "1.3-μm quantum-well InGaAsP, AlGaInAs, and InGaAsN laser material gain: a theoretical study," *Quantum Electronics, IEEE Journal Of*, vol. 38, pp. 1553-1564, 2002.

[129] K. D. Choquette, J. F. Klem, A. J. Fischer, O. Blum, A. A. Allerman, I. Fritz, S. R. Kurtz, W. G. Breiland, R. Sieg and K. M. Geib, "Room temperature continuous wave InGaAsN quantum well vertical-cavity lasers emitting at 1.3 μm," *Electron. Lett.*, vol. 36, pp. 1388-1390, 2000.

[130] S. Calvez and N. Laurand, "Vertical cavity semiconductor optical amplifiers based on dilute nitrides," in *Dilute III-V Nitride Semiconductors and Material Systems*, A. Erol, Ed. Springer, 2008, pp. 525-561.

[131] O. Okhotnikov, T. Jouhti, J. Konttinen, S. Karirinne and M. Pessa, "1.5-μm monolithic GaInNAs semiconductor saturable-absorber mode locking of an erbium fiber laser," *Opt. Lett.*, vol. 28, pp. 364-366, 2003.

[132] J. -. Hopkins, S. A. Smith, C. W. Jeon, H. D. Sun, D. Burns, S. Calvez, M. D. Dawson, T. Jouhti and M. Pessa, "0.6 W CW GaInNAs vertical external-cavity surface emitting laser operating at 1.32 μm," *Electron. Lett.*, vol. 40, pp. 30-31, 2004.

[133] D. Bisping, D. Pucicki, S. Hofling, S. Habermann, D. Ewert, M. Fischer, J. Koeth and A. Forchel, "High-temperature high-power operation of GaInNAs laser diodes in the 1220–1240-nm wavelength range," *Photonics Technology Letters, IEEE*, vol. 20, pp. 1766-1768, 2008.

[134] S. L. Vetter, J. E. Hastie, V. -. Korpijarvi, J. Puustinen, M. Guina, O. Okhotnikov, S. Calvez and M. D. Dawson, "Short-wavelength GaInNAs/GaAs semiconductor disk lasers," *Electron. Lett.*, vol. 44, pp. 1069-1070, 2008.

[135] J. Konttinen, A. Härkönen, P. Tuomisto, M. Guina, J. Rautiainen, M. Pessa and O. Okhotnikov, "High-power (>1 W) dilute nitride semiconductor disk laser emitting at 1240 nm," *New Journal of Physics*, vol. 9, 2007.

[136] D. Bisping, D. Pucicki, M. Fischer, J. Koeth, C. Zimmermann, P. Weinmann, S. Hofling, M. Kamp and A. Forchel, "GaInNAs-based high-power and tapered laser diodes for pumping applications," *Selected Topics in Quantum Electronics, IEEE Journal Of*, vol. 15, pp. 968-972, 2009.

[137] G. C. Papen, W. M. Pfenninger and D. M. Simonich, "Sensitivity analysis of Na narrowband wind—temperature lidar systems," *Appl. Opt.*, vol. 34, pp. 480-498, 1995.

[138] E. B. Kim, W. Lee, C. Y. Park, D. Yu and S. E. Park, "Narrow linewidth 578 nm light generation using frequency-doubling with a waveguide PPLN pumped by an optical injection-locked diode laser," *Optics Express*, vol. 18, pp. 10308-10314, 2010.

[139] J. M. Schmitt, "Optical coherence tomography (OCT): a review," *Selected Topics in Quantum Electronics, IEEE Journal Of*, vol. 5, pp. 1205-1215, 1999.

[140] S. L. Vetter, L. J. McKnight, S. Calvez, M. D. Dawson, F. Fusari, A. A. Lagatsky, W. Sibbett, C. T. A. Brown, V. Korpijarvi, M. D. Guina, B. Richards, G. Jose and A. Jha, "GaInNAs semiconductor disk lasers as pump sources for Tm3+ (,Ho3+)-doped glass, crystal and fibre laser," in 2009, pp. 719317-11.

[141] E. Yoshida, N. Shimizu and M. Nakazawa, "A 40-GHz 0.9-ps regeneratively mode-locked fiber laser with a tuning range of 1530-1560 nm," *Photonics Technology Letters, IEEE*, vol. 11, pp. 1587-1589, 1999.

[142] D. J. Richardson, J. Nilsson and W. A. Clarkson, "High power fiber lasers: current status and future perspectives," *J Opt Soc Am B*, vol. 27, pp. B63-B92, Nov, 2010.

[143] D. Lorenser, D. J. H. C. Maas, H. J. Unold, A. -. Bellancourt, B. Rudin, E. Gini, D. Ebling and U. Keller, "50-GHz passively mode-locked surface-emitting semiconductor laser with 100-mW average output power," *Quantum Electronics, IEEE Journal Of*, vol. 42, pp. 838-847, 2006.

[144] Z. Zhao, S. Bouchoule, J. Song, E. Galopin, J. Harmand, J. Decobert, G. Aubin and J. Oudar, "Subpicosecond pulse generation from a 1.56 µm mode-locked VECSEL," *Opt. Lett.*, vol. 36, pp. 4377-4379, Nov, 2011.

[145] E. Gerster, C. Hahn, S. Lorch, S. Menzel and P. Unger, "Frequency-doubled GaAsSb/GaAs semiconductor disk laser emitting at 589 nm," in *Lasers and Electro-Optics Society, 2003. LEOS 2003. the 16th Annual Meeting of the IEEE*, 2003, pp. 981-982.

[146] E. Gerster, I. Ecker, S. Lorch, C. Hahn, S. Menzel and P. Unger, "Orange-emitting frequency-doubled GaAsSb/GaAs semiconductor disk laser," *J. Appl. Phys.*, vol. 94, pp. 7397-7401, 2003.

[147] T. D. Germann, A. Strittmatter, U. W. Pohl, D. Bimberg, J. Rautiainen, M. Guina and O. G. Okhotnikov, "Quantum-dot semiconductor disk lasers," *J. Cryst. Growth*, vol. 310, pp. 5182-5186, 11/15, 2008.

[148] J. Rautiainen, I. Krestnikov, M. Butkus, E. U. Rafailov and O. G. Okhotnikov, "Optically pumped semiconductor quantum dot disk laser operating at 1180 nm," *Opt. Lett.*, vol. 35, pp. 694-696, 2010.

[149] J. Rautiainen, I. Krestnikov, J. Nikkinen and O. G. Okhotnikov, "2.5 W orange power by frequency conversion from a dual-gain quantum-dot disk laser," *Opt. Lett.*, vol. 35, pp. 1935-1937, 2010.

[150] D. Al Nakdali, M. Gaafar, M. Shakfa, F. Zhang, M. Vaupel, K. Fedorova, A. Rahimi-Iman, E. Rafailov and M. Koch, "High-Power Operation of Quantum-Dot Semiconductor Disk Laser at 1180 nm," *Photonics Technology Letters, IEEE,* vol. 27, pp. 1128-1131, 2015.

[151] A. Rantamäki, G. S. Sokolovskii, S. A. Blokhin, V. V. Dudelev, K. K. Soboleva, M. A. Bobrov, A. G. Kuzmenkov, A. P. Vasil'ev, A. G. Gladyshev, N. A. Maleev, V. M. Ustinov and O. Okhotnikov, "Quantum dot semiconductor disk laser at 1.3 μm," *Opt. Lett.,* vol. 40, pp. 3400-3403, Jul, 2015.

[152] H. Lindberg, M. Strassner, E. Gerster and A. Larsson, "0.8 W optically pumped vertical external cavity surface emitting laser operating CW at 1550 nm," *Electron. Lett.,* vol. 40, pp. 601-602, 2004.

[153] J. Rautiainen, J. Lyytikäinen, A. Sirbu, A. Mereuta, A. Caliman, E. Kapon and O. G. Okhotnikov, "2.6 W optically-pumped semiconductor disk laser operating at 1.57-μm using wafer fusion," *Opt.Express,* vol. 16, pp. 21881-21886, Dec, 2008.

[154] J. Lyytikäinen, J. Rautiainen, L. Toikkanen, A. Sirbu, A. Mereuta, A. Caliman, E. Kapon and O. G. Okhotnikov, "1.3-μm optically-pumped semiconductor disk laser by wafer fusion," *Optics Express,* vol. 17, pp. 9047-9052, 2009.

[155] J. Rautiainen, L. Toikkanen, J. LyytikaInen, A. Sirbu, A. Mereuta, A. Caliman, E. Kapon and O. G. Okhotnikov, "Wafer fused optically-pumped semiconductor disk laser operating at 1220- nm," in *Lasers and Electro-Optics 2009 and the European Quantum Electronics Conference. CLEO Europe - EQEC 2009. European Conference On,* 2009, pp. 1-1.

[156] J. Tourrenc, S. Bouchoule, A. Khadour, J. Harmand, A. Miard, J. Decobert, N. Lagay, X. Lafosse, I. Sagnes, L. Leroy and J. Oudar, "Thermal optimization of 1.55 μm OP-VECSEL with hybrid metal–metamorphic mirror for single-mode high power operation," *Opt. Quant. Electron.,* vol. 40, pp. 155-165, 2008.

[157] A. Tropper and S. Hoogland, "Extended cavity surface-emitting semiconductor lasers," *Progress in Quantum Electronics,* vol. 30, pp. 1-43, 2006.

[158] A. Maclean, R. Birch, P. Roth, A. Kemp and D. Burns, "Limits on efficiency and power scaling in semiconductor disk lasers with diamond heatspreaders," *JOSA B,* vol. 26, pp. 2228-2236, 2009.

[159] S. Haupt, M. Furitsch, H. H. Lindberg, I. Pietzonka, U. Strauss and G. Bacher, "Analysis of the Pump Wavelength Dependence of a 1060-nm VECSEL," *Photonics Technology Letters, IEEE,* vol. 24, pp. 341-343, 2012.

[160] M. Schmid, S. Benchabane, F. Torabi-Goudarzi, R. Abram, A. I. Ferguson and E. Riis, "Optical in-well pumping of a vertical-external-cavity surface-emitting laser," *Appl. Phys. Lett.*, vol. 84, pp. 4860-4862, 2004.

[161] N. Schulz, M. Rattunde, C. Ritzenthaler, B. Rosener, C. Manz, K. Kohler, J. Wagner and U. Brauch, "Resonant optical in-well pumping of an (AlGaIn)(AsSb)-based vertical-external-cavity surface-emitting laser emitting at 2.35 μm," *Appl. Phys. Lett.*, vol. 91, pp. 091113-091113-3, 2007.

[162] W. Zhang, T. Ackemann, S. McGinily, M. Schmid, E. Riis and A. I. Ferguson, "Operation of an optical in-well-pumped vertical-external-cavity surface-emitting laser," *Appl. Opt.*, vol. 45, pp. 7729-7735, 2006.

[163] S. Beyertt, M. Zorn, T. Kübler, H. Wenzel, M. Weyers, A. Giesen, G. Tränkle and U. Brauch, "Optical in-well pumping of a semiconductor disk laser with high optical efficiency," *IEEE J. Quant. Electron.*, vol. 41, pp. 1439-1449, 2005.

[164] E. Kühn, A. Thränhardt, C. Bückers, S. W. Koch, J. Hader and J. V. Moloney. Numerical study of the influence of an antireflection coating on the operating properties of vertical-external-cavity surface-emitting lasers. *J. Appl. Phys. 106(6)*, 2009.

[165] T. Leinonen, *The Design and Fabrication of Lasing Semiconductor Nanostructures Employing Vertical-Cavity Geometry*. Tampere University of Technology, 2007.

[166] S. W. Corzine, R. S. Geels, J. W. Scott, R. Yan and L. A. Coldren, "Design of Fabry-Perot surface-emitting lasers with a periodic gain structure," *Quantum Electronics, IEEE Journal Of*, vol. 25, pp. 1513-1524, 1989.

[167] M. Y. A. Raja, S. R. Brueck, M. Osinski, C. F. Schaus, J. G. McInerney, T. Brennan and B. Hammons, "Resonant periodic gain surface-emitting semiconductor lasers," *Quantum Electronics, IEEE Journal Of*, vol. 25, pp. 1500-1512, 1989.

[168] S. Ranta, T. Hakkarainen, M. Tavast, J. Lindfors, T. Leinonen and M. Guina, "Strain compensated 1120 nm GaInAs/GaAs vertical external-cavity surface-emitting laser grown by molecular beam epitaxy," *J. Cryst. Growth*, vol. 335, pp. 4-9, 11/15, 2011.

[169] S. R. Bank, L. L. Goddard, M. A. Wistey, H. B. Yuen and J. S. Harris, "On the temperature sensitivity of 1.5-μm GaInNAsSb lasers," *Selected Topics in Quantum Electronics, IEEE Journal Of*, vol. 11, pp. 1089-1098, 09, 2005.

[170] D. Houghton, M. Davies and M. Dion, "Design criteria for structurally stable, highly strained multiple quantum well devices," *Appl. Phys. Lett.*, vol. 64, pp. 505-507, 1994.

[171] R. Paschotta, "Power scalability as a precise concept for the evaluation of laser architectures," *arXiv Preprint arXiv:0711.3987*, 2007.

[172] S. Giet, A. Kemp, D. Burns, S. Calvez, M. Dawson, S. Suomalainen, A. Harkonen, M. Guina, O. Okhotnikov and M. Pessa, "Comparison of thermal management techniques for semiconductor disk lasers," in *Lasers and Applications in Science and Engineering*, 2008, pp. 687115-687115-10.

[173] S. Smith, J. Hopkins, J. Hastie, D. Burns, S. Calvez, M. Dawson, T. Jouhti, J. Kontinnen and M. Pessa, "Diamond-microchip GaInNAs vertical external-cavity surface-emitting laser operating CW at 1315 nm," *Electron. Lett.*, vol. 40, pp. 935-936, 2004.

[174] J. Hastie, J. Hopkins, C. Jeon, S. Calvez, D. Burns, M. Dawson, R. Abram, E. Riis, A. Ferguson and W. Alford, "Microchip vertical external cavity surface emitting lasers," *Electron. Lett.*, vol. 39, pp. 1324-1326, 2003.

[175] A. J. Maclean, A. J. Kemp, S. Calvez, J. Kim, T. Kim, M. D. Dawson and D. Burns, "Continuous tuning and efficient intracavity second-harmonic generation in a semiconductor disk laser with an intracavity diamond heatspreader," *Quantum Electronics, IEEE Journal Of*, vol. 44, pp. 216-225, 2008.

[176] A. J. Kemp, J. Hopkins, A. J. Maclean, N. Schulz, M. Rattunde, J. Wagner and D. Burns, "Thermal management in 2.3-μm semiconductor disk lasers: a finite element analysis," *Quantum Electronics, IEEE Journal Of*, vol. 44, pp. 125-135, 2008.

[177] N. Schulz, J. Hopkins, M. Rattunde, D. Burns and J. Wagner, "High-brightness long-wavelength semiconductor disk lasers," *Laser & Photonics Reviews*, vol. 2, pp. 160-181, 2008.

[178] B. Heinen, T. -. Wang, M. Sparenberg, A. Weber, B. Kunert, J. Hader, S. W. Koch, J. V. Moloney, M. Koch and W. Stolz, "106 W continuous-wave output power from vertical-external-cavity surface-emitting laser," *Electronics Letters*, vol. 48, pp. 516-517, 2012.

[179] E. J. Saarinen, S. Suomalainen and O. G. Okhotnikov, "Power scalable semiconductor disk laser using multiple gain cavity," *Optics Express*, vol. 14, pp. 12868-12871, 2006.

[180] L. Fan, M. Fallahi, J. Hader, A. R. Zakharian, J. V. Moloney, J. T. Murray, R. Bedford, W. Stolz and S. W. Koch, "Multichip vertical-external-cavity surface-emitting lasers: a coherent power scaling scheme," *Opt. Lett.*, vol. 31, pp. 3612-3614, 2006.

[181] L. E. Hunziker, Q. Shu, D. Bauer, C. Ihli, G. J. Mahnke, M. Rebut, J. R. Chilla, A. L. Caprara, H. Zhou and E. S. Weiss, "Power-scaling of optically pumped semiconductor lasers," in *Lasers and Applications in Science and Engineering*, 2007, pp. 64510A-64510A-6.

[182] A. Härkönen, "Optically-pumped semiconductor disk lasers for generating visible and infrared radiation," *Tampereen Teknillinen Yliopisto.Julkaisu-Tampere University of Technology.Publication; 724*, 2008.

[183] A. Zakharian, J. Hader, J. Moloney and S. Koch, "VECSEL threshold and output power-shutoff dependence on the carrier recombination rates," *Photonics Technology Letters, IEEE*, vol. 17, pp. 2511-2513, 2005.

[184] J. L. Shen, C. Chang, W. Chou, M. Wu and Y. Chen, "Temperature dependence of the reflectivity in absorbing Bragg reflectors," *Optics Express*, vol. 9, pp. 287-293, 2001.

[185] B. Elman, E. S. Koteles, P. Melman, K. Ostreicher and C. Sung, "Low substrate temperature molecular beam epitaxial growth and the critical layer thickness of InGaAs grown on GaAs," *J. Appl. Phys.*, vol. 70, pp. 2634-2640, 1991.

[186] S. M. Wang, T. G. Andersson and M. J. Ekenstedt, "Temperature-dependent transition from two-dimensional to three-dimensional growth in highly strained InxGa1−xAs/GaAs ($0.36 \leq x \leq 1$) single quantum wells," *Appl. Phys. Lett.*, vol. 61, pp. 3139-3141, 1992.

[187] M. Guina, T. Leinonen, A. Härkönen and M. Pessa, "High-power disk lasers based on dilute nitride heterostructures," *New Journal of Physics*, vol. 11, pp. 125019, 2009.

[188] A. H. Quarterman and K. G. Wilcox, "Design of a solar-pumped semiconductor laser," *Optica*, vol. 2, pp. 56-61, Jan, 2015.

[189] D. G. McConville, S. J. Sweeney, A. R. Adams, S. Tomic and H. Riechert, "Temperature and pressure dependence of the recombination mechanisms in 1.3 μm and 1.5 μm GaInNAs lasers," *Physica Status Solidi (B)*, vol. 244, pp. 208-212, 2007.

[190] M. Achtenhagen, N. V. Amarasinghe and G. A. Evans, "High-power distributed Bragg reflector lasers operating at 1065nm," *Electronics Letters,* vol. 43, 2007.

[191] H. K. Nguyen, S. Coleman, N. J. Visovsky, Y. Li, K. Song, R. W. Davis, M. H. Hu and C. Zah, "Reliable high-power 1060nm DBR lasers for second-harmonic generation," *Electronics Letters,* vol. 43, pp. 716-717, 2007.

[192] C. Fiebig, G. Blume, C. Kaspari, D. Feise, J. Fricke, M. Matalla, W. John, H. Wenzel, K. Paschke and G. Erbert, "12W high-brightness single-frequency DBR tapered diode laser," *Electronics Letters,* vol. 44, pp. 1253-1255, 2008.

[193] G. Giannoulis, V. -. Korpijarvi, N. Iliadis, J. Makela, J. Viheriala, D. Apostolopoulos, M. Guina and H. Avramopoulos, "Bringing High-Performance GaInNAsSb/GaAs SOAs to True Data Applications," *Photonics Technology Letters, IEEE,* vol. 27, pp. 1691-1694, 2015.

[194] D. Fitsios, G. Giannoulis, V. -. Korpijärvi, J. Viheriälä, A. Laakso, N. Iliadis, S. Dris, M. Spyropoulou, H. Avramopoulos, G. T. Kanellos, N. Pleros and M. Guina, "High-gain 1.3 μm GaInNAs semiconductor optical amplifier with enhanced temperature stability for all-optical signal processing at 10 Gb/s," *Appl. Opt.,* vol. 54, pp. 46-52, Jan, 2015.

P1

Publication 1

V.-M. Korpijärvi, M. Guina, J. Puustinen, P. Tuomisto, J. Rautiainen, A. Härkönen, A. Tukiainen, O. Okhotnikov and M. Pessa, "MBE grown GaInNAs-based multi-Watt disk lasers," *Journal of Crystal Growth*, vol. 311, pp. 1868-1871, 2009.

Journal of Crystal Growth 311 (2009) 1868–1871

Contents lists available at ScienceDirect

Journal of Crystal Growth

journal homepage: www.elsevier.com/locate/jcrysgro

MBE grown GaInNAs-based multi-Watt disk lasers

V.-M. Korpijärvi [a,*], M. Guina [a], J. Puustinen [a], P. Tuomisto [b], J. Rautiainen [a], A. Härkönen [a], A. Tukiainen [a], O. Okhotnikov [a], M. Pessa [a]

[a] Optoelectronics Research Centre, Tampere University of Technology, P.O. Box 692, FIN-33101 Tampere, Finland
[b] EpiCrystals Inc., Sinitaival 6, Tampere FIN-33720, Finland

ARTICLE INFO

Available online 5 November 2008

Keywords:
A3. Molecular beam epitaxy
A3. Quantum wells
B2. Semiconductor III–V materials
B3. Semiconductor lasers

ABSTRACT

We report the fabrication and characterization of high-quality GaInNAs/GaAs gain mirror as an active media for semiconductor disk lasers emitting at the 12XX nm spectral range. The structure was fabricated by molecular beam epitaxy using a radio frequency plasma source for incorporating the nitrogen. The growth parameters have been optimized to reduce detrimental effects of nitrogen on the emission efficiency. Using the gain mirror, which comprised 10 GaInNAs quantum wells with a relatively low content of nitrogen, we demonstrated semiconductor disk laser with an output power of ~5 W and a differential efficiency of ~20%.

1. Introduction

Optically pumped semiconductor disk lasers (SDLs), also known as vertical external cavity surface emitting lasers (VECSELs), have recently sparked a high scientific and industrial interest particularly due to their potential for high-power visible light generation. These lasers exhibit many advantageous features, such as the wavelength versatility offered by a semiconductor gain material, the possibility to use optical pumping with low-cost multi-mode diode lasers, remarkable capabilities for high-power operation and power scaling, while preserving a high quality of the output beam and the possibility to use nonlinear crystals for intra-cavity frequency doubling. Intra-cavity frequency doubled 940–1060 nm InGaAs/GaAs disk lasers have been studied intensively. They can currently generate multi-Watt power at blue [1] and green [2] wavelengths. On the contrary, the generation of high-power red laser radiation using SDLs still remains a challenge that requires an efficient source emitting at a fundamental wavelength of 1.2X μm.

The lattice mismatch between InGaAs and GaAs makes it difficult to reach an emission wavelength beyond 1180 nm [3]. The spectral region between 1200 nm $< \lambda <$ 1300 nm can be covered by introducing a small amount of nitrogen into the InGaAs/GaAs quantum wells (QWS) [4]. Similar to the InGaAs/GaAs compound, dilute nitride GaInNAs/GaAs takes advantage of high-reflectivity GaAs/AlAs distributed Bragg reflectors (DBRs). GaAsSb/GaAs QWs can also be used with the GaAs-based DBRs [5]. However, the dilute nitride QWs are preferred because of their stronger carrier confinement that allows operation even at elevated temperatures and high photo-carrier densities. It should also be noted that the incorporation of nitrogen into the InGaAs lattice is usually accompanied by generation of non-radiative recombination centres which have detrimental effects on the emission efficiency and long-term device reliability, ultimately limiting the use of dilute nitride lasers in practical applications. To overcome these limitations, extensive optimization of growth parameters, for example nitrogen plasma source settings, and post-growth annealing are usually needed [6–9].

Compared to the results reported earlier [10], in this paper we demonstrate significant improvement in emission efficiency and output power generated by dilute nitride disk lasers. The results prove that GaInNAs/GaAs QW material renders important opportunities for the development of SDLs emitting at 12XX nm.

2. Fabrication of the gain mirror and laser design

The monolithic gain mirror structure was grown on an n-type GaAs (100) substrate by solid source molecular beam epitaxy (MBE) equipped with a radio frequency (RF) plasma source for incorporating nitrogen into the crystal. The structure, shown in Fig. 1, consisted of a 30-pair GaAs/AlAs DBR and an active region with 10 GaInNAs QWs having a relatively low nitrogen content of ~0.6–0.7%.

Compared to the previous design [10], the number of QWs was reduced by two in order to decrease the overall lattice strain. The QWs, each having a thickness of 7 nm, were distributed in five identical pairs placed at the standing wave anti-nodes formed within the Fabry–Pérot cavity defined by the DBR and the semiconductor–air interface. The compressive lattice strain

*Corresponding author. Tel.: +358 50 546 9651; fax: +358 3 3115 3400.
E-mail address: ville-markus.korpijarvi@tut.fi.

0022-0248/$ - see front matter © 2008 Elsevier B.V. All rights reserved.
doi:10.1016/j.jcrysgro.2008.10.083

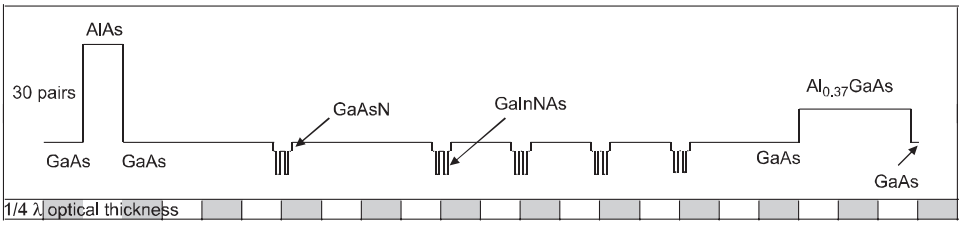

Fig. 1. Conduction band profile of the gain mirror structure showing the position of the QWs.

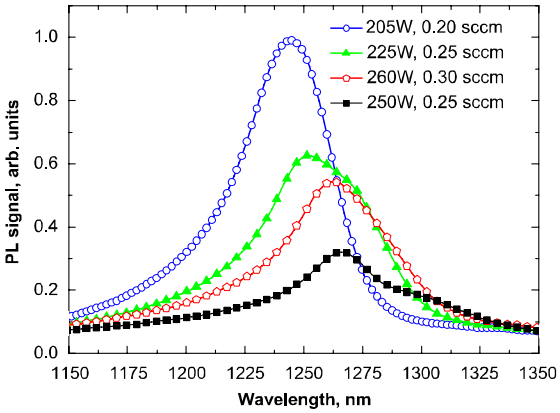

Fig. 2. Effect of plasma RF-power (W) and nitrogen flow (sccm) on the PL spectrum.

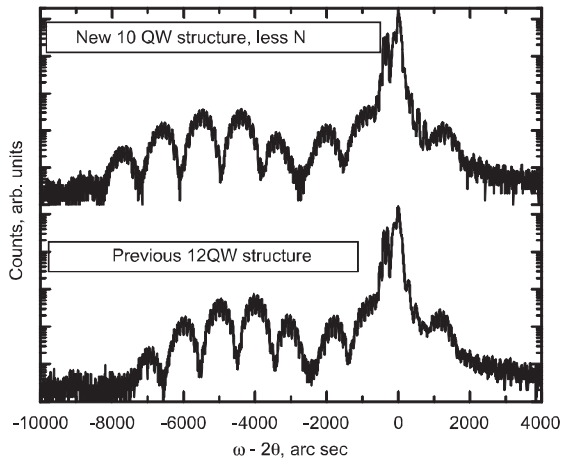

Fig. 3. XRD (0 0 4)-rocking curve measured from the as-grown semiconductor gain mirror plotted for comparison with data for the 12 QW gain mirror structure reported previously.

caused by the QWs was partially compensated by 4 nm thick tensile-strained GaAsN layers grown on both sides of each QW. These strain compensating layers also caused a beneficial spectral red-shift [11]. A 0.75λ thick $Al_{0.37}Ga_{0.63}As$ window layer was grown on top of the active region to confine the photo-generated carriers within the active region and to avoid non-radiative surface recombination. Finally, a thin GaAs capping layer was grown to prevent oxidation of the window layer.

The settings of the nitrogen plasma source were optimized in an attempt to improve the optical quality of the active region. Several samples were grown using different combinations for the RF-power and nitrogen flow. Corresponding photoluminescence (PL) spectra are shown in Fig. 2. The actual settings of the plasma source used during growth of the gain mirror were ~200 W for the power and 0.2 sccm for the nitrogen flow. These settings corresponded to a relatively low nitrogen concentration of about 0.6%. This made the QWs to be more strained compared to the structure reported earlier; an effect which can be observed from the XRD (0 0 4)-rocking curves shown in Fig. 3. The growth temperature, measured by an optical pyrometer, was 450 °C for the QWs, 580 °C for the GaAs barriers, and 590 °C for the DBR and the AlGaAs window layer. The structure was *in situ* post-growth annealed at 680 °C for 5 min. An atomic force microscope (AFM) was used to study the surface quality of the gain mirror. AFM image shown in Fig. 4 reveals that the surface of the gain mirror was smooth on an atomic level indicating high-quality growth. The PL and reflectance spectra measured from an as-grown wafer are shown in Fig. 5. We should note that the PL signal from the gain mirror peaks at the resonant wavelength of the Fabry–Pérot vertical-cavity confining the active region. To avoid the cavity influence on the PL spectrum, a separate PL sample was prepared by removing the substrate and the DBR. The PL spectrum obtained from this sample is presented in Fig. 5 for comparison with the gain mirror PL spectrum. The figure reveals that the spectral detuning between the QWs peak emission and the resonance of the sub-cavity is about 15 nm.

A $2.5 \times 2.5\,mm^2$ laser chip was cut from the as-grown wafer and capillary-bonded with water to a $\sim 3 \times 3 \times 0.3\,mm^3$ type IIa natural diamond heat spreader to ensure efficient heat removal from the gain region. The bonded chip was fixed between two copper plates with indium foil to ensure a good thermal and mechanical contact. The pump light and the 1220 nm signal were coupled through a circular aperture in the top copper plate. The mounted sample was attached to a water-cooled copper heat sink.

Two different cavity configurations were used: a linear cavity and a V-shaped cavity, which are schematically shown in Figs. 6 and 7, respectively. The linear cavity consisted of the gain mirror pumped by an 808 nm laser and a partially reflective curved mirror with a radius of curvature (RoC) of 75 mm and a transmission of 1% at the signal wavelength. The output coupler was placed at 68.5 mm from the gain mirror to match the fundamental mode size on the gain mirror with the pump spot of about 180 μm in diameter. The V-shaped cavity consisted of the gain mirror, a high-reflectivity curved mirror with a RoC of 250 mm placed at a distance of 170 mm from the gain mirror and a planar output coupler placed at 265 mm from the curved mirror. This V-shaped SDL was pumped with a more powerful 50 W 788 nm laser. With this configuration, the mode diameter on the

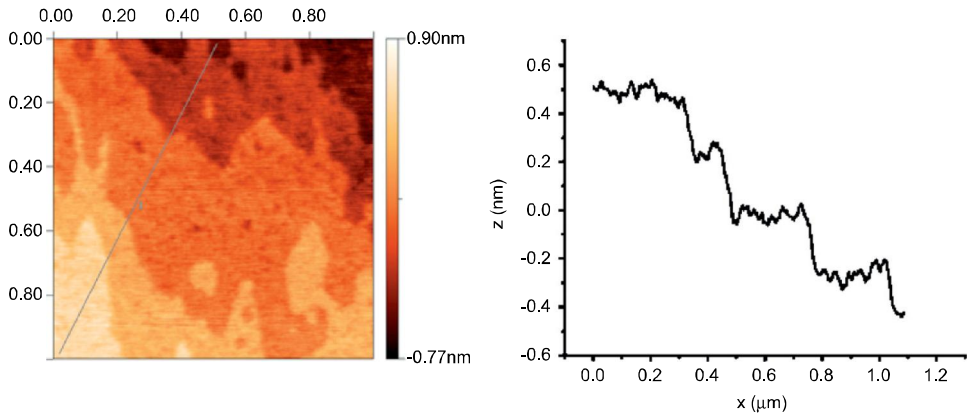

Fig. 4. AFM picture and corresponding line profile measured from the surface of the as-grown gain mirror.

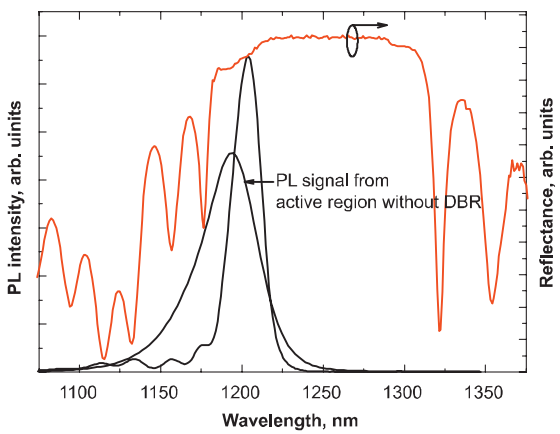

Fig. 5. Room temperature reflectivity and PL spectra of the as-grown sample and a PL sample that was prepared by removing the DBR from the gain mirror. PL intensities are not in scale.

gain mirror was approximately 290 μm, which matches the increased pump spot size.

3. Results and discussion

The SDL with the linear cavity was used for studying lasing characteristics of the gain mirror at different mount temperatures as shown in Fig. 8. The output power at 8 °C and 20 W of incident pump power reached a value of 3.14 W. This value, which is limited by the pump power, corresponds to a slope efficiency of 20%. The threshold pump power increased with temperature, as shown in the inset of Fig. 8. The minimum threshold pump power was observed at a mount temperature of 10 °C. The slight decrease in threshold when the temperature was raised from 8 to 10 °C could be explained by a better match between the peak gain wavelength and the Fabry–Pérot cavity resonance of the gain chip. The emission spectra at the maximum pump power are shown in Fig. 9 for two mount temperatures. The multiple spikes in the spectra originate from the resonant modes of the intra-cavity etalon formed by the diamond heat spreader.

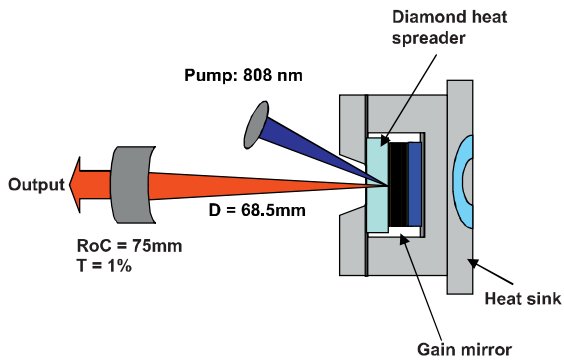

Fig. 6. Schematic representation of the linear cavity. RoC=radius of curvature, T=transmission of the mirror at the operating wavelength.

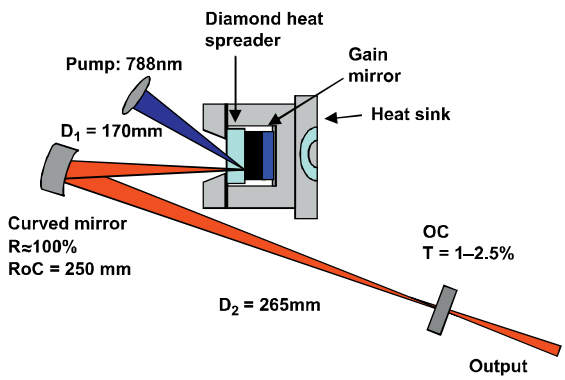

Fig. 7. Schematic representation of the V-shaped cavity. RoC=radius of curvature, OC=output coupler, T=transmission of the mirror at the operating wavelength.

To scale up the output power, a 2-layer SiO_2/TiO_2 antireflection coating was deposited onto the diamond surface resulting in reflectivities of about 0.5% and 5% at the signal and pump wavelengths, respectively. This gain mirror was then inserted into the V-shaped cavity. With this configuration, we were able to

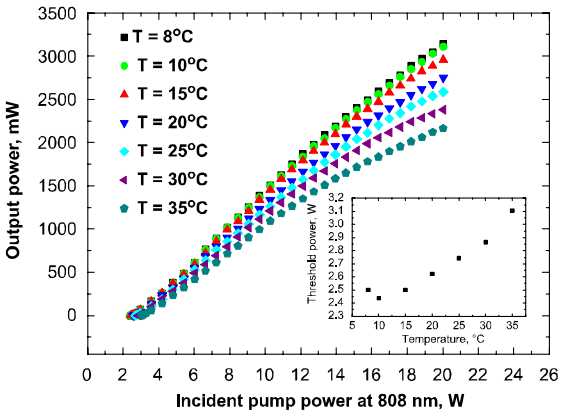

Fig. 8. Power characteristics of the linear cavity SDL for different mount temperatures. Threshold pump power at different temperatures is shown in the inset.

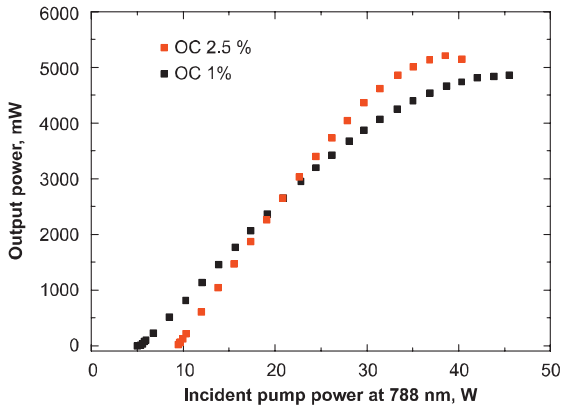

Fig. 10. Power characteristics of the V-shaped SDL. After antireflection coating the reflectivity at the pump wavelength was about 5%. The mount temperature was set to 15 °C.

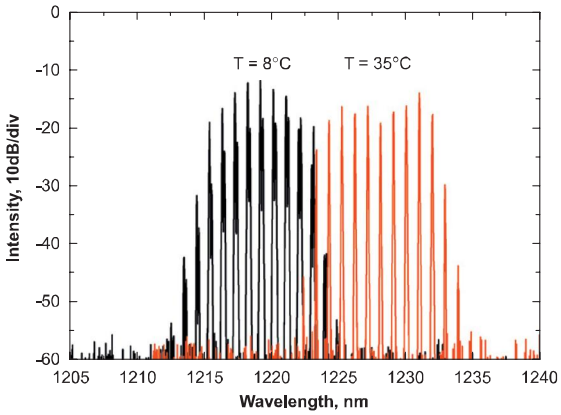

Fig. 9. Spectra of the linear cavity SDL at two mount temperatures; the incident pump power was 20 W.

compare two different output couplers and to increase cavity mode size on the gain mirror. Because the output power of the linear cavity SDL was limited by the available pump power, a more powerful 788 nm pump laser was introduced for this measurement. The mount temperature was kept at 15 °C. As can be seen in Fig. 10, we obtained output power exceeding 5 W at 38 W of incident pump power by using 2.5% output coupler. This corresponds to slope efficiency close to 20%. With 1% output coupler, we reached output power of 4.9 W at a pump power of 45 W. Threshold pump powers for SDLs with 2.5% and 1% output couplers were 9.5 W and 5.0 W, respectively.

Recently, we have used this gain material to demonstrate 2.7 W of orange–red laser radiation by intra-cavity frequency doubling [12], and picosecond pulse generation by passive mode locking [13]. No degradation of the gain material performance has been observed over many months of successive laboratory experiments.

4. Conclusions

We have demonstrated a GaInNAs-based SDL with an output power of 5 W and a slope efficiency of 20%. These results show the best performance for a 1220 nm GaInNAs disk laser reported to date. They are ascribed to the optimization of the nitrogen plasma source settings and the reduction of the number of QWs. While the low nitrogen concentration made the QWs more strained, we expect that the overall strain was reduced because of the smaller number of QWs. Further improvements are still possible by optimizing the growth conditions, the number of QWs, and the pump absorption capability. Our results prove that the GaInNAs/GaAs QW heterostructures render opportunities for the development of SDLs emitting at 12XX nm.

Acknowledgements

We gratefully acknowledge Kimmo Haring and Risto Ahorinta for their help concerning material characterization. This work was supported in part by the EU FP6 project NATAL (IST-NMP-016769) and the "Nanoscience and Nanophotonics" program financed by the Finnish Ministry of Education.

References

[1] L. Fan, T.-C. Hsu, M. Fallahi, J.T. Murray, R. Bedford, Y. Kaneda, J. Hader, A.R. Zakharian, J.V. Moloney, S.W. Koch, W. Stolz, Appl. Phys. Lett. 88 (2006) 251117.
[2] J.H. Lee, S.M. Lee, T. Kim, Y.J. Park, Appl. Phys. Lett. 89 (2006) 241107.
[3] L. Fan, C. Hessenius, M. Fallahi, J. Hader, L. Hongbo, J.V. Moloney, W. Stolz, S.W. Koch, J.T. Murray, R. Bedford, Appl. Phys. Lett. 91 (2007) 131114.
[4] M. Kondow, T. Kitatani, S. Nakatsuka, M.C. Larson, K. Nakahara, Y. Yazawa, M. Okai, K. Uomi, IEEE J. Sel. Top. Quantum Electron. 3 (1997) 719.
[5] E. Gerster, I. Ecker, S. Lorch, C. Hahn, S. Menzel, P. Unger, J. Appl. Phys. 94 (2003) 7397.
[6] J.M. Hopkins, S.A. Smith, C.W. Jeon, H.D. Sun, D. Burns, S. Calvez, M.D. Dawson, T. Jouhti, M. Pessa, Electron. Lett. 40 (2004) 30.
[7] A. Rutz, V. Liverini, E. Müller, S. Schön, U. Keller, J. Crystal Growth 301–302 (2007) 525.
[8] M.A. Wistey, S.R. Bank, H.B. Yuen, H. Bae, J.S. Harris Jr., J. Crystal Growth 278 (2005) 229.
[9] J. Pakarinen, C.S. Peng, J. Puustinen, P. Laukkanen, V.-M. Korpijärvi, A. Tukiainen, M. Pessa, Appl. Phys. Lett. 92 (2008) 232105.
[10] J. Konttinen, A. Härkönen, P. Tuomisto, M. Guina, J. Rautiainen, M. Pessa, O. Okhotnikov, New J. Phys. 9 (2007) 140.
[11] E.-M. Pavelescu, C.S. Peng, T. Jouhti, J. Konttinen, W. Li, M. Pessa, M. Dumitrescu, S. Spânulescu, Appl. Phys. Lett. 80 (2002) 3054.
[12] J. Rautiainen, A. Härkönen, V.-M. Korpijärvi, P. Tuomisto, M. Guina, O.G. Okhotnikov, Opt. Express 15 (2007) 18345.
[13] J. Rautiainen, V.-M. Korpijärvi, J. Puustinen, M. Guina, O.G. Okhotnikov, Opt. Express 16 (2008) 15964.

Publication 2

P2

R. Kudrawiec, V.-M. Korpijärvi, P. Poloczek, J. Misiewicz, P. Laukkanen, J. Pakarinen, M. Dumitrescu, M. Guina and M. Pessa, "The influence of As/III pressure ratio on nitrogen nearest-neighbor environments in as-grown GaInNAs quantum wells," *Applied Physics Letters*, vol. 95, pp. 261909-3, 2009.

The influence of As/III pressure ratio on nitrogen nearest-neighbor environments in as-grown GaInNAs quantum wells

R. Kudrawiec,[1,a)] V.-M. Korpijärvi,[2] P. Poloczek,[1] J. Misiewicz,[1] P. Laukkanen,[2] J. Pakarinen,[2] M. Dumitrescu,[2] M. Guina,[2] and M. Pessa[2]
[1]*Institute of Physics, Wrocław University of Technology, Wybrzeże Wyspiańskiego 27, 50-370 Wrocław, Poland*
[2]*Optoelectronics Research Centre, Tampere University of Technology, FIN-33101 Tampere, Finland*

(Received 6 October 2009; accepted 23 November 2009; published online 31 December 2009)

The energy fine structure, corresponding to different nitrogen nearest-neighbor environments, was observed in contactless electroreflectance (CER) spectra of as-grown GaInNAs quantum wells (QWs) obtained at various As/III pressure ratios. In the spectral range of the fundamental transition, two CER resonances were detected for samples grown at low As pressures whereas only one CER resonance was observed for samples obtained at higher As pressures. This resonance corresponds to the most favorable nitrogen nearest-neighbor environment in terms of the total crystal energy. It means that the nitrogen nearest-neighbor environment in GaInNAs QWs can be controlled in molecular beam epitaxy process by As/III pressure ratio. © *2009 American Institute of Physics*. [doi:10.1063/1.3275712]

GaInNAs/GaAs quantum wells (QWs) are a very promising solution for low-cost GaAs-based laser diodes operating in the 1.3–1.55 μm optical fiber windows.[1] However, the utility of as-grown GaInNAs material is limited by its poor quality of luminescence properties. Therefore, the post-growth heat treatment (annealing) has been employed in this material as a standard process to remove as-grown defects and improve its optical quality. So far, many studies have shown that the annealing process can increase the intensity of luminescence efficiency. However, this process also leads to a blueshift of GaInNAs energy gap for a certain composition of $Ga_{1-x}In_xN_yAs_{1-y}$ alloy.[2–5] This effect has been explained to be caused by the reconfiguration of N atom environment from Ga-rich to In-rich and simultaneous change in the QW profile due to atom diffusion across QW interfaces.[3,6]

In general, the scenario is that during the epitaxial growth the chemical dynamical processes occurring at the surface favor Ga–N bonds instead of In–N ones. The surface state is frozen in during the nonequilibrium growth process. Hence, after the growth process a N atom is surrounded by four Ga atoms. It leads to a crystal structure with "small atom—small atom" and "large atom—large atom" arrangements which is less preferable in terms of strain than "small atom—large atom" environment. Therefore, the annealing process leads to a formation of different nitrogen nearest-neighbor environments, i.e., N-centered $N-In_mGa_{4-m}$ ($0 \le m \le 4$) short-range-order clusters. The reconfiguration of nitrogen surrounding from four Ga atoms ($N-Ga_4$) to four In atoms ($N-In_4$) leads to an effective blue shift of band-gap energy at the same compound composition (x and y). This scenario has been confirmed by many experimental data,[2–11] however the issue of nitrogen nearest-neighbor environments in as-grown materials is still the open question. Recently, it has been concluded that In–N bonds exist already in the as-grown material.[12] It suggests that the nitrogen nearest-neighbor environment is not only sensitive to the annealing temperature but also depends on the growth conditions. In general, it is expected that the control of nitrogen environments during the growth process (i.e., in as-grown materials) can be very profitable since it can improve luminescence efficiency already for the as-grown material and reduce the energy gap blueshift after annealing. So far, the influence of growth parameters on nitrogen surroundings has never been explored for as-grown materials. In this letter, we show that the nitrogen nearest-neighbor environment in GaInNAs can be controlled in molecular beam epitaxy (MBE) process by As/III pressure ratio.

The GaInNAs/GaAs QW samples were grown on *n*-type GaAs:Si (100) substrates by a solid-source MBE system equipped with rf nitrogen plasma source. After depositing a 105 nm GaAs buffer layer at $T_{sub} \approx 580$ °C, the temperature was decreased to 455 °C during a deposition of additional 30 nm of GaAs. Then triple QW structures of the nominal alloy compositions of $Ga_{0.62}In_{0.38}As_{0.0995}N_{0.005}$, each QW being 6.5 nm thick and separated by 20 nm GaAs barriers, were grown and capped with a 80 nm GaAs layer. T_{sub} was raised back to 580 °C during the deposition of the top GaAs layer. Two sets of GaInNAs/GaAs QW samples were grown. The first set of four samples was grown at various As/III beam equivalent pressure (BEP) ratio. The nitrogen plasma source settings for the four samples were the same and equaled 205 W rf power and 0.2 SCCM flow. The second set of samples was grown at As/III=7.9 and with various nitrogen plasma settings (five samples). Annealing was performed at three different temperatures (650, 750, and 850 °C) for 60 s, see details in Ref. 13. In order to investigate the nitrogen nearest-neighbor environments in GaInNAs QWs, we applied contactless electroreflectance (CER). This technique, like photoreflectance spectroscopy,[2–5] is able to probe energy gaps related to individual nitrogen nearest neighbor environments. Relevant details of CER measurements are described in Ref. 14.

Figure 1 shows room temperature CER spectra for the set of as-grown GaInNAs/GaAs QW samples obtained at various As/III BEP ratios. It is clearly visible that for samples

[a)]Electronic mail: robert.kudrawiec@pwr.wroc.pl.

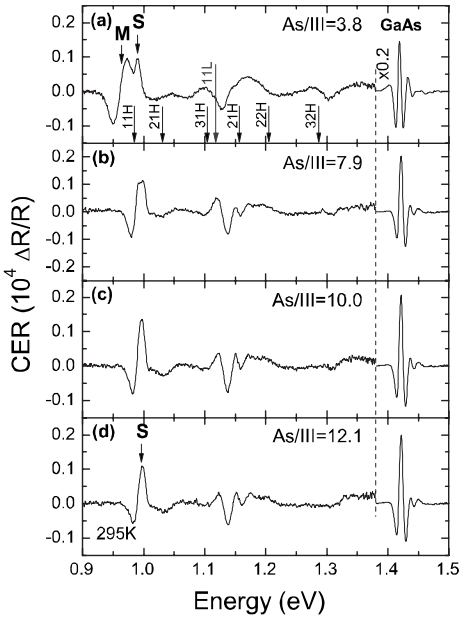

FIG. 1. Room temperature CER spectra for the set of GaInNAs/GaAs QWs obtained at various As/III pressure ratios. The plasma settings are 205 W rf power and 0.2 SCCM flow. Arrows show the calculated energies of optical transition for this QW. The notation *ij*H(L) denotes the transition between *i*th heavy(light) hole subband and *j*th conduction subband.

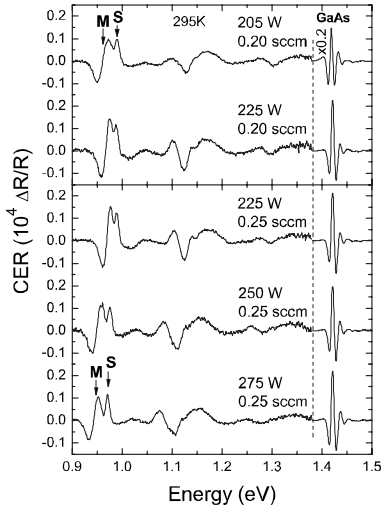

FIG. 2. Room temperature CER spectra for the set of GaInNAs/GaAs QWs obtained at low As pressure (As/III=7.9) and various nitrogen plasma settings.

obtained at lower As pressure CER signal at the energy of ~0.95 eV is composed of two CER resonances, one broader resonance (labeled M) and the second narrower one (labeled S). Broader resonance is strong for samples grown at low As pressure. This resonance corresponds to various nitrogen nearest-neighbor environments but none of them is dominant.[3] With the increase in As pressure the M resonance disappears. Instead of this resonance the second resonance (see the S resonance), which is narrower and located at higher energy, starts to dominate CER spectrum features.

A clear double resonance structure of CER signal in this spectral range is also observed for the second set of GaInNAs/GaAs QW samples obtained at low As pressure (As/III=7.9) but different nitrogen plasma settings, see Fig. 2. The observed redshift of QW transitions with the increase in rf power is associated with the increase in nitrogen concentration in GaInNAs layer. In this work, we focus on the energy fine structure of CER signal at ~0.95 eV.

Figure 3 shows CER spectrum for one sample in the vicinity of ~0.95 eV fitted by two resonances according to Aspnes formula,[15] as in Ref. 3. This fit clearly shows that CER signal in this spectral range is composed of two CER resonances which are separated by an energy difference of ~30 meV. Taking into account all electron and hole levels in GaInNAs/GaAs QW the two resonances have been attributed to the fundamental transition in this QW, since any of the two resonances (M nor S) cannot be associated with the optical transition involving the first light-hole state or the second heavy-hole state. For a better illustration of this aspect, the energies of the optical transitions in this QW have been calculated[16] and marked in Fig. 1(a) by arrows.

The energy fine structure of the fundamental transition in GaInNAs/GaAs QW is a result of various nitrogen nearest-neighbor environments in GaInNAs alloy.[2–4] We concluded that this environment changes with the growth conditions and, therefore, the relative intensities between the S and M transition varies with the increase in As/III pressure ratio. This issue is very well illustrated in Fig. 4 where the S/(M+S) intensity ratio is plotted for the two sets of samples. We suppose that the narrow CER resonance (S transition) corresponds to the most probable nitrogen nearest-neighbor environment in terms of the total crystal energy whereas the broader CER resonance (M transition) represents remaining nitrogen environments which are unfavorable in terms of the total crystal energy and therefore they should disappear after annealing. In order to verify this presumption we measured CER spectra for annealed samples, see Fig. 5. The obtained results confirm this scenario, i.e., in the case of GaInNAs/GaAs QWs obtained at lower arsenic pressures [Figs. 5(a) and 5(b)] both M and S resonances are observed for as-grown samples and the M resonance disappears after annealing. In the case of GaInNAs/GaAs QWs obtained at higher

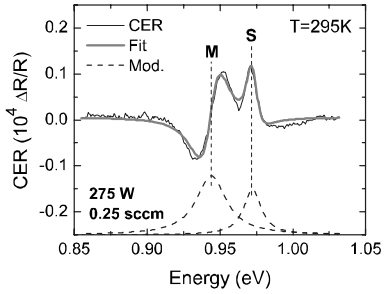

FIG. 3. Room temperature CER spectrum for GaInNAs/GaAs QW sample obtained at low As/III pressure (As/III=7.9) and nitrogen plasma settings of 275 W rf power and 0.25 SCCM flow in the vicinity of the fundamental QW transition together with the fitting curve (gray line) and the decomposition of CER signal for individual modulus of CER resonances (dashed lines).

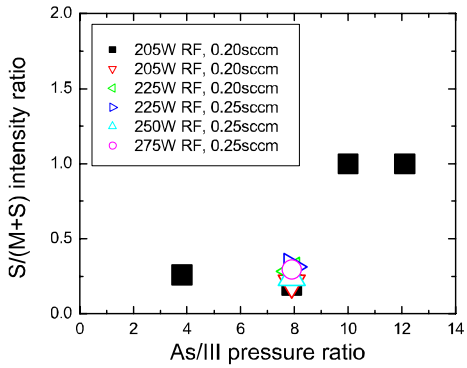

FIG. 4. (Color online) S/(M+S) intensity ratio obtained from the fitting of CER data by Eq. (1).

arsenic pressures [Figs. 5(c) and 5(d)], only one resonance (S one) is observed for as-grown and annealed samples. The slight blueshift of this resonance upon annealing can be attributed to a small atom interdiffusion across QW interfaces,[3] i.e., "so called" QW intermixing.

According to theoretical calculations for GaInNAs alloy[17] and our previous studies for GaInNAs/GaAs QWs,[3] we attributed the S resonance to the $N-In_3Ga_1$ atom configuration since this configuration is the most favorable for this system. The presence of this configuration already for as-grown material clearly shows that not only the energy of atom bonds, but also As/III pressure ratio determines the nitrogen surroundings in as-grown GaInNAs material. We suppose that in the microscopic picture the effectiveness of formation of Ga–As and In–As bonds depends on the As/III pressure ratio as well the relation between gallium and indium fluxes. It means that at fixed gallium and indium fluxes the nitrogen nearest-neighbor environment can vary with the As/III pressure ratio. Also the nitrogen flux can influence atom environments as well the nitrogen concentration. In our case the nitrogen flux is controlled by the nitrogen plasma settings. In the applied range of plasma setting the nitrogen flux does not change significantly and, therefore, the nitrogen nearest-neighbor environment does not change significantly in the second set of samples (i.e., samples grown at the same As/III pressure ratio).

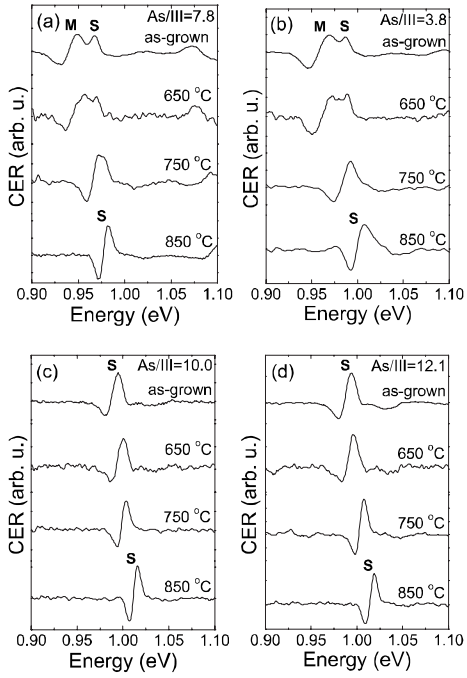

FIG. 5. Room temperature CER for as-grown and annealed GaInNAs/GaAs QW samples obtained at various As/III BEP ratios: (a) As/III=7.9 (nitrogen plasma settings 275 W rf power and 0.25 SCCM flow), (b) As/III=3.8, (c) As/III=10.0, and (d) As/III=12.1. Nitrogen plasma settings for (b), (c), and (d) are the same and equal 205 W rf power and 0.2 SCCM flow.

In conclusion, it has been clearly shown that besides the postgrowth annealing the As/III pressure ratio also influences the nitrogen nearest-neighbor environment in GaInNAs/GaAs QWs. For samples obtained at low As pressures two CER resonances were detected in the spectral range corresponding to the fundamental transition in GaInNAs/GaAs QW whereas for samples obtained at higher As pressures only one CER resonance was observed in this spectral range. This resonance corresponds to the most favorable nitrogen nearest-neighbor environment in terms of the total crystal energy. This observation is very valuable from the viewpoint of finding of the optimal growth conditions for GaInNAs/GaAs QWs.

This study was performed within the framework of European Union project DeLight (Grant No. FP7 224366) and COST Action under Grant No. MP0805 focused on study of dilute-nitrides. In addition, R.K. acknowledges for support from the Foundation for Polish Science and the MNiSzW under Grant no. N N202 285634.

[1]M. Kondow, K. Uomi, A. Niwa, T. Kikatani, S. Watahiki, and Y. Yazawa, Jpn. J. Appl. Phys., Part 1 **35**, 1273 (1996).
[2]P.J. Klar, H. Grüning, J. Koch, S. Schäfer, K. Volz, W. Stolz, W. Heimbrodt, A. M. Kamal Saadi, A. Lindsay, and E.P. O'Reilly, Phys. Rev. B **64**, 121203(R) (2001).
[3]R. Kudrawiec, G. Sek, J. Misiewicz, D. Gollub, and A. Forchel, Appl. Phys. Lett. **83**, 2772 (2003).
[4]R. Kudrawiec, E.-M. Pavelescu, J. Wagner, G. Sęk, J. Misiewicz, M. Dumitrescu, J. Konttinen, A. Gheorghiu, and M. Pessa, J. Appl. Phys. **96**, 2576 (2004).
[5]V. Lordi, S. Friedrich, T. Funk, T. Takizawa, K. Uno, and J. S. Harris, Phys. Rev. Lett. **90**, 145505 (2003).
[6]M. Albrecht, H. Abu-Farsakh, T. Remmele, L. Geelhaar, H. Riechert, and J. Neugebauer, Phys. Rev. Lett. **99**, 206103 (2007).
[7]J. Wagner, T. Geppert, K. Kohler, P. Ganser, and N. Herres, J. Appl. Phys. **90**, 5027 (2001).
[8]H. D. Sun, M. D. Dawson, M. Othman, J. C. L. Yong, J. M. Rorison, P. Gilet, L. Grenouillet, and A. Million, Appl. Phys. Lett. **82**, 376 (2003).
[9]T. Kitatani, M. Kondow, and M. Kudo, Jpn. J. Appl. Phys., Part 2 **40**, L750 (2001).
[10]S. R. Kurtz, J. F. Klem, A. A. Allerman, R. M. Sieg, C. H. Seager, and E. D. Jones, Appl. Phys. Lett. **80**, 1379 (2002).
[11]S. Kurtz, J. Webb, L. Gedvilas, D. Friedman, J. Geisz, J. Olson, R. King, D. Joslin, and N. Karam, Appl. Phys. Lett. **78**, 748 (2001).
[12]V. Lordi, H. B. Yuen, S. R. Bank, M. A. Wistey, J. S. Harris, and S. Friedrich, Phys. Rev. B **71**, 125309 (2005).
[13]J. Pakarinen, C. S. Peng, J. Puustinen, P. Laukkanen, V.-M. Korpijärvi, A. Tukiainen, and M. Pessa, Appl. Phys. Lett. **92**, 232105 (2008).
[14]R. Kudrawiec and J. Misiewicz, Rev. Sci. Instrum. **80**, 096103 (2009).
[15]D. E. Aspnes, Surf. Sci. **37**, 418 (1973).
[16]R. Kudrawiec, H. B. Yuen, M. Motyka, M. Gladysiewicz, J. Misiewicz, S. R. Bank, H. P. Bae, M. A. Wistey, and J. S. Harris, J. Appl. Phys. **101**, 013504 (2007).
[17]K. Kim and A. Zunger, Phys. Rev. Lett. **86**, 2609 (2001).

Publication 3

P3

V. Korpijärvi, T. Leinonen, J. Puustinen, A. Härkönen and M. D. Guina, "11 W single gain-chip dilute nitride disk laser emitting around 1180 nm," *Optics Express*, vol. 18, pp. 25633-25641, 2010.

11 W single gain-chip dilute nitride disk laser emitting around 1180 nm

Ville-Markus Korpijärvi, Tomi Leinonen, Janne Puustinen, Antti Härkönen, and Mircea D. Guina*

Optoelectronics Research Centre, Tampere University of Technology, Korkeakoulunkatu 3, Tampere, 33720 Finland
**mircea.guina@tut.fi*

Abstract: We report power scaling experiments of a GaInNAs/GaAs-based semiconductor disk laser operating at ~1180 nm. Using a single gain chip cooled to mount temperature of ~10 °C we obtained 11 W of output power. For efficient thermal management we used a water-cooled microchannel mount and an intracavity diamond heat spreader. Laser performance was studied using different spot sizes of the pump beam on the gain chip and different output couplers. Intracavity frequency-doubling experiments led to generation of ~6.2 W of laser radiation at ~590 nm, a wavelength relevant for the development of sodium laser guide stars.

OCIS codes: (140.5960) Semiconductor lasers; (140.7270) Vertical emitting lasers.

References and links

1. M. Kuznetsov, F. Hakimi, R. Sprague, and A. Mooradian, "High-Power (>0.5-W CW) diode-pumped vertical-external-cavity surface-emitting semiconductor lasers with circular TEM_{00} beams," IEEE Photon. Technol. Lett. **9**(8), 1063–1065 (1997).
2. N. Schulz, J.-M. Hopkins, M. Rattunde, D. Burns, and J. Wagner, "High-brightness long-wavelength semiconductor disk lasers," Laser Photon. Rev. **2**(3), 160–181 (2008).
3. S. Calvez, J. E. Hastie, M. Guina, O. G. Okhotnikov, and M. D. Dawson, "Semiconductor disk lasers for the generation of visible and ultraviolet radiation," Laser Photon.Rev. **3**(5), 407–434 (2009).
4. J. M. Hopkins, S. A. Smith, C. W. Jeon, H. D. Sun, D. Burns, S. Calvez, M. D. Dawson, T. Jouhti, and M. Pessa, "0.6 W CW GaInNAs vertical external-cavity surface emitting laser operating at 1.32 μm," IET Electron. Lett. **40**(1), 30–31 (2004).
5. S. L. Vetter, J. E. Hastie, V.-M. Korpijärvi, J. Puustinen, M. Guina, O. Okhotnikov, S. Calvez, and M. D. Dawson, "Short-wavelength GaInNAs/GaAs semiconductor disk lasers," IET Electron. Lett. **44**(18), 1069–1070 (2008).
6. V.-M. Korpijärvi, M. Guina, J. Puustinen, P. Tuomisto, J. Rautiainen, A. Härkönen, A. Tukiainen, O. Okhotnikov, and M. Pessa, "MBE grown GaInNAs-based multi-Watt disk lasers," J. Cryst. Growth **311**(7), 1868–1871 (2009).
7. L. Fan, C. Hessenius, M. Fallahi, J. Hader, H. Li, J. V. Moloney, W. Stolz, S. Koch, J. T. Murray, and R. Bedford, "Highly strained InGaAs/GaAs multiwatt vertical-external-cavity surface-emitting laser emitting around 1170 nm," Appl. Phys. Lett. **91**(13), 131114 (2007).
8. M. Kondow, T. Kitatani, S. Nakatsuka, M. C. Larson, K. Nakahara, Y. Yazawa, M. Okai, and K. Uomi, "GaInNAs: a novel material for long wavelength semiconductor lasers," IEEE J. Sel. Top. Quantum Electron. **3**(3), 719–730 (1997).
9. J. Rautiainen, A. Härkönen, V.-M. Korpijärvi, P. Tuomisto, M. Guina, and O. G. Okhotnikov, "2.7 W tunable orange-red GaInNAs semiconductor disk laser," Opt. Express **15**(26), 18345–18350 (2007).
10. T. Leinonen, A. Härkönen, V.-M. Korpijärvi, M. Guina, R.J. Epstein, J.T. Murray, and G.J. Fetzer, "High-power narrow-linewidth optically pumped dilute nitride disk laser with emission at 589 nm," SPIE Photon. Europe Proc. **7720**, 772016–1–772016–7, 12– 16 April 2010, Brussels.
11. M. Guina, T. Leinonen, A. Härkönen, and M. Pessa, "High-power disk lasers based on dilute nitride heterostructures," N. J. Phys. **11**(12), 125019 (2009), http://iopscience.iop.org/1367-2630/11/12/125019/fulltext.
12. C. F. Blodi, S. R. Russell, J. S. Pulido, and J. C. Folk, "Direct and feeder vessel photocoagulation of retinal angiomas with dye yellow laser," Ophthalmology **97**(6), 791–795, discussion 796–797 (1990).
13. C. W. Hoyt, Z. W. Barber, C. W. Oates, T. M. Fortier, S. A. Diddams, and L. Hollberg, "Observation and absolute frequency measurements of the 1S0-3P0 optical clock transition in neutral ytterbium," Phys. Rev. Lett. **95**(8), 083003 (2005).
14. C. E. Max, S. S. Olivier, H. W. Friedmann, K. An, K. Avicola, B. V. Beeman, H. D. Bissinger, J. M. Brase, G. V. Erbert, D. T. Gavel, K. Kanz, M. C. Liu, B. Macintosh, K. P. Neeb, J. Patience, and K. E. Waltjen, "Image

#133719 - $15.00 USD Received 20 Aug 2010; revised 5 Nov 2010; accepted 14 Nov 2010; published 23 Nov 2010

improvement from a sodium-layer laser guide star adaptive optics system," Science **277**(5332), 1649–1652 (1997).
15. D. B. Calia, Y. Feng, W. Hackenberg, R. Holzlöhner, L. Taylor, and S. Lewis, "Laser development for sodium laser guide stars at ESO", The Messenger, **139**, 12–19 (2009), *http://www.eso.org/sci/publications/messenger/archive/no.139-mar10/messenger-no139-12-19.pdf*.
16. A. Giesen, and J. Speiser, ""Fifteen years of work on thin-disk lasers: results and scaling laws", IEEE J. of Select," Top. in Quantum Electron. **13**(3), 598–609 (2007).
17. E.-M. Pavelescu, C. S. Peng, T. Jouhti, J. Konttinen, W. Li, M. Pessa, M. Dumitrescu, and S. Spânulescu, "Effects of insertion of strain-mediating layers on luminescence properties of 1.3-μm GaInNAs/GaNAs/GaAs quantum-well structures," Appl. Phys. Lett. **80**(17), 3054 (2002).
18. R. Kudrawiec, V.-M. Korpijärvi, P. Poloczek, J. Misiewicz, P. Laukkanen, J. Pakarinen, M. Dumitrescu, M. Guina, and M. Pessa, "The influence of As/III pressure ratio on nitrogen nearest-neighbor environments in as-grown GaInNAs quantum wells," Appl. Phys. Lett. **95**(26), 261909 (2009).
19. J. E. Hastie, J. M. Hopkins, S. Calvez, C. W. Jeon, D. Burns, R. Abram, E. Riis, A. I. Ferguson, and M. D. Dawson, "0.5-W single transversemode operation of an 850-nm diode-pumped surface-emitting semiconductor laser," IEEE Photon. Technol. Lett. **15**(7), 894–896 (2003).
20. S. Giet, A. J. Kemp, D. Burns, S. Calvez, M. D. Dawson, S. Suomalainen, A. Härkönen, M. Guina, O. Okhotnikov, and M. Pessa, "Comparison of thermal management techniques for semiconductor disk lasers", Proceedings SPIE **6871**, Solid State Lasers: Technology and Devices, 687115 (2008).

1. Introduction

The advantages offered by the optically-pumped semiconductor disk lasers (OP-SDLs), also referred to as vertical external cavity surface-emitting lasers [1], have been proved using a large variety of semiconductor gain media for generating high-brightness radiation at visible, infrared, and mid-IR wavelengths [2,3]. Demonstrated first for the generation of radiation at 1.32 μm [4], dilute nitride (GaInNAs/GaAs) OP-SDLs have recently emerged as a viable solution for developing high-power laser sources emitting in the wavelength range between 1.17 μm [5] and 1.24 μm [6]. The increased interest in dilute nitride SDLs has been largely motivated by their ability to produce orange-red laser light via intracavity frequency doubling [3]. GaInNAs/GaAs quantum wells (QWs) can be monolithically integrated with AlAs/GaAs distributed Bragg reflectors (DBRs), which exhibit superior optical and thermal properties compared to InP-based DBRs. By alloying only a few percent of nitrogen into GaInAs, both the band-gap and lattice constant of GaIn(N)As/GaAs QWs are simultaneously decreased. Thus the use of dilute nitrides offers a higher flexibility in designing the gain mirrors and alleviates the problems related to the high compressive lattice strain present in GaInAs/GaAs QWs emitting at wavelengths above 1100 nm [7]. Another important aspect for SDL operation is that GaInNAs/GaAs QWs exhibit a large conduction-band offset and electron effective mass providing efficient carrier confinement and excellent temperature behaviour [8].

On the other hand, the incorporation of nitrogen is usually accompanied by the introduction of lattice defects which ultimately decrease the performance of dilute nitride lasers. However, dilute nitride OP-SDLs with emission wavelengths in the range of 1180–1240 nm require a nitrogen content of less than 1% and can exhibit multi-watt output powers in both fundamental [6] and frequency-doubled operation [9,10]. The highest reported output power (~7 W) and slope efficiency (~30%) exhibited by a dilute nitride OP-SDL incorporating one gain element have been obtained for operation at ~1180 nm [11]. This wavelength range is of particular interest for important applications in medicine [12], optical frequency metrology [13], and astrophysics [14]. For example, high power emission at the frequency doubled wavelength of 589 nm is required to create sodium laser guide stars employed in earth-based telescopes with adaptive optics systems. Frequency doubled SDLs emitting at the 589 nm D_2-sodium absorption line are anticipated to fulfill the specifications of future generation sodium laser guide stars [15], providing that significant advances are made in increasing the output power and achieving stable operation with narrow linewidth.

Assuming that sufficient heat dissipation is ensured, the output power of an OP-SDL can be scaled up by increasing the mode size on the laser gain mirror or by using multiple gain chips in a single SDL cavity or both [16]. The first approach is attractive due to its simplicity;

#133719 - $15.00 USD Received 20 Aug 2010; revised 5 Nov 2010; accepted 14 Nov 2010; published 23 Nov 2010

in particular for a laser guide star application, the narrow linewidth and the spectral stability requirements might be hard to achieve by using multiple gain elements. Increasing the mode size allows for keeping the power density, and therefore the heat generated per unit area constant while increasing the pump and output power. In this paper, we report power scaling of an OP-SDL based on a dilute nitride gain mirror emitting at ~1180 nm. We used a water-cooled microchannel mount for thermal management and studied the influence of pump spot diameter and output coupler transmission on the laser performance. As a result, a record-high output power of 11 W is demonstrated.

2. Gain mirror fabrication

The dilute nitride gain mirror was grown on n-GaAs(100) substrate using solid source molecular beam epitaxy (SS-MBE) equipped with a radio frequency (RF) plasma source for incorporating nitrogen into the crystal. The design of the resonant periodic gain (RPG) structure is shown in Fig. 1.

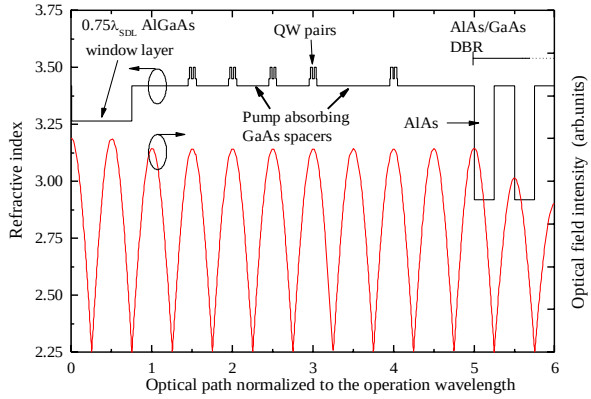

Fig. 1. Schematic representation of the gain mirror design revealing the positioning of the QWs at the antinodes of the optical field distribution at 1180 nm.

The main elements of the gain mirror are a 25.5-pair AlAs/GaAs DBR and a gain region with 10 GaInNAs QWs. The QWs are distributed in five identical pairs at the standing wave anti-nodes formed within the Fabry–Pérot (FP) cavity defined by the DBR and the semiconductor-air interface. The quantum well pairs are embedded within GaAs, which absorbs the pump light and supplies carriers to QWs for providing optical gain. The GaAs layers surrounding the QW group located deepest in the structure are thicker than those surrounding the QW groups placed closer to the surface; this configuration reflects the pump intensity depletion due to absorption and should ensure a more uniform carrier distribution between the QW groups. The compressive lattice strain of the QWs was partially compensated by 4-nm thick tensile-strained GaAsN layers grown on both sides of each QW. The GaAsN layers have a beneficial effect also in terms of red-shifting the emission wavelength [17]. A 0.75λ thick $Al_{0.31}Ga_{0.69}As$ window layer was grown on top of the structure to confine the photo-generated carriers within the active region and to avoid non-radiative surface recombination. Finally, a 5 nm thick GaAs cap layer was grown to prevent oxidation of the window layer. The QWs were grown at a low temperature of about 450 °C with a growth rate of 0.95 μm/h and a high As/III beam equivalent pressure ratio of 25, which was found to lead to preferential formation of N-In bonds and better stability and optical quality of

#133719 - $15.00 USD Received 20 Aug 2010; revised 5 Nov 2010; accepted 14 Nov 2010; published 23 Nov 2010

the as-grown material [18]. The N_2 flow rate to the plasma source was 0.18 sccm and the RF power was 175 W. These settings correspond to a relative small amount, estimated to be ~0.6%, of nitrogen incorporated into the QWs. After the growth, the structure was in situ annealed in the MBE chamber for 7 minutes at a temperature of 680 °C.

Figure 2 reveals the evolution of the reflectivity spectra and photoluminescence (PL) signal with increasing gain chip temperature. The reflectivity spectra were measured from an as-grown gain mirror whereas the PL was measured in the laser setup from a gain mirror bonded to a diamond heat spreader with an anti-reflection coating. The reason for making the PL measurement in the laser setup was to take advantage of the temperature control. The power of the PL excitation laser was kept low (a few tens of mW) in order to prevent undesired heating of the sample.

From these measurements we estimated that the DBR stop-band red-shifts at a rate of only 0.06 nm/K while the PL peak wavelength red-shifts at a rate of 0.3 nm/K. Hence, the detuning between QW absorption edge and the resonant wavelength of the gain mirror decreases with increasing temperature, as revealed by the resonance-enhanced absorption dip in the stop-band. However, owing to a higher rate of non-radiative recombination, the PL intensity decreases with increasing temperature regardless of the better match between luminescence spectrum and the resonant wavelength of the gain mirror. This behavior emphasizes the importance of wavelength detuning between the PL and resonant wavelength and, on the other hand, reveals the detrimental effect of temperature rise on light emission. For the gain mirror studied here, the room temperature PL peak wavelength (as measured from a quantum well sample grown prior to the gain mirror) was detuned to about 30 nm below the desired laser operation wavelength; this is the same detuning as for the chip used in Ref [11].

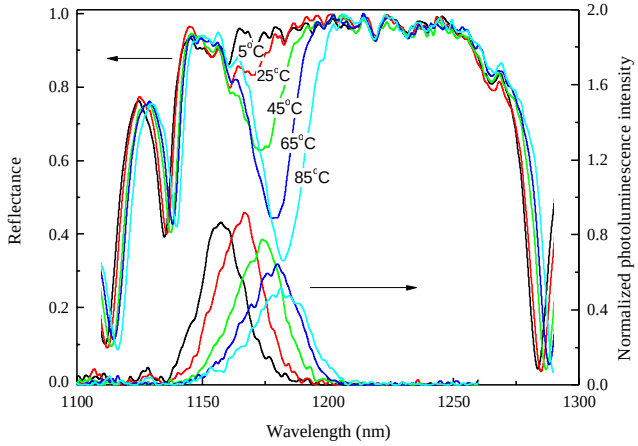

Fig. 2. Reflectivity and photoluminescence spectra of the gain mirror measured at different temperatures.

#133719 - $15.00 USD Received 20 Aug 2010; revised 5 Nov 2010; accepted 14 Nov 2010; published 23 Nov 2010

3. Laser characterization

3.1 Laser cavity and thermal management

The V-shaped laser cavity (Fig. 3) comprised the gain mirror, a high-reflectivity curved folding mirror and a planar output coupler. A fibre-coupled 808 nm diode laser was used for optical pumping of the gain mirror. The pump beam was incident onto the gain mirror at a 27° angle relative to the surface normal. The diameter of the pump spot on the gain chip was varied between ~320 μm and ~460 μm. The cavity was adjusted to achieve high power operation with a good beam shape. The as-grown gain chip was 2.5 × 2.5 mm^2 in size and was capillary-bonded with water to a ~3 × 3 × 0.3 mm^3 synthetic single-crystal diamond heat spreader to ensure efficient heat removal from the gain region [19]. The diamond had a 2° wedge angle with respect to semiconductor surface and was antireflection coated to avoid etalon effects and to minimize the pump reflection. The bonded chip was mechanically clamped to a water-cooled microchannel mount.

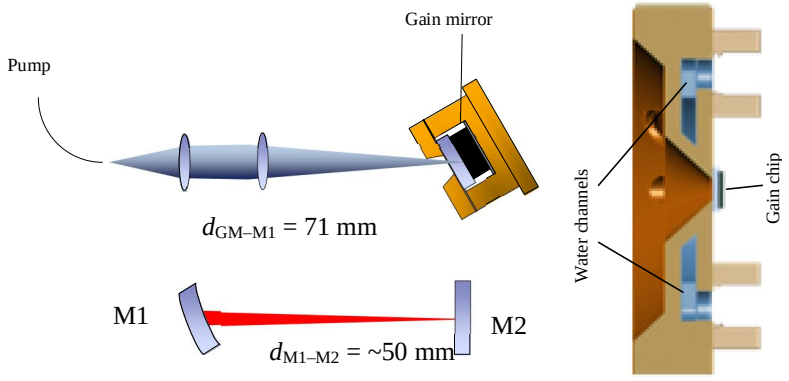

Fig. 3. The cavity design of the SDL (left) and a drawing of the water-cooled microchannel mount (right).

One of the factors limiting the output power of the 1180 nm SDLs we reported earlier [11] was linked to the use of a cooling mount that did not provide sufficient heat extraction from the gain chip at high pump powers. To ensure efficient heat extraction for the experiments reported here, we developed a metallic water-cooled microchannel mount (see Fig. 3). The microchannels were machined as close as possible to the diamond heat spreader, i.e. at a distance of about 1 mm from the closest edge of the diamond. The channel cross section was about 2 mm^2 at the narrowest point. The thermal dissipation ability was simulated using COMSOL finite element tools. The pressure difference between the water at the input and output of the microchannels was estimated to be about 100 kPa. With this pressure difference, the water flow and the geometry of the mount was not sufficient to maintain constant temperature when the pump power was increased; the variation of the mount temperature with the pump power for constant pressure of the circulating water is shown in Fig. 4. Nevertheless, the mount enabled more efficient heat dissipation compared to a standard mount without microchannels placed in the proximity of the diamond heat-spreader.

#133719 - $15.00 USD Received 20 Aug 2010; revised 5 Nov 2010; accepted 14 Nov 2010; published 23 Nov 2010

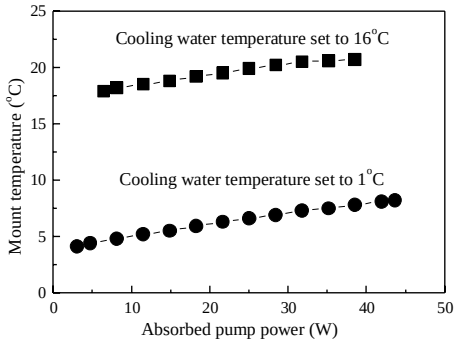

Fig. 4. The dependence of the mount temperature (T_{Mount}) on the pump power absorbed by the gain mirror during lasing at a constant water flow through the microchannel mount(measurements for pump spot diameter of 320 μm and output coupler transmission of 1.5%).

3.2 Influence of the output coupler on the output characteristics

The power conversion characteristics corresponding to different output couplers are shown in Fig. 5. For these measurements, the pump spot diameter on the gain mirror was ~320 μm and the temperature for the cooling water was ~16 °C. As revealed in Fig. 6, the slope efficiency and the threshold pump power increased with increasing output coupling. The maximum slope efficiency of 27%, estimated between the threshold and a pump power of 20 W, was reached with a 3% output coupling. However, it is noticed that regardless of the higher value at low pump powers, the slope efficiency with the 2.5% and 3% output couplers decreased more rapidly at high pump powers than it did with smaller output coupling. This is most likely due to higher gain required to match the increased output coupling, which means higher carrier concentration and, thus, higher rate of non-radiative recombination. Ultimately, the 1.5% output coupler resulted in the highest output power of ~7.5 W at a pump power of ~41.1 W and at the measured mount temperature of T_{Mount} = 21 °C. The maximum power conversion efficiency of 21% (pump light to signal light) was achieved with this output coupler at a pump power of 30.3 W. The pump power reflected from the gain mirror surface was measured to be 7% of the incident power.

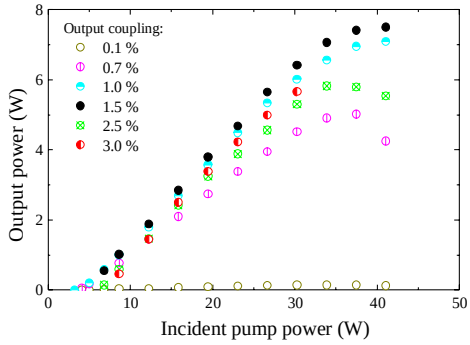

Fig. 5. Output characteristics of the 1.18 μm SDL corresponding to output couplers with different transmission. The temperature of the cooling water was set to 16 °C and the diameter of the pump spot was ~320 μm.

#133719 - $15.00 USD Received 20 Aug 2010; revised 5 Nov 2010; accepted 14 Nov 2010; published 23 Nov 2010

The deterioration of the slope efficiency at high pump powers due to non-radiative recombination can be alleviated by reducing the gain mirror temperature. In order to further increase the output power, the temperature of the cooling water was set to 1°C. Accordingly, the slope efficiency was increased, especially for higher output coupling, and the thermal roll-over point was shifted to higher pump powers. The maximum output power of ~9 W was achieved with T_{Mount} = 8 °C, again for the output coupler with a transmission of 1.5% as revealed in Fig. 7.

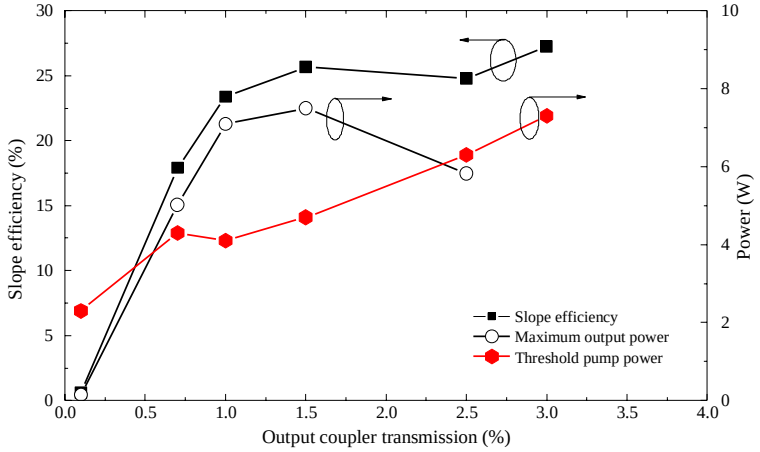

Fig. 6. Variation of the slope efficiency, maximum output power, and the threshold pump power with the output coupling ratio, for a cooling water temperature of 16 °C and a pump spot diameter of ~320 µm. The slope efficiency was determined from linear fit in the range between threshold and a pump power of 20 W.

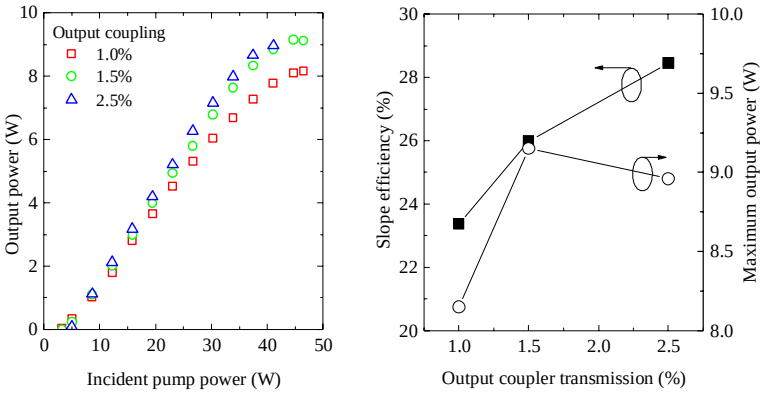

Fig. 7. Output characteristics of the 1.18 µm SDL with cooling water temperature set to 1 °C. Pump spot diameter was ~320 µm.

#133719 - $15.00 USD Received 20 Aug 2010; revised 5 Nov 2010; accepted 14 Nov 2010; published 23 Nov 2010

3.3 Power scaling by increasing the pump spot size

Next, different pump spot sizes were tested with the temperature of the cooling water set to 1°C. For each of the pump spot sizes, we also tested the operation with different output couplers. In all cases, the 1.5% output coupler was found to be optimal with respect to maximum achievable output power. Thus, only the results with this particular output coupler are presented below. The pump spot size was changed by modifying the focusing lens between the pump laser and the gain mirror, followed by cavity readjustment. Figure 8 reveals that over 11 W of output power was generated by the SDL with increased pump spot diameter of 390 µm and with T_{Mount} = 10 °C. As the figure suggests, this was achieved by shifting the thermal roll-over to higher pump powers by decreasing the pump intensity. The slope efficiency, however, decreased with increasing spot size and, thus, thermal roll-over prevented the maximum output power from being increased further when pump spot diameter was increased to 460 µm. This can be explained by the non-ideal heat extraction from the gain mirror, as the heat extraction efficiency increases at a rate smaller than area [20]. Another, potentially important, limiting factor for the power scaling with the pump spot size, is the increase of the number of nonradiative defects within the optically pumped area. The larger the pump spot, the greater the risk to reach areas with higher density of defects or dislocation lines. We believe that further power scaling is possible by improving the heat dissipation and selecting gain chips with a lower density of defects.

Figure 8 reveals also a typical output spectrum corresponding to an output power of 5 W. Multiple peaks with spacing of about 0.156 nm were observed in the spectra, which were otherwise relatively broad and flat. The peaks originate from the etalon effect taking place in the 3 mm thick output coupler, despite the use of an antireflective coating on its back surface. To provide a smooth spectral shape, also the output coupler should be wedged. The origin of the dip in the spectrum around 1177.5 nm is not obvious, but we suspect it to be caused by the competition between etalon effects associated with the output coupler, diamond heat-spreader, and the resonant wavelength of the RPG mirror.

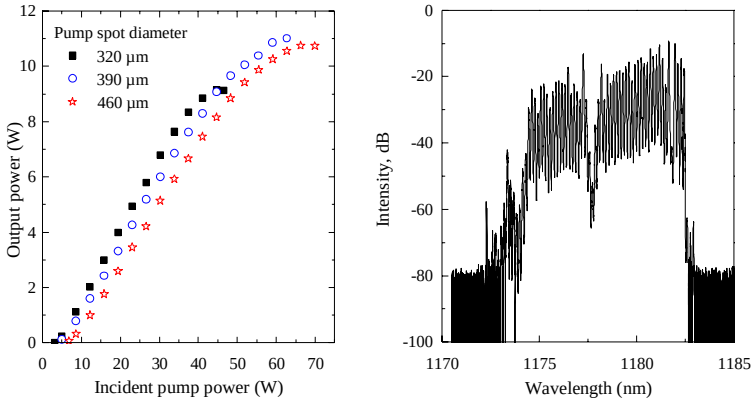

Fig. 8. Left: Output characteristics of the 1.18 µm SDL for three pump spot sizes. Cooling water temperature was set to 1 °C and the transmission of the output coupler was 1.5%. Right: Typical output spectrum at an output power of 5 W.

#133719 - $15.00 USD Received 20 Aug 2010; revised 5 Nov 2010; accepted 14 Nov 2010; published 23 Nov 2010

3.4 Frequency doubling to yellow

The same V-cavity SDL (Fig. 3) was used for frequency doubling experiments. For these experiments the output coupler M2 was replaced by a flat mirror with high reflectivity for both the fundamental and frequency doubled radiation. The folding mirror M1 had high transmission (of more than 90%) for the frequency doubled light and high reflectivity for the fundamental laser radiation. A 4 mm long type-I critically phase-matched BBO crystal, which was antireflection coated for 1220 nm radiation, was inserted into the cavity about 5 mm away from the flat mirror. The estimated mode diameter within the BBO crystal was 180 μm. With T_{Mount} = 9 °C (cooling water was set to 1 °C), we achieved about 6.2 W of frequency doubled output power. The power conversion characteristics are shown in Fig. 9 together with a typical output spectrum. With cooling water temperature set to 16 °C (T_{Mount} = 22 °C), the maximum output power of the frequency converted beam decreased to 5.2 W. A more thorough study of the frequency doubling behavior of the laser is currently underway.

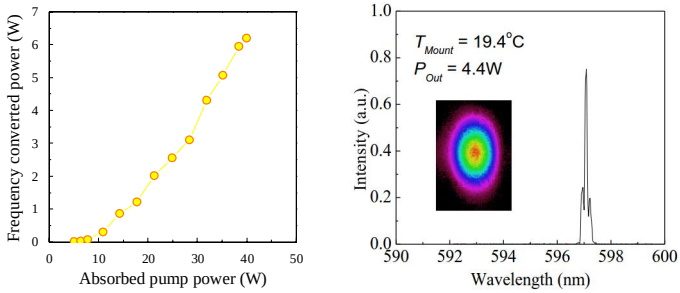

Fig. 9. Frequency doubled output power as a function of absorbed pump power (left), and output spectrum and output beam shape corresponding to 4.4 W of output power (right). Cooling water temperature was set to 1 °C (T_{Mount} = 9 °C) during the output power measurement. The output spectrum and beam shape were measured close to room temperature.

4. Conclusions

We demonstrated a GaInNAs/GaAs-based semiconductor disk laser emitting a record-high output power of 11 W at ~1180 nm. This performance was achieved by using a single gain chip attached to a water-cooled microchannel mount with the temperature of ~10 °C. We studied the laser operation with various cavity arrangements corresponding to different sizes of the pump spot on the gain chip and different output couplers. The results are encouraging for future developments, which will aim at making dilute nitride SDLs reliable and practical sources of high-brightness yellow-orange laser radiation. In particular we will focus on further improvements of the gain structure and heat management and on the demonstration of narrow linewidth operation for meeting the laser guide star specifications.

Acknowledgments

We acknowledge the help received from Jari Nikkinen for the antireflection coating deposition. This work was financially supported by the Academy of Finland within the Mignon project (number 128364), Pirkanmaa TE-center and Areté Associates.

#133719 - $15.00 USD Received 20 Aug 2010; revised 5 Nov 2010; accepted 14 Nov 2010; published 23 Nov 2010

Publication 4

V.-M. Korpijärvi, A. Aho, P. Laukkanen, A. Tukiainen, A. Laakso, M. Tuominen and M. Guina, "Study of nitrogen incorporation into GaInNAs: The role of growth temperature in molecular beam epitaxy," *Journal of Applied Physics*, vol. 112, pp. 023504-5, 2012.

P4

Study of nitrogen incorporation into GaInNAs: The role of growth temperature in molecular beam epitaxy

V.-M. Korpijärvi,[1,a)] A. Aho,[1] P. Laukkanen,[2] A. Tukiainen,[1] A. Laakso,[1] M. Tuominen,[2] and M. Guina[1]
[1]*Optoelectronics Research Centre (ORC), Tampere University of Technology, Tampere 33720, Finland*
[2]*Department of Physics and Astronomy, University of Turku, Turku 20014, Finland*

(Received 18 April 2012; accepted 9 June 2012; published online 18 July 2012)

GaInNAs has an important impact on developing GaAs-based optoelectronics and multijunction solar cells, but the complex nature of the nitrogen incorporation into GaInAs is still not fully understood. By combining x-ray diffraction, photoluminescence, reflection high-energy electron diffraction, and photoelectron spectroscopy measurements, we show that nitrogen incorporation is enhanced with increasing growth temperature in the range of 300–450 °C. We study the growth front and show that the surface reconstruction is (1×3) regardless of growth temperature in this range. The enhanced nitrogen incorporation can be modeled as a thermally activated process with activation energy of about 0.1 eV. © *2012 American Institute of Physics*.
[http://dx.doi.org/10.1063/1.4737127]

I. INTRODUCTION

The dilute nitride GaInNAs material has been studied actively, because it offers an opportunity of having a small band gap, lattice matched material grown epitaxially on GaAs substrates. This material system has made a high impact on the development of novel optoelectronic devices by increasing the wavelength coverage of the GaAs-based quantum wells (QWs) up to telecom wavelengths.[1] Short-wavelength (1.2 μm) GaInNAs QWs, on the other hand, can be used for generating high-power yellow-red radiation, which is difficult to produce otherwise.[2] Maybe the highest potential of GaInNAs is in producing high-quality bulk layers lattice-matched on GaAs or Ge and having band gap of 1 eV. Such heterostructures are instrumental for increasing the efficiency of multijunction solar cells.[3,4] However, many of these advantages have been hindered by difficulties in the epitaxy of GaInNAs. The growth-related challenges are largely due to the low miscibility of N into Ga(In)As and the related metastable nature of the GaInNAs material. Accordingly, GaInNAs crystals need to be grown at relatively low temperatures (<500 °C) where the surface kinetics has a significant role and where the phase separation of the material is limited by weakened diffusion of constituting atoms. Obviously, the understanding of the N incorporation into GaInNAs is the key to further developments of the GaInNAs technology.

Detailed *ab initio* calculations[5–7] have elucidated the mechanisms behind the N incorporation, which is indeed a complex interplay of several factors, including the growth temperature and the surface reconstruction of the GaInNAs growth front. It has been recently shown that the N incorporation (which should be assisted by activation of N_2 molecules, for example by a plasma source) is restricted to the topmost group-V layer, because the energy barrier between the topmost and subsurface layers is too high for N atoms to overcome at 500 °C.[7]

Although the growth temperature (T_g) is one of the most important parameters affecting the N solubility, the experimental findings for the effects of T_g are still controversial.[8–12] In particular, the redshift of emission wavelength with increasing T_g is not well understood. Previously, the annealing during the growth of other layers above GaInNAs has been found to induce this redshift.[8–11] In fact, the annealing causes a blueshift through short range ordering within GaInNAs, which takes place more readily in the samples grown at lower T_g.[8–11] Another explanation is phase separation of GaInNAs at elevated growth temperatures, which leads to formation of clusters or quantum dot like structures with redshifted emission.[12] Still another factor affecting the GaInNAs properties could be changes in defect concentration and type.[13,14] Nevertheless, the previous experiments have shown that T_g of GaInNAs itself does not significantly affect the amount of N incorporated, except for the surface segregation and desorption, which lead to reduced N composition and emission blueshift at elevated growth temperatures ($T_g > 450$ °C).[15,16]

In this article, an unexpected effect of T_g on N incorporation is reported. In particular, we show that both the band gap and the lattice constant of GaInNAs decrease with increasing T_g at the range of 300–450 °C. These changes, measured by x-ray diffraction (XRD) and photoluminescence (PL), can be fully explained by enhancement of N incorporation with increasing T_g, which is supported also by x-ray photoelectron spectroscopy (XPS) measurements. Reflection high-energy electron diffraction (RHEED) observations made during the GaInNAs growth reveal that for T_g within 300–450 °C, the surface reconstruction remains the same: (1×3). It appears that this growth front geometry has not been considered in previous computational studies. By combining XRD and PL measurements with post-growth thermal annealing of samples grown at different

a)Electronic mail: ville-markus.korpijarvi@tut.fi.

temperatures, we also elucidate the relation between T_g and effects of thermal annealing.

II. EXPERIMENT

This study is based on two sets of samples: a set of compressively strained $Ga_{0.75}In_{0.25}N_{0.01}As_{0.99}$ QWs and a set of three nominally lattice-matched bulk $Ga_{0.921}In_{0.079}N_{0.03}As_{0.97}$ samples. All the samples were grown on n-doped GaAs(100) substrates by a Veeco GEN20 solid source molecular beam epitaxy (MBE) system equipped with a radio frequency plasma source for nitrogen incorporation. RHEED experiments were performed with a separate bulk sample of $Ga_{0.921}In_{0.079}N_{0.03}As_{0.97}$. The growth temperature was measured by a commercial BandiT band edge thermometer. After the growth, the room temperature PL was measured by a RPM2000 system using a 532 nm Nd:YAG excitation laser and a GaInAs detector. For high-resolution XRD measurements, we used a 5-crystal X'Pert Pro MRD system with ω–2θ geometry and Cu Kα1 radiation.

Each QW sample consists of two 7 nm thick $Ga_{0.75}In_{0.25}N_yAs_{1-y}$ QWs with nominal nitrogen composition of about $y = 1\%$ and separated by a 20-nm thick GaAs spacer. The QW pair was sandwiched between 100 nm GaAs layers on both sides and further surrounded by $Al_{0.6}Ga_{0.4}As$ layers with thickness of 150 nm below the QWs and 50 nm above the QWs. The upper $Al_{0.6}Ga_{0.4}As$ layer was protected against oxidation by a 10-nm thick GaAs layer. All the growth parameters, except for the T_g of GaInNAs, were kept constant for the entire sample series. The growth rates were 1.5, 0.6, and 0.8 μm/h for AlGaAs, GaAs, and GaInNAs, respectively. The As/III beam equivalent pressure (BEP) ratio ($(As/III)_{BEP}$) was about six. The (Al)GaAs layers were grown at 580 °C. The T_g for GaInNAs QWs (at which also the GaAs spacer and 5 nm GaAs layers surrounding the QW pair were grown) was varied between 310 and 460 °C. The growth was interrupted for T_g ramps to and from the QW temperature.

Eight of the eleven QW samples were used for rapid thermal annealing (RTA) experiments carried out in a separate furnace at 700 °C. During RTA, the sample surfaces were protected by covering them with an n-GaAs substrate. Several RTA treatments were done on the same sample chips and their PL spectra were measured between the consecutive annealing steps.

The second sample set used for this study consisted of samples comprising a 500 nm thick $Ga_{0.921}In_{0.079}N_{0.03}As_{0.97}$ layer grown on GaAs. Again, the GaInNAs T_g is the only difference between these samples: T_g values for the three samples were 307, 335, and 363 °C. The $(As/III)_{BEP}$ used for the GaInNAs growth was about ten. The growth rate was 0.75 μm/h.

III. RESULTS AND DISCUSSION

Figure 1 shows XRD from the 500 nm thick $Ga_{0.921}In_{0.079}N_yAs_{1-y}$ samples. The rocking curves reveal that tensile strain of the layers increases with increasing T_g. Although decreasing In composition could explain the changes in strain,[17,18] it cannot account for the observed PL

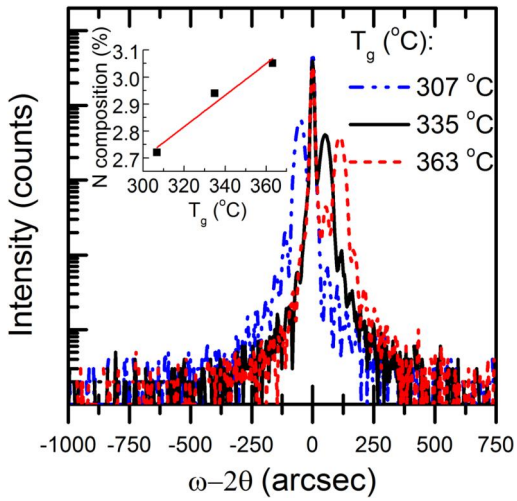

FIG. 1. XRD rocking curves measured from 500 nm thick $Ga_{0.921}In_{0.079}N_{0.03}As_{0.97}$ samples showing the decrease of compressive strain with increasing T_g. Inset shows the increase of nitrogen composition assuming that it is the only cause for the changing strain.

emission redshift with increasing T_g. Moreover, the segregation effects are most likely diminished at the low growth temperatures studied here.[15,19] Figure 1 also shows that the width of the GaInNAs related diffraction peaks is constant within the used measurement accuracy (4 arcsec), which indicates that there is no change in the homogeneity and coherency of the layers. Thus, by assuming that enhanced N incorporation causes the observed change in strain, dynamical XRD simulations fitted to the measurements show that the N composition changes with T_g at a slope of 0.006%/°C (linear fit in the inset of Fig. 1). This corresponds to a slope of 0.002%/°C if normalized by the nominal N composition of 3%. In addition, XPS was used to confirm the relative N composition of these samples. Although the sample surfaces were oxidized, the relative N 1s intensities (not shown in figures) of the samples clearly revealed that the N concentration systematically increases with T_g.

Figure 2 shows RHEED patterns observed on the GaInNAs surface with changing the sample temperature in the As flux. At 500–600 °C, RHEED showed a (2×4) surface reconstruction (Figs. 2(a) and 2(b)). If the As flux was closed at 500–600 °C, the (2×4) pattern changed to a (3×1) one (not shown), which can be the same as found recently.[20] Between 300 and 500 °C in the As flux, RHEED showed a (1×3) reconstruction as presented in Figs. 2(c) and 2(d). Decreasing the temperature below 300 °C changed the pattern to c(4×4). Varying the BEP value between 10 and 30 did not significantly affect these RHEED results. The (1×3) pattern was the only one seen during the growth of GaInNAs at 300–450 °C. Previously, 1×3 reconstruction has been observed for InGaAs at low growth temperatures.[21] Increase of the growth temperature above 500 °C led to a spotty RHEED indicating a rough surface. The (1×3) reconstruction is interesting because it has not been used as a surface

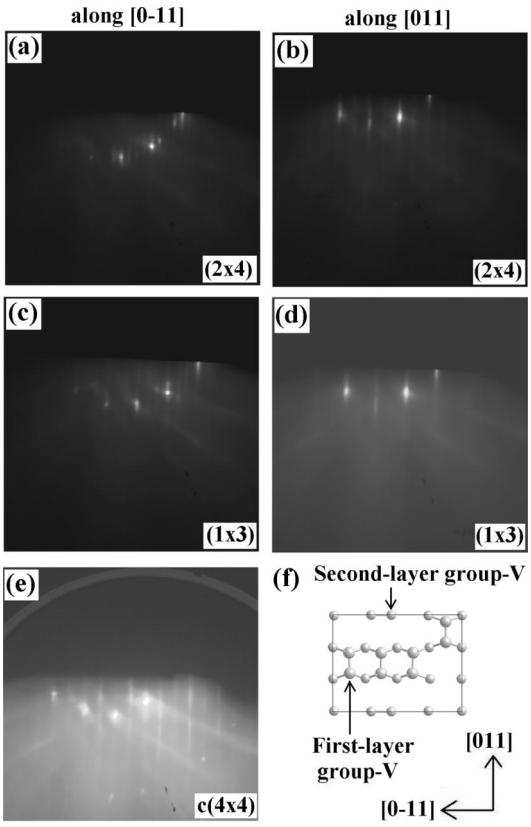

FIG. 2. (a)-(e) RHEED patterns from (2×4)-, (1×3)-, and $c(4\times4)$-reconstructed GaInNAs surfaces observed with decreasing the substrate temperature under the As flux (see text). (f) Possible (4×3) structural building block for the surface showing the (1×3) RHEED.

model in the previous N-solubility calculations, according to our knowledge. The (1×3) RHEED observation, however, agrees with recent calculations[22] showing that the (4×3) reconstructions are almost stable on the GaAs(100) and are likely important in kinetically limited growth conditions as well as for strain-stabilized III-V alloy surfaces. Thus, our RHEED observation provide an experimental evidence for the calculated results; the surfaces producing the (1×3) pattern are most likely composed of (4×3) building blocks[23] like that shown in Fig. 2(f). To recapitulate, the RHEED results show that the above described increase in the N concentration with T_g is not related to the surface reconstruction change.

Figure 3 shows the PL characteristics measured before annealing from the QW samples grown at different temperatures. The emission wavelength increases monotonously with increasing T_g up to 434 °C after which it starts to decrease. The peak intensity, on the other hand, increases with decreasing T_g until a rapid decrease at the lowest T_g of 307 °C. The PL peak width decreases with decreasing T_g throughout the studied temperature range. The samples were grown one after another starting from the highest T_g and continuing sample by sample towards the lowest T_g. After the complete series was grown, the growth of the sample with $T_g = 448$ °C was repeated in order to evaluate the repeatability of the growths. As shown in Fig. 3, the difference in PL wavelengths between the two samples is only 5 nm.

According to simulations based on band anticrossing model,[24] the wavelength increase of the QWs for T_g within the range of 307–434 °C (Fig. 3(a)) corresponds to a N composition increase of about 0.006%/°C. However, taking into account that nominal nitrogen composition of the QWs is only one third of the nitrogen composition of the bulk samples, this value is higher than expected. The surprisingly strong increase of emission wavelength with increasing T_g could be partly explained by growth temperature dependent short range ordering.[8–11] In order to minimize the effect of short range ordering and to be able to investigate the effects of changing nitrogen composition, we studied annealed QW samples.

Figure 4 shows the blueshift of the PL peak wavelength with respect to as-grown wavelength as a function of the cumulative annealing time. The blueshift first increases up to 1200 s but then saturates almost entirely as the annealing is continued. It is also observed that the amount of the blue shift increases with increasing T_g except for the highest T_g of 462 °C. The sample grown at the lowest T_g of 307 °C stopped emitting after 600 s at 700 °C. The main blueshift mechanisms during annealing are usually the change in composition due to interdiffusion of atoms across the QW interfaces and the short-range ordering of nearest neighborhood of N atoms from Ga-rich to In-rich.[6,25,26] The short range ordering is shown to be the dominant blueshift mechanism if low

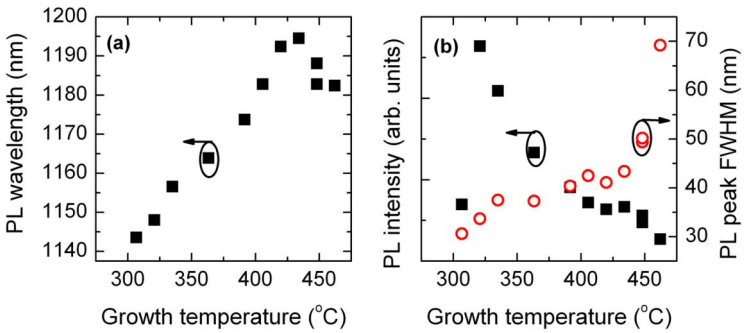

FIG. 3. (a) PL peak wavelength, (b) peak intensity and full width at half maximum (FWHM) measured before annealing from the samples grown at different temperatures.

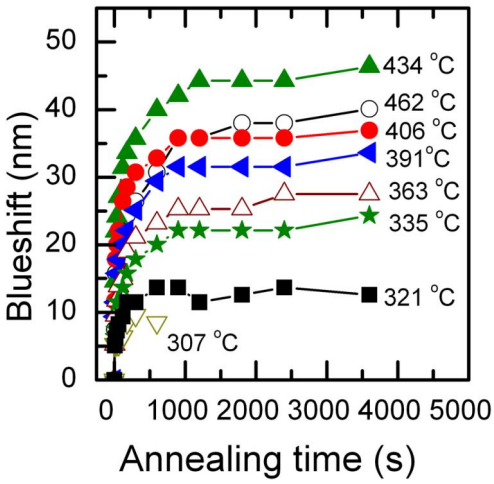

FIG. 4. Blueshift of the PL peak wavelength as compared to the as-grown wavelength. Data points correspond to measurements between consecutive annealing treatments. Growth temperatures for different samples are indicated in the figure.

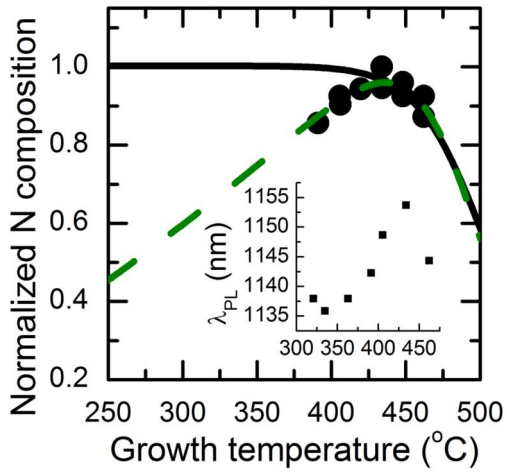

FIG. 5. Nitrogen composition of annealed QW samples based on the PL peak wavelength simulation and normalized by the nominal composition of 1%. Figure shows also kinetic nitrogen incorporation model fitted to the measurement data: The solid curve assumes constant incorporation and activated desorption,[15] whereas the dashed curve is based on the same model modified so that also incorporation is an activated process. Inset shows the PL peak wavelengths with respect to growth temperature after 2400 s of annealing at 700 °C.

annealing temperature and GaAs proximity capping are used[25,26]—as they were in this study. Thus, the increase of blueshift with increasing T_g agrees well with the reported[27] increase of the number of Ga-N bonds, which are favored at the growth front, relative to In-N bonds. The sample grown at the highest T_g of 462 °C might have reached the threshold temperature for phase separation and three dimensional growth mode.[27,28] XRD measurements did not reveal considerable or systematic change of strain due to RTA, neither for the QW samples nor for the bulk samples. This indicates that their composition does not change in annealing.

The inset of Fig. 5 shows the PL peak wavelength as a function of T_g as measured after 2400 s annealing, i.e., after the saturation of the blueshift. Now, the wavelength differences between the samples, which were annealed for prolonged time, are more related to variations in composition than in short-range ordering.[6,29,30] According to simulations, the wavelength redshift in the T_g range of 321–434 °C corresponds to a nitrogen composition increase of 0.002%/°C. This increase matches the slope increase measured by XRD for the bulk samples if the slope values are normalized to nominal nitrogen compositions. This relatively small change in the absolute nitrogen composition of the QWs would be hardly detectable by XRD.

Short range ordering around N atoms, which depends on the T_g, can explain part of the wavelength differences in the as-grown materials (Fig. 3).[8–11] However, here the wavelength differences are shown to exist even after prolonged annealing, which is consistent with the assumed increase of N composition with increasing T_g. The increase of N composition deduced from XRD measurements of bulk GaInNAs samples (Fig. 1, inset) matches very well the wavelength red shift observed for the annealed QW samples.

Now the kinetic nitrogen incorporation model[15] can be modified so that, in addition to desorption, also incorporation from the surface into lattice is modeled as an activated process, i.e., by an Arrhenius exponential (Ae^{-E_a/kT_g}). This gives the following expression for the nitrogen composition [N] in the crystal

$$[N] = \frac{A\exp(-E_a/kT_g)}{C + D\exp(-E_d/kT_g)}, \quad (1)$$

where E_a and E_d are the activation energies for incorporation and desorption, respectively. A, C, and D are constants independent of temperature, but can be related to growth conditions as suggested in the literature.[15] Using this model, we can estimate the activation energies by fitting $[N]$ with the measured data (Fig. 5). This gives an activation energy of $E_a \approx 0.1$ eV for incorporation. Figure 5 shows the fitting also with constant, non-activated incorporation rate, as modeled previously.[15] In both cases, the previously reported[15,31,32] activation energy for desorption ($E_d = 2.1$ eV) was used and gave a good fit with the measurements. Compared to previous reports,[15] nitrogen surface segregation seems to play only a minor role at the growth conditions studied here, and thus was not included in the calculations.

IV. CONCLUSIONS

In conclusion, the nitrogen composition in GaInNAs has been found to increase with increasing T_g in the range of 300–450 °C. The RHEED observations made during the growth show that there are no reconstruction changes related to the enhanced N solubility. We described the nitrogen incorporation as a thermally activated process. Accordingly, we could present a refinement to the kinetic nitrogen incorporation model. Fitting the refined model (Eq. (1)) with our

measurement data gave an activation energy of about 0.1 eV for nitrogen incorporation. The presented results are helpful to testing physical models of the N incorporation.

ACKNOWLEDGMENTS

Authors would like to acknowledge the technical assistance from Mr. Pekka Malinen and the financial support from EU through the FP7-ICT project RAMPLAS and from the Finnish Funding Agency for Technology and Innovation (TEKES) through Solar III-V (project 40120/09). V.-M.K. acknowledges the financial support from Graduate School in Electronics, Telecommunications and Automation (GETA), TTY:n tukisäätiö, the Emil Aaltonen Foundation, and the Walter Ahlström Foundation.

[1]G. Jaschke, R. Averbeck, L. Geelhaar, and H. Riechert, J. Cryst. Growth **278**, 224 (2005).
[2]V.-M. Korpijärvi, T. Leinonen, J. Puustinen, A. Härkönen, and M. D. Guina, Opt. Express **18**, 25633 (2010).
[3]D. J. Friedman and S. R. Kurtz, Prog. Photovoltaics **10**, 331 (2002).
[4]D. B. Jackrel, S. R. Bank, H. B. Yuen, M. A. Wistey, J. James, S. Harris, A. J. Ptak, S. W. Johnston, D. J. Friedman, and S. R. Kurtz, J. Appl. Phys. **101**, 114916 (2007).
[5]S. B. Zhang and A. Zunger, Appl. Phys. Lett. **71**, 677 (1997).
[6]M. Albrecht, H. Abu-Farsakh, T. Remmele, L. Geelhaar, H. Riechert, and J. Neugebauer, Phys. Rev. Lett. **99**, 206103 (2007).
[7]H. Abu-Farsakh and J. Neugebauer, Phys. Rev. B **79**, 155311 (2009).
[8]E.-M. Pavelescu, J. Wagner, H.-P. Komsa, T. T. Rantala, M. Dumitrescu, and M. Pessa, J. Appl. Phys. **98**, 083524 (2005).
[9]R. Kudrawiec, E.-M. Pavelescu, J. Andrzejewski, J. Misiewicz, A. Gheorghiu, T. Jouhti, and M. Pessa, J. Appl. Phys. **96**, 2909 (2004).
[10]E.-M. Pavelescu, T. Jouhti, M. Dumitrescu, P. J. Klar, S. Karirinne, Y. Fedorenko, and M. Pessa, Appl. Phys. Lett. **83**, 1497 (2003).
[11]S. Karirinne, E.-M. Pavelescu, J. Konttinen, T. Jouhti, and M. Pessa, New J. Phys. **6**, 192 (2004).
[12]W. M. McGee, R. S. Williams, M. J. Ashwin, T. S. Jones, E. Clarke, J. Zhang, and S. Tomić, Phys. Rev. B **76**, 085309 (2007).
[13]Q. D. Zhuang, A. Krier, and C. R. Stanley, J. Appl. Phys. **101**, 103536 (2007).
[14]G. Stenuit and S. Fahy, Phys. Rev. B **76**, 035201 (2007).
[15]Z. Pan, L. H. Li, W. Zhang, Y. W. Lin, and R. H. Wu, Appl. Phys. Lett. **77**, 214 (2000).
[16]V. A. Odnoblyudov, A. Y. Egorov, A. R. Kovsh, A. E. Zhukov, N. A. Maleev, E. S. Semenova, and V. M. Ustinov, Semicond. Sci. Technol. **16**, 831 (2001).
[17]E. Luna, A. Trampert, E.-M. Pavelescu, and M. Pessa, New J. Phys. **9**, 405 (2007).
[18]H. F. Liu, V. Dixit, and N. Xiang, J. Appl. Phys, **100**, 083518 (2006).
[19]K. Muraki, S. Fukatsu, Y. Shiraki, and R. Ito, Appl. Phys. Lett. **61**, 557 (1992).
[20]A. Ohtake, J. Appl. Phys. **110**, 033506 (2011).
[21]P. A. Bone, J. M. Ripalda, G. R. Bell, and T. S. Jones, Surf. Sci. **600**, 973 (2006).
[22]J. C. Thomas, N. A. Modine, J. Mirecki Millunchick, and A. Van der Ven, Phys. Rev. B **82**, 165434 (2010).
[23]W. Barvosa-Carter, A. S. Bracker, J. C. Culbertson, B. Z. Nosho, B. V. Shanabrook, L. J. Whitman, H. Kim, N. A. Modine, and E. Kaxiras, Phys. Rev. Lett. **84**, 4649 (2000).
[24]W. Shan, W. Walukiewicz, J. W. Ager, E. E. Haller, J. F. Geisz, D. J. Friedman, J. M. Olson, and S. R. Kurtz, Phys. Rev. Lett. **82**, 1221 (1999).
[25]M. Hugues, B. Damilano, J.-M. Chauveau, J.-Y. Duboz, and J. Massies, Phys. Rev. B **75**, 045313 (2007).
[26]J. Pakarinen, C. S. Peng, J. Puustinen, P. Laukkanen, V.-M. Korpijarvi, A. Tukiainen, and M. Pessa, Appl. Phys. Lett. **92**, 232105 (2008).
[27]X. Kong, A. Trampert, E. Tournié, and K. H. Ploog, Appl. Phys. Lett. **87**, 171901 (2005).
[28]A. Hierro, J.-M. Ulloa, J.-M. Chauveau, A. Trampert, M.-A. Pinault, E. Tournié, A. Guzmán, J. L. Sánchez-Rojas, and E. Calleja, J. Appl. Phys. **94**, 2319 (2003).
[29]V. Lordi, H. B. Yuen, S. R. Bank, M. A. Wistey, J. S. Harris, and S. Friedrich, Phys. Rev. B **71**, 125309 (2005).
[30]V. Lordi, V. Gambin, S. Friedrich, T. Funk, T. Takizawa, K. Uno, and J. S. Harris, Phys. Rev. Lett. **90**, 145505 (2003).
[31]R. J. Hauenstein, D. A. Collins, X. P. Cai, M. L. O'Steen, and T. C. McGill, Appl. Phys. Lett. **66**, 2861 (1995).
[32]Z. Z. Bandic, R. J. Hauenstein, M. L. O'Steen, and T. C. McGill, Appl. Phys. Lett. **68**, 1510 (1996).

Publication 5

V.-M. Korpijarvi, E. L. Kantola, T. Leinonen, R. Isoaho and M. Guina, "Monolithic GaInNAsSb/GaAs VECSEL Operating at 1550 nm," *IEEE Journal of Selected Topics in Quantum Electronics*, vol. 21, pp. 1700705, 2015.

P5

Monolithic GaInNAsSb/GaAs VECSEL operating at 1550 nm

Ville-Markus Korpijärvi, Emmi L. Kantola, Tomi Leinonen, Riku Isoaho, and Mircea Guina

***Abstract*—The first monolithic GaAs-based vertical-external-cavity surface-emitting laser (VECSEL) operating at 1550 nm is reported. VECSEL operation is based on a gain mirror which was grown in a single growth run by plasma-assisted molecular beam epitaxy. The gain mirror comprised 8 GaInNAsSb/GaAs quantum wells with a photoluminescence peak at 1505 nm and an AlAs/GaAs distributed Bragg reflector ensuring high reflectivity. The VECSEL chip was pumped with an 808 nm diode laser that had a large quantum defect in respect to the lasing wavelength. An output power of 80 mW in continuous wave mode and 210 mW in pulsed pump mode are demonstrated close to room temperature.**

***Index Terms*—GaInNAsSb, gallium arsenide, quantum well lasers, semiconductor disk lasers, semiconductor lasers, surface emitting lasers, vertical-external-cavity surface-emitting lasers**

I. Introduction

Availability of high quality compound semiconductor heterostructures has enabled a rapid progress of vertical-external-cavity surface-emitting lasers (VECSELs) to cover a broad spectral range from ultraviolet to mid-infrared, yet not without gaps [1]. Because of efficient heat removal and good control of transverse modes by the external cavity, VECSELs are well suited for power scaling while preserving high beam quality [2]. Furthermore, their output characteristics can be modified by including optical components in the external cavity. These components can be for example SESAMs for mode locking [3], nonlinear crystals for frequency conversion [4] and wavelength selective components for narrow-linewidth operation [5].

So far GaAs-based VECSELs emitting at 1.0–1.1 µm have shown the best performance [6, 7]. At these wavelengths the high-gain InGaAs quantum wells (QWs) and AlAs/GaAs distributed Bragg reflectors (DBRs) can be grown monolithically on GaAs substrates. High refractive index contrast, low lattice mismatch and high thermal conductance make AlAs and GaAs an excellent choice of DBR materials, also for VECSELs that inherently have to handle a high thermal load.

This work was supported in part by the European Commission through project FP7-ICT RAMPLAS (270773). The work of V.-M. Korpijärvi was supported by the Graduate School in Electronics, Telecommunications and Automation (GETA), HPY research foundation and Ulla Tuominen Foundation.

Authors are with Optoelectronics Research Centre, Tampere University of Technology, Tampere, Finland (email: ville-markus.korpijarvi@tut.fi, web: www.tut.fi/orc).

At the telecom wavelength of 1.55 µm, the AlAs/GaAs DBRs retain their good characteristics but high lattice mismatch between InGaAs and GaAs limits the use of InGaAs/GaAs QWs. Because of the lack of suitable gain materials, monolithic GaAs-based VECSELs operating at 1.55 µm have not been demonstrated so far. To this end, GaAs-based GaInNAsSb is an attractive material because nitrogen allows both to reduce the band gap for reaching longer wavelengths and to compensate for the compressive strain of the InGaAs. The use of antimony as an incorporating surfactant improves the optical quality of the QWs, widens the usable growth parameter window and also decreases the band gap for emission at longer wavelengths [8, 9]. Yet, the growth parameters of 1.55 µm dilute nitride QWs should be carefully chosen in order to obtain material quality suitable for device fabrication, even if only 1–2 QWs are needed as it is the case for in-plane lasers [8, 10, 11]. Indeed, these requirements can become even more critical for VECSELs that usually require a high number of QWs (typically from 8 to14) to reach as high as possible single-pass gain.

GaInNAsSb/GaAs materials have already been used to demonstrate long-wavelength (> 1.5 µm) vertical-cavity surface-emitting lasers [12, 13] (VCSELs), edge-emitting lasers [8] and semiconductor optical amplifiers [14, 15]. Also VECSELs based on GaInNAs/GaAs have been previously demonstrated but at shorter wavelengths of 1.18 µm [16, 17], 1.22 µm [18] and 1.32 µm [19]. Here we use dilute nitride GaInNAsSb QWs to demonstrate the first monolithic 1.55 µm GaAs-based VECSEL.

Previous demonstrations of 1.55 µm VECSELs have made use of monolithic InP-based gain mirrors [5], wafer fused gain mirrors with AlAs/GaAs DBR and InP-based gain region [4, 20] or gain mirrors with InP-based gain region and hybrid metal–metamorphic AlAs/GaAs mirror [21]. InP-based DBRs do not provide sufficient heat removal for high power VECSELs and are difficult to fabricate because of high number of layer pairs required due to low refractive index contrast. In contrast, monolithic AlAs/GaAs DBRs can reach high reflectivity with relatively few layer pairs and their thermal conductance is much higher than that of DBRs of monolithic InP-based VECSELs. On the other hand, fabrication of wafer-fused or metamorphic hybrid mirrors is much more complicated as compared to monolithic GaInNAsSb VECSEL approach that we demonstrate here.

1550 nm VECSELs are of interest for example for telecom

applications as mode-locked pulsed sources. Longitudinally single-mode 1550 nm VECSELs could be used in laser communications, light detection and ranging (LIDAR), spectroscopy, sensing, and as seed lasers for high power amplified systems [22]. Ultralow noise VECSELs at 1550 nm could be used also in optical links of microwave antenna systems [23]. When frequency doubled to 700 – 800 nm, these lasers could provide an alternative to bulky Ti:sapphire lasers, or to GaAs-based diode lasers in applications where high beam quality is required [4]. VECSELs at slightly shorter wavelengths around 1480 nm could find application as pump sources of Raman amplifiers [24].

II. Gain Mirror Design and Fabrication

The semiconductor growths were carried out monolithically on n-GaAs(100) substrate by molecular beam epitaxy (MBE) equipped with a radio frequency plasma source for nitrogen. As and Sb were supplied by valved crackers and Al, Ga and In by normal effusion cells.

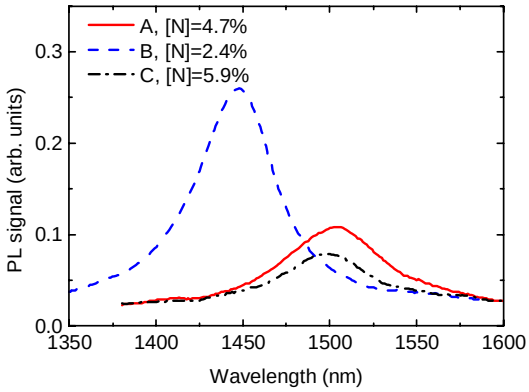

Fig. 1. Effect of nitrogen composition of GaNAs barriers surrounding the QWs on the photoluminescence spectra measured from test samples.

Before the growth of the full VECSEL gain mirror wafer, the compositions of the GaInNAsSb QW and the surrounding GaNAs barriers were optimized. For this, single-QW separate confinement heterostructures were grown that could be processed into edge emitting lasers for testing the material quality. The layer structure of these test laser diode wafers is described in [8]. As a starting point we used 7.5 nm $Ga_{0.625}In_{0.375}N_{0.030}AsSb$ QW surrounded by 21 nm tensile-strained $GaN_{0.047}As$ layers on both sides for compensating the compressive strain of the QWs (Sample A). The beam equivalent pressure of Sb used for the growth was 1.3E-8 Torr. As compared with this sample, increasing the nitrogen composition to 5.9 % (Sample C) in GaNAs decreased the photoluminescence (PL) intensity. Whereas, decreased nitrogen composition of 2.4 % (Sample B) led to remarkable increase of the PL intensity as shown in Fig. 1. Decreased nitrogen composition in the barrier improved also the laser diode characteristics of 80 µm x 1600 µm broad area oxide stripe lasers with as-cleaved facets. Lasing threshold current density decreased from 2500 A/cm^2 (sample A) to 920 A/cm^2 (sample B) (pulsed mode and at room temperature). However, reducing the nitrogen composition in GaNAs increases the conduction band offset of the QWs, which leads to blue shift of the emission wavelength (Fig. 1). Thus we grew another set of samples with $GaN_{0.024}As$ barriers but smaller band gap of the QWs. This second set consisted of three additional samples with increased Sb (Sample D), In (Sample E) or N (Sample F) composition in the QWs. From these samples the one with increased nitrogen composition in the QW (from 3.0 % to 3.7%) showed the best PL characteristics and reached the targeted emission wavelength of 1500 nm, as shown in Fig. 2. When this material was processed into a laser diode, it showed slightly increased lasing threshold of 1050 A/cm^2 but, on the other hand, also the highest slope efficiency of all these samples. With fine-tuned growth conditions the threshold current density could be pushed down to 800 A/cm^2 using the same structure and the optimized QW compositions.

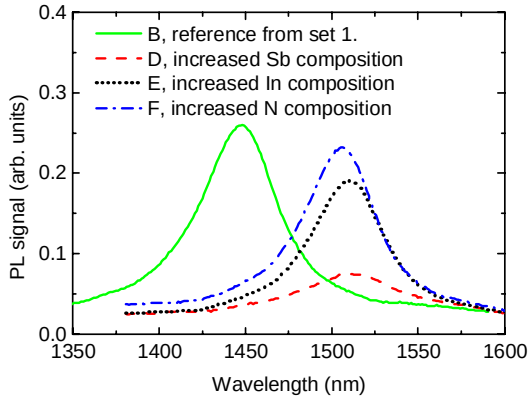

Fig. 2. Photoluminescence spectra measured from test wafers: effect of increasing emission wavelength by increasing Sb, In or N composition in the QWs.

The VECSEL gain mirror comprised 4 pairs of the GaInNAsSb QWs located at the antinodes of the optical standing wave formed in the semiconductor microcavity, as shown in Fig. 3. Design wavelength for the structure was 1545 nm. The QWs were surrounded by the strain compensating GaNAs layers with a thickness of 21 nm between the QWs and also at the outer edges of the QW pairs. The QW pairs were separated by GaAs layers. On the top of the structure, an $Al_{0.35}GaAs$ window layer finalized the structure to confine the carriers to the active region. Below the active region, a 29.5-pair AlAs/GaAs DBR mirror formed one end of the VECSEL cavity.

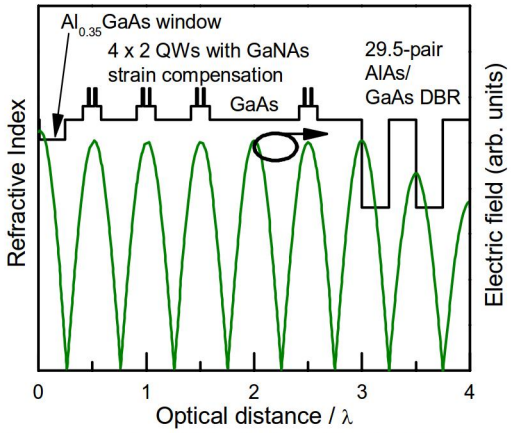

Fig. 3. Refractive index profile showing the position of the QWs at the maxima of simulated electric field.

The reflectance stop-band measured from the as-grown gain mirror was centered at ~1530 nm, as shown in Fig. 4. The PL of the as-grown gain mirror peaked at 1508 nm, which is very close to the peak wavelength (1504 nm) of the double-QW calibration sample reported in Fig. 4. It is also to be noted that the gain mirror PL spectrum is enhanced around 1545 nm which is the designed resonance wavelength of the gain mirror microcavity. Thus, the detuning between the room temperature PL peak wavelength and the resonance wavelength is about 40 nm (22 meV) to account for heating due to the large quantum defect between the energy of the pump and emitted photons.

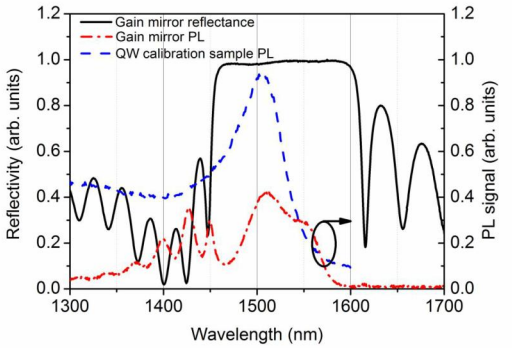

Fig. 4. PL and reflectance spectra measured from as-grown gain mirror wafer. PL spectrum of a calibration sample shows QW emission peak without the effect of VECSEL's semiconductor microcavity.

III. Laser Characterization

Laser characterization was carried out in a straight cavity, which is schematically shown in Fig. 5. The cavity was formed between the gain mirror and a highly reflective (R > 99.8 %) output coupler with a radius of curvature of 100 mm. The distance between the output coupler and the gain mirror was 53 mm. The gain mirror was pumped by an 808 nm diode laser. Diameter of the pump spot on the gain mirror was about 380 µm.

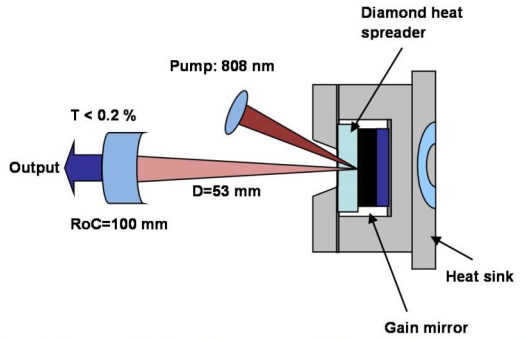

Fig. 5. Setup used for laser characterization. 808 nm diode laser was used for pumping. Laser cavity was formed between the gain mirror and the highly reflective (transmission < 0.2 %) mirror with a radius of curvature of 100 mm. Distance between the gain mirror and output coupler was 53 mm.

Heat was extracted from the gain mirror using a flat 300 µm thick diamond heat spreader that was attached to the as-grown gain mirror surface by capillary bonding. No coatings were deposited on the diamond. From the diamond, heat was further conducted to a water-cooled copper mount. Reported temperatures correspond to the temperature of this mount.

Lasing was observed above the incident threshold pump power of 10.3 W. Incident pump power refers to the pump power measured after pumping optics that is incident on the diamond heat spreader. Thus this power includes the pump power reflected from the diamond surface as well as the power absorbed in the DBR. Output power of the VECSEL increased monotonously, although not linearly, up to a pump power of 30.2 W. At this pump power, a maximum output power of 78 mW was recorded, as shown in Fig. 6. Cooling water temperature was set to 10 °C and mount temperature was 16 °C at the highest pump powers.

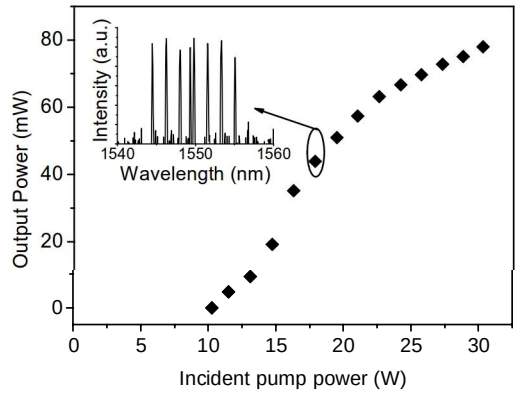

Fig. 6. VECSEL output power versus incident 808 nm pump power and an output spectrum measured at an output power of 42 mW.

The lasing spectrum, which is shown in the inset of Fig. 6 for output power of 42 mW, was centered at 1550 nm. The spectrum consisted of several peaks, which originate from the uncoated heat spreader. The peaks are separated by 1.75 nm (except for one additional peak), which corresponds to free

spectral range of the ~300 µm heat spreader diamond forming an etalon inside the cavity.

Because the output power of the VECSEL was limited to 78 mW in continuous wave mode, power conversion characteristics were measured also in pulsed pump mode. In pulsed mode average power and thus the heating of the gain mirror can be reduced. The 808 nm pump laser was pulsed by a driver that produced 1.5 µs pulses at 10 kHz repetition rate. The cooling water temperature was set to 16 °C. In pulsed mode, the mount temperature corresponded closely to the water temperature, and so the mount temperatures were similar in pulsed and CW measurements (16 °C). In pulsed mode, the VECSEL reached a maximum peak power of 210 mW at a peak pump power of 70 W, as shown in Fig. 7. With a driver current pulse of 1.5 µs, the VECSEL yielded an output pulse with a full width at half maximum (FWHM) of 0.94 µs at the maximum output power. The duration of the optical output pulses decreased with decreasing pump and output powers, as marked in the Fig. 7 for each measurement point.

It is known that 1.55 µm GaInNAsSb QWs are more sensitive to temperature increase than GaInNAs at shorter wavelengths [25, 26]. This problem might be strengthened here by the heat load related to the large quantum defect between the pump and operation wavelengths. Furthermore, rough estimation (using GaAs absorption coefficient of 13900 cm^{-1} [27] for the 0.9 µm thick active region) shows that in the current design only 71 % of the pump power is absorbed in the active region and as much as 29 % is transmitted to the DBR and lost there as harmful heat. Thus, it is expected that increasing active region thickness would improve the pump absorption efficiency and, as a result, also the overall efficiency of the laser. At the same time, the number of quantum wells could be increased. This should reduce the gain per QW required to reach the threshold, and thus, reduce the carrier density in each QW during lasing. The reduced carrier density should reduce the Auger recombination rate leading to higher efficiency of the laser. Still, further improvement of the pumping efficiency can be achieved by the use of antireflection coatings to minimize the pump power that is reflected from the diamond surface. Longer pump wavelengths and alternative designs can also be considered for reducing the quantum defect. Moreover we note that strain management techniques, similar to those reported in [28], should significantly reduce the number of defects associated with the growth of the highly strained layers.

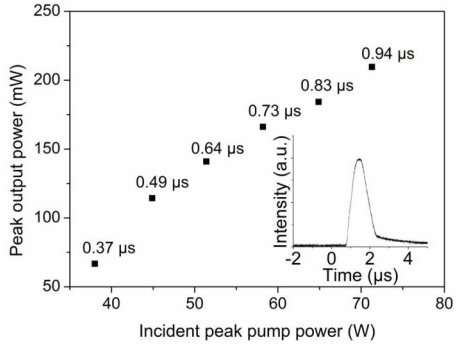

Fig. 7. Power conversion characteristics in pulsed pump mode. Inset shows shape of the output pulse at maximum output power. Output pulse duration (FWHM) is shown for each measurement point.

IV. Conclusions

We have demonstrated the first monolithic GaAs-based 1.55 µm VECSEL. For this, we used MBE-grown gain mirror comprising GaInNAsSb QWs with optimized compositions and AlAs/GaAs DBR. The VECSEL emitted an output power of 78 mW with spectrum centered at 1550 nm. In pulsed pump mode, a peak power of 210 mW was obtained. Future developments should involve alternative gain mirror designs for higher gain and smaller heat load, which would enable the usage of higher output coupling ratios. With these changes and optimized material quality, watt-level output powers are expected to be attained.

Acknowledgment

The authors are grateful to Arto Aho and Pekka Malinen for their support in MBE and to Jussi-Pekka Penttinen for his help in VECSEL processing and characterization. Jukka Viheriälä and his team are acknowledged for diode laser processing.

References

1. O. G. Okhotnikov, Semiconductor Disk Lasers: Physics and Technology. John Wiley & Sons, 2010.
2. M. Kuznetsov, F. Hakimi, R. Sprague and A. Mooradian, "Design and characteristics of high-power (> 0.5-W CW) diode-pumped vertical-external-cavity surface-emitting semiconductor lasers with circular TEM 00 beams," Selected Topics in Quantum Electronics, IEEE Journal Of, vol. 5, pp. 561-573, 1999.
3. A. Aschwanden, D. Lorenser, H. J. Unold, R. Paschotta, E. Gini and U. Keller, "2.1-W picosecond passively mode-locked external-cavity semiconductorlaser," Opt. Lett., vol. 30, pp. 272-274, Feb, 2005.
4. A. Rantamäki, J. Rautiainen, J. Lyytikäinen, A. Sirbu, A. Mereuta, E. Kapon and O. G. Okhotnikov, "1 W at 785 nm from a frequency-doubled wafer-fused semiconductor disk laser," Opt.Express, vol. 20, pp. 9046-9051, Apr, 2012.
5. H. Lindberg, A. Larsson and M. Strassner, "Single-frequency operation of a high-power, long-wavelength semiconductor disk laser," Opt. Lett., vol. 30, pp. 2260-2262, Sep, 2005.
6. B. Heinen, T.-L. Wang, M. Sparenberg, A. Weber, B. Kunert, J. Hader, S. W. Koch, J. V. Moloney, M. Koch and W. Stolz, "106 W continuous-wave output power from vertical-external-cavity surface-emitting laser," Electronics Letters, vol. 48, pp. 516-517, 2012.
7. T. L. Wang, Y. Kaneda, J. M. Yarborough, J. Hader, J. V. Moloney, A. Chernikov, S. Chatterjee, S. W. Koch, B. Kunert and W. Stolz, "High-

Power Optically Pumped Semiconductor Laser at 1040 nm," Photonics Technology Letters, IEEE, vol. 22, pp. 661-663, 2010.
8. S. R. Bank, H. Bae, L. L. Goddard, H. B. Yuen, M. A. Wistey, R. Kudrawiec and J. S. Harris, "Recent Progress on 1.55- μm Dilute-Nitride Lasers," Quantum Electronics, IEEE Journal Of, vol. 43, pp. 773-785, 2007.
9. H. B. Yuen, S. R. Bank, H. Bae, M. A. Wistey and J. S. Harris, "The role of antimony on properties of widely varying GaInNAsSb compositions," J. Appl. Phys., vol. 99, 2006.
10. G. Jaschke, R. Averbeck, L. Geelhaar and H. Riechert, "Low threshold InGaAsN/GaAs lasers beyond 1500 nm," J. Cryst. Growth, vol. 278, pp. 224-228, 5/1, 2005.
11. D. Bisping, D. Pucicki, M. Fischer, S. Höfling and A. Forchel, "Influence of arsenic flux on the annealing properties of GaInNAs quantum wells for long wavelength laser applications around 1.6 μm," J. Cryst. Growth, vol. 311, pp. 1715-1718, 2009.
12. M. A. Wistey, S. R. Bank, H. P. Bae, H. B. Yuen, E. R. Pickett, L. L. Goddard and J. S. Harris, "GaInNAsSb/GaAs vertical cavity surface emitting lasers at 1534 nm," Electronics Letters, vol. 42, pp. 282-283, 2006.
13. T. Sarmiento, H. Bae, T. D. O'Sullivan and J. S. Harris, "1528 nm GaInNAsSb/GaAs vertical cavity surface emitting lasers," in Lasers and Electro-Optics, 2009 and 2009 Conference on Quantum Electronics and Laser Science Conference. CLEO/QELS 2009. Conference On, 2009, pp. 1-2.
14. V.-M. Korpijarvi, G. Giannoulis, J. Makela, J. Viheriala, N. Iliadis, H. Avramopoulos, A. Laakso and M. Guina, "1.55 μm GaInNAsSb/GaAs ridge waveguide lasers and semiconductor optical amplifiers for photonic integrated circuits," in Semiconductor Laser Conference (ISLC), 2014 International, 2014, pp. 151-152.
15. T. Piwonski, J. Pulka, G. Madden, G. Huyet, J. Houlihan, J. Pozo, N. Vogiatzis, P. Ivanov, J. M. Rorison, P. J. Barrios and J. A. Gupta, "Ultrafast gain and refractive index dynamics in GaInNAsSb semiconductor optical amplifiers," J. Appl. Phys., vol. 106, 2009.
16. V. Korpijärvi, T. Leinonen, J. Puustinen, A. Härkönen and M. D. Guina, "11 W single gain-chip dilute nitride disk laser emitting around 1180 nm," Optics Express, vol. 18, pp. 25633-25641, 2010.
17. M. Guina, T. Leinonen, A. Härkönen and M. Pessa, "High-power disk lasers based on dilute nitride heterostructures," New Journal of Physics, vol. 11, pp. 125019, 2009.
18. V.-M. Korpijärvi, M. Guina, J. Puustinen, P. Tuomisto, J. Rautiainen, A. Härkönen, A. Tukiainen, O. Okhotnikov and M. Pessa, "MBE grown GaInNAs-based multi-Watt disk lasers," J. Cryst. Growth, vol. 311, pp. 1868-1871, 3/15, 2009.
19. J.-M. Hopkins, S. A. Smith, C. W. Jeon, H. D. Sun, D. Burns, S. Calvez, M. D. Dawson, T. Jouhti and M. Pessa, "0.6 W CW GaInNAs vertical external-cavity surface emitting laser operating at 1.32 μm," Electron. Lett., vol. 40, pp. 30-31, 2004.
20. J. Rautiainen, J. Lyytikäinen, A. Sirbu, A. Mereuta, A. Caliman, E. Kapon and O. G. Okhotnikov, "2.6 W optically-pumped semiconductor disk laser operating at 1.57-μm using wafer fusion," Opt.Express, vol. 16, pp. 21881-21886, Dec, 2008.
21. J. Tourrenc, S. Bouchoule, A. Khadour, J. Harmand, A. Miard, J. Decobert, N. Lagay, X. Lafosse, I. Sagnes, L. Leroy and J. Oudar, "Thermal optimization of 1.55 μm OP-VECSEL with hybrid metal–metamorphic mirror for single-mode high power operation," Opt. Quant. Electron., vol. 40, pp. 155-165, 2008.
22. A. Rantamäki, J. Rautiainen, A. Sirbu, A. Mereuta, E. Kapon and O. G. Okhotnikov, "1.56 μm 1 watt single frequency semiconductor disk laser," Opt.Express, vol. 21, pp. 2355-2360, Jan, 2013.
23. G. Baili, L. Morvan, G. Pillet, S. Bouchoule, Z. Zhao, J. Oudar, L. Ménager, S. Formont, F. V. Dijk, M. Faugeron, M. Alouini, F. Bretenaker and D. Dolfi, "Ultralow Noise and High-Power VECSEL for High Dynamic Range and Broadband RF/Optical Links," J. Lightwave Technol., vol. 32, pp. 3489-3494, Oct, 2014.
24. J. Lyytikainen, J. Rautiainen, A. Sirbu, V. Iakovlev, A. Laakso, S. Ranta, M. Tavast, E. Kapon and O. G. Okhotnikov, "High-Power 1.48-μm Wafer-Fused Optically Pumped Semiconductor Disk Laser," Photonics Technology Letters, IEEE, vol. 23, pp. 917-919, July, 2011.
25. S. R. Bank, L. L. Goddard, M. A. Wistey, H. B. Yuen and J. S. Harris, "On the temperature sensitivity of 1.5-μm GaInNAsSb lasers," Selected Topics in Quantum Electronics, IEEE Journal Of, vol. 11, pp. 1089-1098, 09, 2005.
26. D. G. McConville, S. J. Sweeney, A. R. Adams, S. Tomic and H. Riechert, "Temperature and pressure dependence of the recombination mechanisms in 1.3 μm and 1.5 μm GaInNAs lasers," Physica Status Solidi (B), vol. 244, pp. 208-212, 2007.
27. S. Haupt, M. Furitsch, H. H. Lindberg, I. Pietzonka, U. Strauss and G. Bacher, "Analysis of the Pump Wavelength Dependence of a 1060-nm VECSEL," Photonics Technology Letters, IEEE, vol. 24, pp. 341-343, 2012.
28. S. Ranta, T. Hakkarainen, M. Tavast, J. Lindfors, T. Leinonen and M. Guina, "Strain compensated 1120 nm GaInAs/GaAs vertical external-cavity surface-emitting laser grown by molecular beam epitaxy," J. Cryst. Growth, vol. 335, pp. 4-9, 11/15, 2011.

Ville-Markus Korpijärvi received his M.Sc. degree from Tampere University of Technology, Finland, in 2010. He majored in physics (semiconductor physics and optoelectronics), and his M.Sc. thesis described the development and use of plasma-assisted molecular beam epitaxy for fabricating GaInNAs/GaAs vertical-external-cavity surface-emitting lasers operating at 1180 nm and 1220 nm. His M.Sc. work was carried out at the Optoelectronics Research Centre (ORC), and he continues this work as a PhD student. He is the main author of three peer-reviewed journal articles.

Emmi Kantola received her MPhys (Hons) degree in 2011 from the University of Kent, Canterbury, England. She joined Tampere University of Technology in 2012 for post-graduate studies and since then she has been working with high-power Vertical-External-Cavity Surface-Emitting Lasers.

Tomi Leinonen joined Tampere University of Technology in 1999 and has since been involved in the development of numerous edge and surface emitting semiconductor lasers. He received his M.Sc. and D.Sc. in 2002 and 2007 in Tampere, and is currently the main investigator of 1100-1250 nm and visible high-power Vertical-External-Cavity Surface-Emitting Lasers. He has published 37 papers in international peer-reviewed journals and has over 67 international peer-reviewed conference publications (2 invited).

Riku Isoaho received his B.Sc. degree from Tampere University of Technology in 2014 and is now continuing his studies towards M.Sc. degree. His work concentrates on molecular beam epitaxy of novel GaInNASb devices.

Prof. Mircea Guina obtained the MSc degree in photonics at the Politehnica University of Bucharest in 1997 and the PhD degree in physics from Tampere University of Technology, Finland, in 2002. In 2008 he was appointed professor and Head of the III-V Optoelectronics Group at the Optoelectronics Research Centre, Tampere University of Technology. He conducts scientific work related to molecular beam epitaxy of novel optoelectronic heterostructures and devices, and their applications. His current projects are concerned with the development of uncooled lasers, amplifiers and modulators for hybrid-PICs, ordered nanostructures for quantum optics, epitaxy of III-Bi-V alloys, the development of high power semiconductor lasers (VECSELs and MOPAs), and the development of ultra-high efficiency multijunction solar cells based on GaInNAsSb-alloys. He has published more than 120 journal papers, several book chapters, holds 4 international patents, has several position of trust in COST Actions and scientific boards, and has given numerous invited talks at major optoelectronics conferences. He is the Director of the International Summer School “New Frontiers in Optical Technologies”, which he established in 2001.

Publication 6

V.-M. Korpijärvi, J. Viheriälä, M. Koskinen, A.T. Aho, M. Guina, “High-power temperature-stable GaInNAs DBR laser emitting at 1180 nm,” Submitted to *Optics Letters.*

For published version, see doi: 10.1364/OL.41.000657.

P6

High-power temperature-stable GaInNAs DBR laser emitting at 1180 nm

VILLE-MARKUS KORPIJÄRVI,[1,*] JUKKA VIHERIÄLÄ,[1] MERVI KOSKINEN,[1] ANTTI T. AHO,[1] MIRCEA GUINA[1]

[1]*Optoelectronics Research Centre (ORC), Tampere University of Technology, P.O. Box 692, FIN-33101, Tampere, Finland*
**Corresponding author: ville-markus.korpijarvi@tut.fi*

Received XX Month XXXX; revised XX Month, XXXX; accepted XX Month XXXX; posted XX Month XXXX (Doc. ID XXXXX); published XX Month XXXX

We report **a** single-mode 1180 nm distributed Bragg reflector (DBR) laser diode with **a** high output power of 340 mW. For the fabrication we employed novel nanoimprint lithography (NIL) that ensures cost-effective, large area, conformal patterning and does not require regrowth. The output characteristic exhibited outstanding temperature insensitivity with **a** power drop of only 30 **%** for an increase of the mount temperature from 20 to 80 °C. The high temperature stability was achieved by using GaInNAs/GaAs quantum wells (QWs), which exhibit improved carrier confinement compared to standard InGaAs/GaAs QWs. The corresponding characteristic temperatures were T_0=110 **K** and T_1=160K. Moreover, we used **a** large detuning between the peak wavelength of the material gain at room temperature and the lasing wavelength determined by the DBR. In addition to good temperature characteristics, GaInNAs/GaAs QWs exhibit relatively low lattice strain with direct impact on improving the lifetime of laser diodes at this challenging wavelength range. The single-mode laser emission could be tuned by changing the mount temperature (0.1 nm/°C) or the drive current (0.5 pm/mA). Laser showed no degradation in **a** room-temperature lifetime test at 900 mA drive-current. These compact and efficient 1180 nm laser diodes are instrumental for the development of compact frequency doubled yellow–orange lasers, which have important applications in medicine and spectroscopy. © 2015 Optical Society of America

OCIS codes: (140.2020) Diode lasers; (140.5960) Semiconductor lasers; (140.3570) Lasers, single-mode; (220.3740) Lithography; (230.1480) Bragg reflectors

http://dx.doi.org/xxx

Many important applications in spectroscopy and medicine, such as treatments of vascular lesions, would benefit from availability of compact semiconductor diode lasers emitting at yellow–orange wavelengths. However, this wavelength range cannot be reached with compact and efficient directly emitting semiconductor lasers typically employed for red wavelengths (GaAs-based compounds) or for blue–green wavelengths (GaN-based materials). Moreover, the frequency doubling approaches, traditionally used for reaching green wavelength range, suffer from the lack of high-power narrow-linewidth frequency stable laser diodes with fundamental emission at 1170 -1200 nm. This is due to the fact that GaInAs/GaAs QWs system would require incorporation of a high amount of In leading to high strain, ultimately generating high amount of defects affecting the laser efficiency and life-time. To cope with this limitation, strain compensation technologies have been employed in external cavity lasers architectures [1, 2] . Recently, strain-compensated GaInAs/GaAs QWs have been used to demonstrate a high power tapered laser diode [3] operating near room temperature. While this recent result is indeed promising, the long-term life-time assessment of such gain structures remains questionable given the high intrinsic strain of the QWs.

Alternatively, 1180 nm wavelength range can be reached using, GaInAs/GaAs QDs [4, 5] or dilute nitrides, i.e. GaInNAs/GaAs QWs [6] . In particular the use of a small amount of N, in the range of 1 %, has been recognized for its benefits related to reduced strain and good carrier confinement enabling demonstration of power levels beyond 10 W in optically pumped vertical-external-cavity surface-emitting lasers (VECSELs) [6] . Adding a small fraction of N to GaInAs can relax the design constraints of the semiconductor structure by avoiding the need for strain compensation and enabling use of higher number of QWs, which could be beneficial for power scaling in integrated amplifiers. The improved carrier confinement translates to improved temperature stability of laser characteristics, a feature that has been recognized since the proposal of GaInNAs/GaAs QWs for uncooled telecom lasers at 1.3 µm [7] . Improved temperature stability is expected to benefit especially miniaturization of frequency-doubled lasers and in general the development of photonic integration approaches, which are currently limited by thermal management issues. For example, ability of lasers to operate at elevated temperatures will reduce the constrains of mounting them close to frequency doubling crystals, which often require elevated operation temperatures [8] .

The single-mode operation with stable wavelength and narrow spectrum, which are essential features for efficient frequency doubling and spectroscopic applications [8] , can be achieved using a distributed

Bragg reflector (DBR) integrated to a narrow ridge waveguide (RWG). To this end, we have developed a process based on using soft stamp UV nanoimprint lithography (NIL) for patterning of the DBR. As compared with other patterning methods (such as electron beam lithography or steppers) NIL is a low-cost and high throughput method, which can imprint features at wafer scale [9] .

In this article we report on the NIL-based development of a temperature-stable single-mode GaInNAs/GaAs DBR laser diode emitting an output power as high as 340 mW at 1180 nm. This was enabled by employing GaInNAs/GaAs QW with improved carrier confinement and low intrinsic strain. The highest power reported so far for a DBR laser operating at 1180 nm, without amplifier or tapering, is ~230 mW [10].

The semiconductor structure was grown by plasma-assisted molecular beam epitaxy (MBE) on an n-GaAs(100) substrate and consisted of a single $GaIn_{0.31}N_{0.005}As$ QW embedded in a 1 µm GaAs waveguide surrounded by $Al_{0.25}GaAs$ claddings, as illustrated in Fig. 1. The QW was grown at low temperature of 380 °C in order to kinetically limit phase separation of metastable GaInNAs [11, 12] . We used an excess arsenic pressure corresponding to a beam equivalent pressure ratio of As/III = 14. A high growth rate of 1.4 µm/h was chosen to keep the nitrogen composition low [13] . On the p-side, thinner cladding was used for alleviating possible problems due to high aspect ratio etching of the DBR and to maximize thermal conductivity towards p-contact.

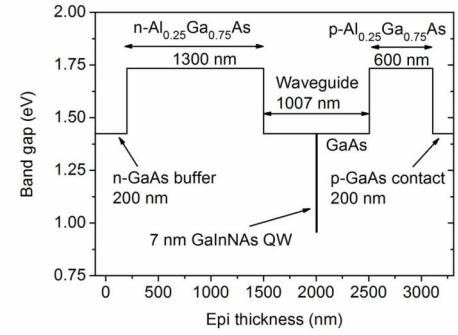

Fig. 1. Semiconductor layer structure grown by plasma-assisted MBE and used for the DBR laser.

In addition to precisely controlled growth conditions, post-growth annealing is of high-importance in GaInNAs device fabrication. Annealing reduces the amount of point defects related to low-temperature growth and nitrogen incorporation and affects nitrogen-induced short range ordering. This improves the luminescence intensity but also induces a blue shift of the emission wavelength. However, the unwanted blue shift is saturable and thus, easily controlled assuming that annealing temperature is not increased above 750 °C [12, 14] . In order to improve material quality for the lasers reported here, we grew three test structures with different annealing temperatures: ~695, ~705 and ~720 °C. The only difference between the test structures and the DBR laser structure was a thinner 900 nm n-AlGaAs cladding used in the test structures. As a result of increased annealing temperature, photoluminescence (PL) intensity of the laser wafers increased by an order of magnitude, and threshold current density of broad area test lasers decreased to one third of the original value (Fig. 2). The best wafer showed PL wavelength of 1173 nm and lasing wavelengths above 1190 nm, which are too high for the targeted 1180 nm DBR laser wavelength. For the DBR laser, we chose an annealing temperature of ~720 °C, fine-tuned the QW emission wavelength by slightly reducing In and N compositions, and increased the n-cladding thickness for suppressing mode-leakage to substrate.

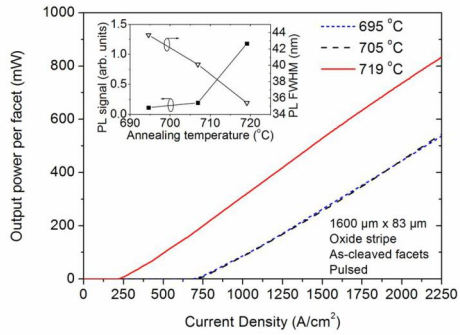

Fig. 2. Output power characteristics of 1600 µm x 83 µm oxide stripe test lasers annealed at different temperatures. Inset shows PL characteristics for the same wafers.

For testing the material characteristics, the heterostructure made for DBR laser was first processed into 83 µm x 1600 µm broad-area oxide stripe lasers without facet coatings. The lasers were mounted p-side up, which leads to poor thermal conductivity from the quantum well region through the substrate to the copper mount. Thus, these lasers were not optimized for high-power continuous wave (CW) operation. Still, they had low threshold current density of 220 A/cm² and reached maximum output of 1.2 W (0.6 W per as-cleaved facet) in CW mode at driving current of 2.8 A and voltage of 1.4 V. This corresponds to electrical to optical conversion efficiency of 31 % and shows clear improvement as compared with characteristics of InGaAs/GaAs QW lasers at the same wavelength and mounted p-side down for efficient cooling [10] . Lasing wavelength shifted from 1160 nm to 1188 when increasing the driving current from 1 A to 3 A. One reason for the good CW results can be the high thermal stability of the GaInNAs/GaAs QWs. Thermal properties can be characterized by characteristic temperatures $T_0 = \ln(I_{th})/\Delta T$ and $T_1 = \ln(slope)/\Delta T$ describing the exponential increase of threshold current I_{th} and decrease of slope efficiency, respectively, with increasing temperature T. The temperature dependence of the output power in pulsed mode is summarized in Fig. 3; the pulsed mode operation enabled to decouple the thermal behavior of the diodes from the heating related to the use of un-optimized mounting scheme (i.e. p-side up). The determined characteristics temperatures were T_0 = 110 K and T_1 = 160 K. For comparison, typical T_0 values for InGaAs/GaAs QWs with similar wavelength are around 80 K [10, 15] . In fact we measured a T_0 = 80 K and T_1 = 130 K for our InGaAs/GaAs laser with similar structure but emitting at 1060 nm. Still, it should be noted that regardless of the QW material these values can be improved using higher number of QWs or AlGaAs barriers. Increasing the number of QWs using dilute nitrides should be easier than with GaInNAs because of the smaller lattice mismatch. Wavelength of the broad-area lasers shifted at a rate of 0.41 nm/°C and was centered at 1180 nm at a mount temperature of 100 °C. The vertical far field had a full width at half maximum of 43°.

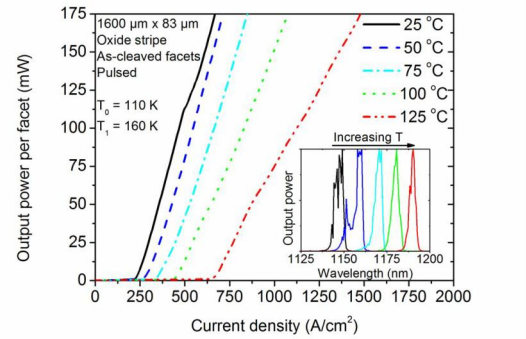

Fig. 3. Peak output power of a broad area laser in pulsed mode and at different mount temperatures. Inset shows output spectra corresponding to different mount temperatures.

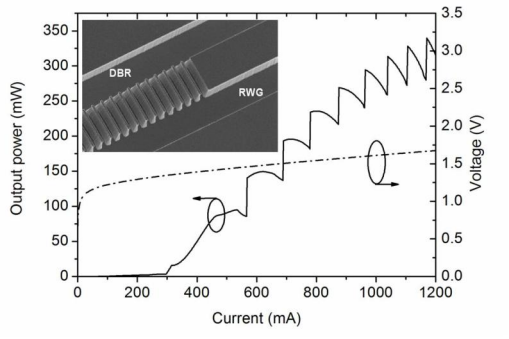

Fig. 4. Current-voltage and light output characteristics of the single-mode 1180 nm DBR laser in CW mode and at mount temperature of 20 °C. Inset shows a scanning electron microscope image taken from a DBR laser.

The DBR laser comprised a 2-mm-long 3rd order DBR section with a reflectivity estimated to be about 15 %. The passive DBR section selected a single longitudinal mode and stabilized the emission wavelength. A 3-mm-long RWG section with a width of 3.2 µm provided gain for lasing in a single transversal mode. DBR and RWG sections were imprinted by soft UV-NIL in one step and etched into semiconductor using inductively coupled plasma (ICP) etching system. Dielectric layer was then deposited on the wafer and removed from top of the ridge waveguide section to define the area where current is injected. P-side metallization (Ti/Pt/Au) was deposited and the wafer was thinned to 150 µm to allow facet cleaving. After thinning, n-metallization (Ni/Au/Ge/Au) was deposited and the metal was annealed to form ohmic contact. Both of the cleaved laser facets were antireflection coated with single layer Al_2O_3 for suppressing Fabry-Perot modes and to increase output power from the front facet. Heat extraction from the DBR lasers was improved by mounting them p-side down. Chips were first soldered with AuSn to AlN submount with thermal conductivity of 170 W/mK. Submount was then bonded on a conductively cooled copper mount with indium solder.

The DBR laser was characterized in continuous wave mode at mount temperature of 20 °C. The corresponding characteristics are presented in FIG. 4. Laser had a threshold current of 300 mA and reached a maximum output power of 340 mW, which was measured at a driving current of 1170 mA and forward voltage of 1.67 V (Fig. 4). This corresponds to electrical-to-optical power efficiency of 17 % whereas the maximum efficiency of 20 % was reached at driving current of 876 mA and output power of 269 mW. This record-high output power is an excellent basis for further increase of the output power using a tapered configuration.

Output spectrum of the DBR laser was centered at 1180 nm and had a full width at half maximum (FWHM) of 0.05 nm. The measured spectrum width was likely limited by the resolution of the optical spectrum analyzer (0.05 nm FWHM) used for the measurement. The wavelength could be adjusted at an average rate of 0.5 pm/mA. Tuning was characterized by abrupt changes due to changing of longitudinal lasing mode, which was observed also in the output power (Fig. 5). Between the mode hops, tuning rate was about 1.1 pm/mA. Although tuning was not continuous, emission wavelength could be tuned to any value in the tuning range of the laser owing to overlap between lasing wavelength ranges of consecutive longitudinal modes.

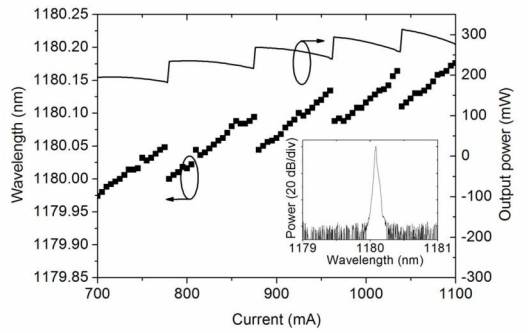

Fig. 5. Wavelength tuning with drive current. Changes between consecutive lasing modes are seen as abrupt changes in wavelength and output power. Inset shows the output spectrum measured at 800 mA.

DBR lasers were also measured at different mount temperatures. It was observed that threshold current decreased from 450 mA to 125 mA with increasing temperature from 10 to 50 °C (Fig. 6). This unusual behavior is explained by large detuning between the lasing wavelength and QW gain spectrum. Large detuning is illustrated by amplified spontaneous emission spectrum centered at 1142 nm at 500 mA driving current (inset of Fig. 6). The wavelength tuning rate with temperature was of 0.1 nm/°C. At high current levels output power was relatively insensitive to changes in mount temperature. For example, output powers measured at 1000 mA driving current were 255, 213 and 181 mW for mount temperatures of 20, 50 and 80 °C, respectively. This shows that excellent laser characteristics at high temperatures can be obtained by using high-confinement GaInNAs QWs together with large detuning between lasing wavelength and room-temperature QW gain wavelength.

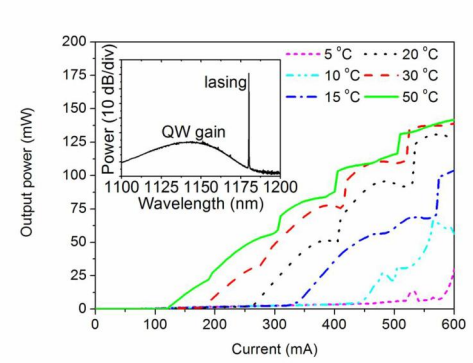

Fig. 6. Output power of DBR laser with respect to driving current measured at different mount temperatures. Inset shows output spectrum at room temperature and current of 500 mA.

A preliminary lifetime test was also carried out by driving the component for 125 hours at 900 mA and mount temperature of 20 °C. Only slight improvement of threshold current and output power were observed after the test.

In conclusion, we have demonstrated an 1180 nm single-mode DBR laser diode with record-high output power of 340 mW. The laser exhibited excellent temperature-stability with only 30 % drop in output power when the mount temperature was increased from 20 to 80 °C. Good high temperature characteristics were enabled by high detuning between lasing wavelength and room-temperature gain wavelength and by temperature-stable GaInNAs/GaAs QWs. Temperature stability of GaInNAs QWs was confirmed by measuring high characteristic temperatures of T_0=110 K and T_1=160 K for broad area laser diodes without DBR. High-power single-mode operation is important for enabling efficient frequency doubling, whereas good laser operation at elevated temperatures is important for future miniaturization of the frequency-doubled lasers. Next development steps include scaling up the output power by fabricating tapered DBR lasers and demonstration of frequency doubling to yellow–orange wavelengths in compact architectures.

Funding. European Commission within the 7th Framework Program projects APACOS and RAPIDO. Project CLEEN funded by the Finnish Agency for Innovation (TEKES).

Acknowledgment. Riku Isoaho's assistance in the epitaxy is gratefully acknowledged.

References

1. S. Ranta, T. Hakkarainen, M. Tavast, J. Lindfors, T. Leinonen, and M. Guina, J. Cryst. Growth 335, 4-9 (2011).
2. S. Ranta, M. Tavast, T. Leinonen, N. Van Lieu, G. Fetzer, and M. Guina, Electronics Letters 49, 59-60 (2013).
3. K. Paschke, F. Bugge, G. Blume, D. Feise, and G. Erbert, Opt. Lett. 40, 100-102 (2015).
4. R. L. Sellin, C. Ribbat, M. Grundmann, N. N. Ledentsov, and D. Bimberg, Appl. Phys. Lett. 78, 1207-1209 (2001).
5. D. Al Nakdali, M. Gaafar, M. Shakfa, F. Zhang, M. Vaupel, K. Fedorova, A. Rahimi-Iman, E. Rafailov, and M. Koch, IEEE Photonics Technology Letters, 27, 1128-1131 (2015).
6. V. Korpijärvi, T. Leinonen, J. Puustinen, A. Härkönen, and M. D. Guina, Optics express 18, 25633-25641 (2010).
7. M. Kondow, T. Kitatani, S. Nakatsuka, M. C. Larson, K. Nakahara, Y. Yazawa, M. Okai, and K. Uomi, IEEE Journal of Selected Topics in Quantum Electronics, 3, 719-730 (1997).
8. A. Jechow, R. Menzel, K. Paschke, and G. Erbert, Laser & Photonics Reviews 4, 633-655 (2010).
9. J. Viheriälä, J. Tommila, T. Leinonen, M. Dumitrescu, L. Toikkanen, T. Niemi, and M. Pessa, Microelectronic Engineering 86, 321-324 (2009).
10. K. Paschke, F. Bugge, G. Blume, D. Feise, W. John, S. Knigge, M. Matalla, H. Wenzel, and G. Erbert, Proc.SPIE 8965, 896509-896509-7 (2014).
11. W. McGee, R. Williams, M. Ashwin, T. Jones, E. Clarke, J. Zhang, and S. Tomić, Physical Review B 76, 085309 (2007).
12. V.-M. Korpijärvi, A. Aho, P. Laukkanen, A. Tukiainen, A. Laakso, M. Tuominen, and M. Guina, J. Appl. Phys. 112, 023504 (2012).
13. A. Aho, V.-M. Korpijärvi, A. Tukiainen, J. Puustinen, and M. Guina, J. Appl. Phys. 116, (2014).
14. M. Hugues, B. Damilano, J. Chauveau, J. Duboz, and J. Massies, Physical Review B 75, 045313 (2007).
15. T. K. Sharma, M. Zorn, F. Bugge, R. Hulsewede, G. Erbert, and M. Weyers, IEEE Photonics Technology Letters, 14, 887-889 (2002).

Tampereen teknillinen yliopisto
PL 527
33101 Tampere

Tampere University of Technology
P.O.B. 527
FI-33101 Tampere, Finland

ISBN 978-952-15-3629-8
ISSN 1459-2045